2013-04-30

A New Shear Test Method for Mortar Bed Joints

Popal, Rashid

UNIVERSITY OF CALGARY

A New Shear Test Method for Mortar Bed Joints

by

Rashid Popal

A THESIS

SUBMITTED TO THE FACULTY OF GRADUATE STUDIES

IN PARTIAL FULFILMENT OF THE REQUIREMENTS FOR THE

DEGREE OF MASTER OF SCIENCE

DEPARTMENT OF CIVIL ENGINEERING

CALGARY, ALBERTA

MARCH 2013

Abstract

From a review of existing test methods devised to determine the shear strength of a mortar joint, it was concluded that among the existing methods, the triplet test is the simplest to perform and the Hofmann & Stöckl test provides the best results in terms of uniform stresses. The advantages of these two tests were combined in a new shear test method designed, constructed, and utilized in this research. In the new test method, simple equipment is used to subject a couplet to a time-dependent horizontal load as well as to a level of normal compression stress. The couplet is placed between two rubber sheets, two steel plates, and two roller rails to accommodate the unevenness of the surface of the bricks, to allow smooth movement of the rollers, and to minimize the friction between the couplet and the vertical support planes, respectively. The results of the experimental investigation show that the developed test method produces uniform shear stress as in the Hofmann & Stöckl test and is as simple to perform as the triplet test.

Acknowledgements

I am deeply indebted to my supervisor Dr. Shelley Lissel for her continuous trust, support, guidance, and patience throughout my research. I am grateful to Dr. Nigel Shrive for all the valuable discussions, useful advice, and his contribution of time. I would also like to thank my committee members Dr. Mamdouh El-Badry, Dr. Nigel Shrive, and Dr. Sudarshan (Raj) Mehta for their time and effort in reviewing this work.

The assistance of the technical staff of the Department of Civil Engineering, University of Calgary, during the experimental work is gratefully appreciated. Also many thanks to Civil Department supporting staff Julie Nagy Kovacs and Chrissy Thatcher for their support during my study time. Further, I would like to acknowledge the support of IXL Masonry Supplies Ltd. and Spec Mix Inc. for supplying the required material for this research. I also want to thank Dr. Andy Take from Queen's University for providing the Geo-PIV program. Also, many thanks to Khaled Abdelrahman for his assistance in applying the Geo-PIV program for the data evaluation.

I am grateful to my friend Mohsen Andayesh for the valuable technical discussions, wonderful time, and for always being there to help and support me. I am also indebted to my mentor and friend Dr. Gerd Birkle for providing encouragement and support from the start of this thesis to its completion. None of this would be possible without him.

At last, but definitely not least, I would like to thank my parents for their unconditional love and support throughout this phase of my life.

To my

sister Zohal A. Popal and brother Jalil A. Popal

Table of Contents

List of Tables

List of Figures and Illustrations

CHAPTER 1: **INTRODUCTION**

Masonry is an assemblage of units (bricks or blocks) connected by mortar joints. The bricks or blocks as well as the mortar are available in different configurations and compositions worldwide. Therefore, masonry has been used by humans for millennia to construct shelter, and thereby a protection against uncomfortable weather conditions and risks. Generally, in a masonry construction, the lateral loads caused by wind or earthquake are resisted and transmitted to the foundation by means of shear walls that are arranged orthogonally, e.g. as shown in Figure 1.1.

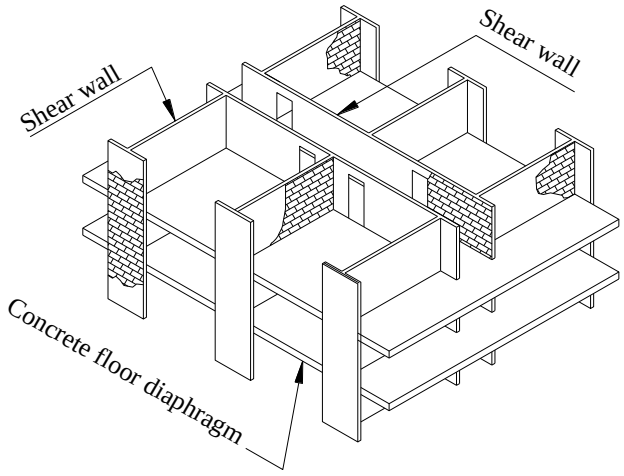

Figure 1.1: Orthogonally arranged masonry shear walls

In case of exceedance of the wall resistance, two different modes of failure are usually observed, namely: flexural (tension) and shear failure, as shown in Figure 1.2. Considering only the shear failure, the crack can propagate either through the head and bed joints or through the head, bed joints, and units and may also propagate mainly along only 1 or 2 bed joints in what is called sliding shear failure. Therefore, the shear resistance of a masonry wall depends on the strength of units and the mortar-unit

interface. In order to study and assess the shear behaviour and the shear strength of a masonry wall, several test methods have been devised and utilized by many researchers, (Jukes & Riddington, 1997).

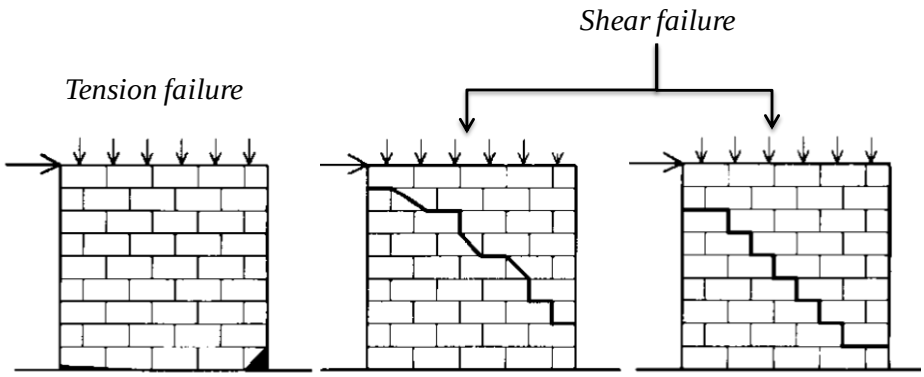

Figure 1.2: Mode of failures, (Lissel, 2001)

The test methods can be classified into three different levels: Macro-level, Meso-level, and Micro-level.

The macro-level includes test methods with larger specimens, typically one story in height, possibly containing an opening. The meso-level includes test methods with specimens in the order of $1\,m$ by $1\,m$, and the micro-level includes test methods with specimens consisting of two, three or four units. In the first two levels, no distinction is drawn between units and mortar joint, while at the micro-level the units and mortar joint are considered separately (van Vliet, 2004). The current research project is only focussed on joint shear test methods at the micro-level, several of which, have been reported in the literature (Jukes & Riddington, 1997). A joint shear test method should meet the following criteria according to Riddington, et al. (1997):

- The normal and shear stress distribution should be uniform.
- Majority of the joint should be close to failure when failure is initiated at one point.
- No tensile stresses should be induced along the joint that could affect the failure load.
- The failure should be initiated away from the edge of a joint.
- The complexity needed to carry out the test should be as simple as possible.

1.1 Objective

The objective of this research is to devise a simple test method that produces uniform shear stress in the mortar bed joint and meets the criteria listed above. It is not intended to evaluate the shear strength of mortar bed joints.

To achieve this objective, a simple finite element analysis of two existing methods and of the devised test method was performed to gain insight into the state of stress imposed in the bed joint. Subsequently, an experimental program using two types of bricks combined with only one type of mortar was conducted to evaluate the devised test arrangement.

1.2 Scope and Thesis organisation

In Chapter 2, a literature review of test methods at the micro-level is presented. Furthermore, some of the factors affecting the shear strength of a masonry wall are discussed. From the literature review, two test methods are identified that meet most of the above criteria: the Hofmann & Stöckl and the Triplet tests. While the Hofmann &

Stöckl test produces the most uniformly distributed normal and shear stresses along the bed joint, it requires very complex equipment, (Stöckl & Hofmann, 1990). The triplet test is much simpler, but does not produce the ideal normal and shear stress distributions (Jukes & Riddington, 1997; Riddington, et al., 1997). While the Hofmann & Stöckl test produces the best results and the triplet test is simpler to perform, the challenge remains to devise a test method that is able to combine the advantages of both test methods

In Chapter 3, the Hofmann & Stöckl test and the triplet test are evaluated and compared based on a two-dimensional finite element analysis assuming linear stress-strain behaviour of the material. Subsequently, a new joint shear test method is proposed for specimens consisting of two units connected by a mortar joint over the entire length in stack bond. Numerical analysis of the new test method is also carried out using finite element method (FEM) for comparison with the Hofmann & Stöckl and triplet tests. In Chapter 4, an experimental program using the new test method is described. In addition, a short description of the measurement systems utilized is included. Linear strain converters (LSCs) are used to prove the reproducibility of the new test method by determining the variation in load-displacement behaviour. A Particle Image Velocimetry measurement system (GeoPIV) is used to gain insight into the state of stress imposed in the bed joint in the new test method.

In Chapter 5, the experimental data obtained using LSCs and the GeoPIV measurement system are evaluated and discussed. The performance of the new test method is evaluated on the basis of these data. In Chapter 6, the research presented in this thesis is summarized, followed by conclusions and recommendations for future work.

CHAPTER 2: **LITERATURE REVIEW**

2.1 Introduction

Within the scope of this research, the existing joint shear test methods at the micro-level are reviewed and discussed. The discussion is primarily concentrated on the test methods that provide bending moment free testing of the mortar bed joint, and on the methods that are simpler to perform. While the test methods are discussed, the criteria, as specified in Chapter 1, are taken into account. The existing test methods are summarized and discussed to distinguish their respective advantages and disadvantages. For this purpose, test methods are ordered by the number of units of the specimens, and the type of applied shearing load. Beyond that, factors having an effect on the results of bond shear strength of a mortar joint are emphasized and reviewed. The knowledge gained will be used to devise a new test method that is able to combine the advantages of the existing test methods.

2.2 Existing shear test methods

A review of the literature reveals that many researchers have utilized different methods to measure the shear strength of a mortar bed joint at the micro level, (Jukes & Riddington, 1997). The existing test methods differ either in their arrangement or in the type of specimen. Considering the test arrangement, the differences are mainly in the load arrangement and application. For example, in some of the tests, the specimen is only subjected to a horizontal load (i.e. the line of action of the load is acting parallel to the mortar joint), and in others the specimen is subjected to a horizontal as well as a vertical load (i.e. the mortar joint is subjected to parallel und normal stress). In addition to these

two types of load application, there exist test methods in which the specimen is subjected to a torque with or without a normal compressive stress. With respect to the specimens, the test methods differ from each other in the number of units and shape of the specimens. In most of the existing test methods, a couplet (two-unit specimen) is utilized to measure the shear strength of a mortar joint, but there also exist test methods which are performed using four or three-unit specimens. For example, a four-unit specimen was used by Hamid & Drysdale, (Hamid, et al., 1979), and a triplet is suggested by the European Committee for Standardization (CEN) to measure the shear strength of a mortar joint, (DIN EN 1052-3, 2007). Generally, couplets are subjected either to shearing force or to torsion, while triplets (three-unit specimen) and four-unit specimens are subjected only to shearing force.

However, regardless of the number of units or the shape of the specimens, it is quite a challenge in practice to apply load to a specimen without inducing bending moment to the mortar bed joint. This is a result of the eccentricity that exists between the line of action of the applied shearing load and the center line of the mortar bed joint. In order to reduce or to eliminate the induced bending moment, researchers have utilized a combination of horizontal and vertical load, or a specific manner of load application, or a particular load and support arrangement. For example, Hofmann & Stöckl (1986) utilized a combination of horizontal and vertical load, van der Pluijm (1993) utilized a specific way of load application, and Jiang & Xiao (1994) used both the load and support condition to perform a shear test free of bending moment. Furthermore, to avoid inducing bending moment in the mortar joint, researchers have devised test methods in which a

couplet is subjected to a torque to determine the bond shear strength of a mortar joint (Samarasinghe & Lawrence, 1994; Khalaf, 1995; Hansen & Pedersen, 2008; Hansen & Pedersen, 2009; Masia, et al., 2010). However, results obtained using these test methods, in which the specimen is subjected to a torque, represent the torsional shear capacity of masonry subjected to flexural about the axis normal to the bed joints, (Samarasinghe & Lawrence, 1994).

2.2.1 Four unit specimens

Hamid et al. (1979) used a four-block specimen for their proposed test method to measure the shear strength of joints in concrete masonry. In this four unit test, the specimen can be tested either with or without normal compressive stress. However, the utilized specimen, as shown in Figure 2.1, is very fragile and vulnerable to collapse before testing. In addition, as a result of their construction, the four joints are pre-stressed due to the self-weight of the concrete blocks. Therefore, the results obtained indicate only the additional load necessary for the mortar joint to fail. Not only do the results represent the strength of the weakest mortar joint, but the eccentrically applied load leads to bending of the blocks which, in turn, causes a non-uniform normal stress distribution along the mortar joints and the mortar joints are subjected to tension as discussed in (Jukes & Riddington, 1997).

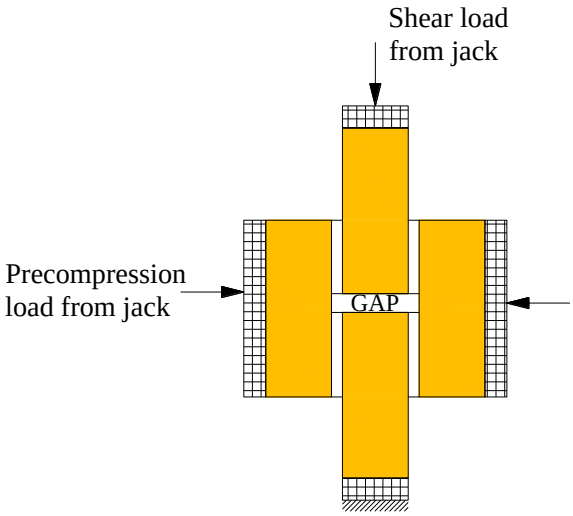

Figure 2.1: Hamid & Drysdale Test

2.2.2 Triplet test

The triplet test without pre-compression was proposed by the European Committee for Standardization (CEN) as a standard test for measuring the bond shear strength of a mortar joint. In the proposal of CEN, the details for the support and load arrangement of the triplet test were unclear. Therefore, a research program was carried out in which the triplet test was performed with different load and support conditions, (Riddington & Ghazali, 1990; Bouzeghoub, et al., 1995). In doing so, the influence of unit aspect ratio and loading arrangement on bond shear strength, as well as the initial mode of failure of the triplet was studied. The results obtained show that the bond shear strength is affected by the amount of bending moment to which the specimen is subjected. Hence, in order to minimize the effect of bending moment as well as the effect of the unit aspect ratio (high/length), a new load and support arrangement, as shown in Figure 2.2, was proposed (Riddington, et al., 1991). However, the proposed load and support arrangement only minimizes, but does not eliminate, the bending moment, and

for this reason as long as the triplet test is conducted without pre-compression, most of the mortar joint will be subjected to a considerable amount of normal tensile stress, (Riddington, et al., 1997) and (Popal & Lissel, 2010). In addition, as was the case with the four unit test, the results obtained represent only the shear strength of the weakest mortar joint of the specimen, and both of these test methods require more material compared to tests using a two unit specimen (couplet). Advantages of the triplet test include the symmetrical nature of the specimen and the load arrangement, since this facilitates a stable load arrangement in comparison to the couplet (Jukes & Riddington, 1997), and in addition, the test is feasible with simple equipment.

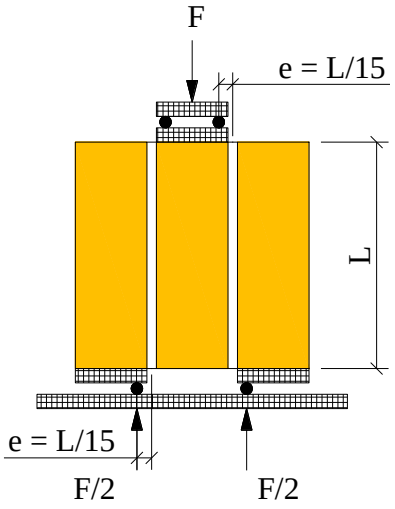

Figure 2.2: Triplet Test

2.2.3 Couplet tests

As mentioned previously, the aim is to devise a test setup that reduces or ideally eliminates the effect of bending moment. Keeping this in mind, one existing test arrangement that measures the shear strength of a mortar joint free from the effect of bending moment was proposed by Hofmann & Stöckl (1986). In this test method, a

combination of a horizontal load and a pair of vertical loads, are applied to a couplet, in which the two bricks are overlapped by about half of the unit length, as shown in Figure 2.3. In order to eliminate the bending moment along the mortar joint, the load combination must be permanently monitored, so that the pair of vertical loads can be automatically adjusted as a function of the increasing horizontal load. In this manner, the vertically applied load creates a counter moment of the same magnitude as the one induced by the horizontal load, and assures a bending moment free measurement of the shear strength of the mortar joint. Numerical evaluation of the test arrangement also indicated that the test method produces the most uniform distributed shear and normal stresses along the mortar joint, (Stöckl & Hofmann, 1990) and (Riddington, et al., 1997). However, the numerical evaluation also indicated that most of the mortar joint is subjected to normal tensile stress. In addition, the test cannot be performed at different levels of normal compressive stress, since the compressive load is applied as function of the horizontal load. Beyond that, the test arrangement also requires the use of complex equipment, see Appendix B, which eliminates its chance to be adopted as a standard test method and limits its application to the best equipped labs.

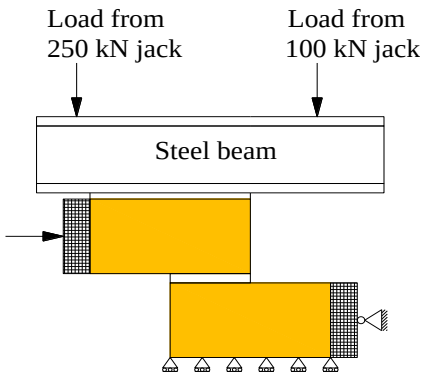

Figure 2.3: Hofmann and Stöckl Test

The second test arrangement that provides a bending moment free evaluation of joint shear was described by van der Pluijm (1993). In this test arrangement, as shown in Figure 2.4, the two-brick specimen is attached by means of adhesive material to the L-shaped members, and the applied shear load is transferred to the specimen through the L-shaped solid steel section. Using the L-shaped steel sections, the shear load is applied to the specimens without any eccentricity. In doing so, it enables determination of the shear strength of the mortar joint without being affected by the bending moment. The principle behind this test method is that by applying moments and shear forces to a specimen, pure shear is achieved at the middle of the specimen as long as the applied moment equals $M = \mathrm{V} * \mathrm{d}/2$, (van der Pluijm, 1992). As a matter of fact, numerical analyses of the test method proved that the test produces a nearly uniform shear stress distribution. However, the FE-analyses also indicated that the distribution of the normal stress along the mortar joint, unlike distribution of the shear stress, varies considerably. The non-uniformity of the normal stress is related to the stiffness of the steel blocks, and can be improved by using thicker or stiffer steel blocks (van der Pluijm, 1992; 1993). Furthermore, the FE-analyses indicated that, as in the case of the Hofmann & Stöckl test, the mortar joint will be subjected to normal tensile stress if the test is conducted without pre-compression, (Riddington, et al., 1997; van der Pluijm, 1993). However, one advantage of this test, compared to the Hofmann & Stöckl test, is that it can be performed at different levels of normal compressive stress, since the load normal to the mortar joint is not applied as a function of the shearing load.

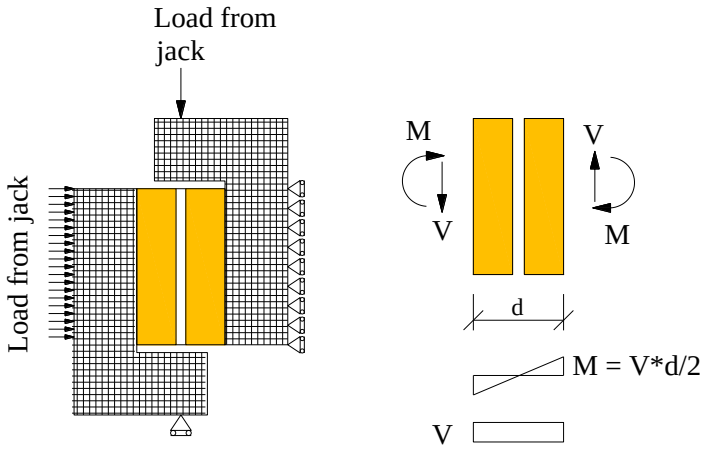

Figure 2.4: van der Pluijm Test

The test method described by Jiang & Xiao (1994) is also one in which the load and support arrangements are utilized in combination to produce a bending moment free shear test. As shown in Figure 2.5, the couplet is bracketed between two T-sections, and is placed in the midspan of a beam. The applied loads (at *B* and *C*) and supports of the beam (at *A* and *D*) create a constant shear force between points *B* and *C*, and a moment that equals zero in the middle of the mortar joint. The finite element analysis, presented by Jiang & Xiao, showed a uniform distribution of shear stress along the mortar joint, but stresses normal to the mortar joint were not reported. Furthermore, the test method only provides results for the initial bond shear strength, τ_0, while the ultimate shear strength of a masonry assemblage, τ_u, is expected to be a function of the initial bond shear strength, the internal coefficient of friction (μ) at the interface, and the normal stress due to gravity. However, this test method can be combined with a simple test apparatus proposed by Ghazali & Riddington (1988) to obtain the ultimate shear strength.

The simple apparatus, as shown in Figure 2.6, is intended for measuring the coefficient of friction and was combined with the triplet test without pre-compression, to

determine the shear strength of a masonry assemblage, (Riddington & Jukes, 1994). In doing so, Riddington & Jukes tested 1300 triplet specimens, and concluded that the combination of the two tests is capable of producing similar values for τ_0 and μ as those produced by the triplet test with pre-compression. However, in the case of bricks with large perforations and smooth top and bottom surfaces, the method is not capable of producing similar results to those produced by the triplet test with compression. Therefore, the use of the inclined test with this type of bricks is not recommended.

Therefore, two disadvantages of the test method reported by Jiang & Xiao are that it is only useful for limited types of brick and mortar combinations and, more importantly, it cannot be performed with pre-compression.

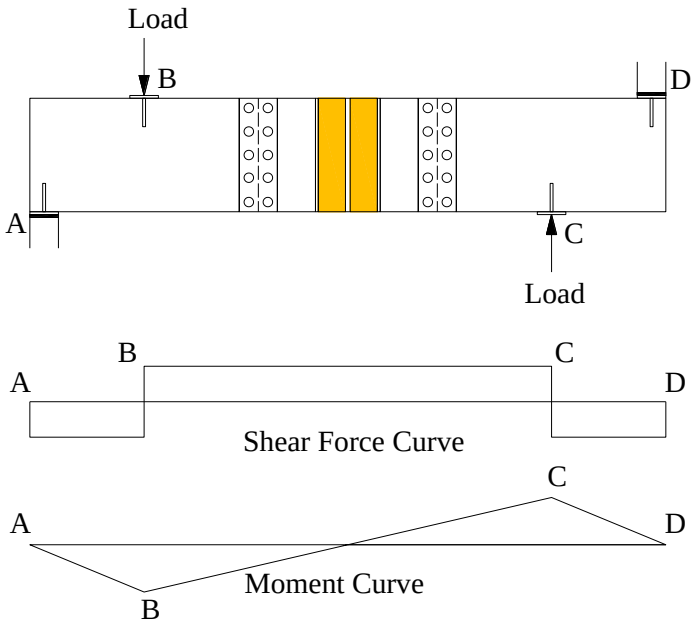

Figure 2.5: Jiang/Xiao Test

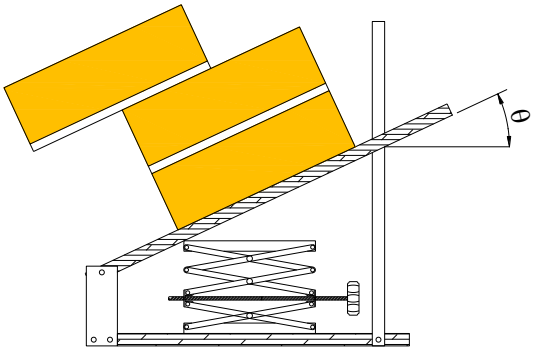

Figure 2.6: Inclined Test

2.2.4 Torsion tests

To characterize the shear behaviour of a mortar joint in masonry, some researchers subjected specimens to a torque. Thereby, they studied the torsional behaviour of brick-mortar joints, and the torsional shear capacity which is activated when stretcher bonded masonry is subjected to flexure about an axis perpendicular to the bed joints. In 1994, Samarasinghe & Lawrence investigated the torsional shear resistance capacity of brick masonry bed joints by subjecting specimens to torsion and compressive load (Samarasinghe & Lawrence, 1994). In this test arrangement, the specimens are constructed of two bricks joined together by a partially filled rectangular mortar joint, and are kept in place by four steel rods which are rigidly connected to two steel plates, as shown in Figure 2.7. The four rods are used to transfer the applied torsion load to the specimen, and the compressive load is applied through the steel plates using a screw jack. While the test arrangement itself is fairly simple, the construction of the specimens, specifically the forming of the reduced size mortar joint is somewhat complicated and likely time-consuming, therefore, the test cannot be declared as simple.

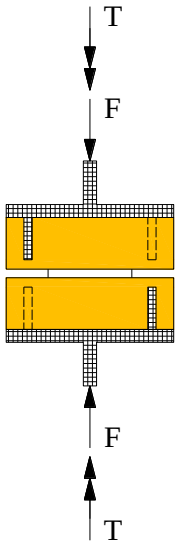

Figure 2.7: Samarasinghe & Lawrence test

In 1995, Khalaf proposed a simple apparatus to test couplets in which the bricks were staggered and joined by means of a mortar joint with a circular cross section, (Khalaf, 1995). This test arrangement, shown in Figure 2.8, provides the initial shear capacity of a mortar joint subject to torsional load. Therefore, the test was conducted in combination with the above mentioned sliding apparatus (shown in Figure 2.6) to determine the ultimate shear strength capacity. As mentioned previously, the inclined test method cannot be used for bricks with large perforations and a smooth surface, therefore the combination of these two tests also has limited application. In addition, despite the relatively simple test apparatus, the construction of the specimens with a circular shaped mortar joint is very time consuming and difficult. However, a similar test setup was reported in 2009 by Hansen & Pedersen, in which the two bricks were joined together by means of rectangular cross section mortar joints instead of circular (Figure 2.8). In addition, the test is feasible with normal compressive load. These two main differences are also improvements in comparison to the original Khalaf test. However, a 3D-finite

element analysis indicated that the distribution of the shear stress varies along the perimeter of the mortar joint as well as with the radius (Hansen & Pedersen, 2009).

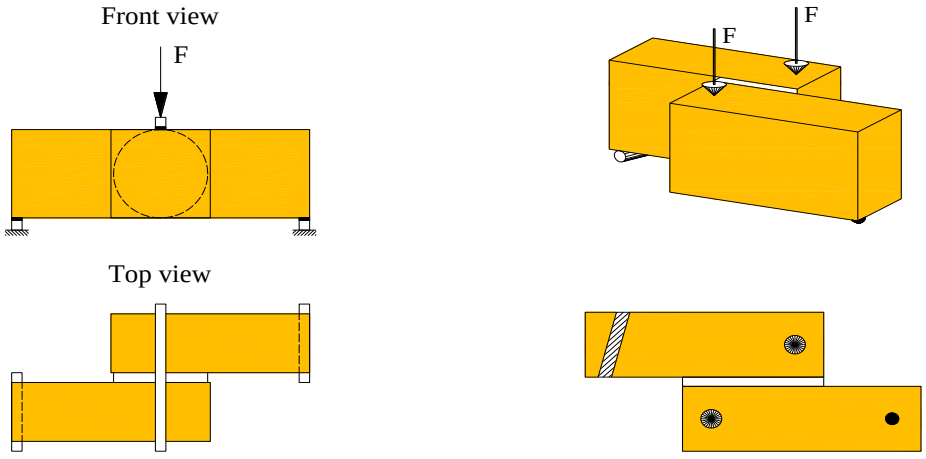

(a) **(b)**

Figure 2.8: (a) Khalaf test, (b) Hansen & Pederson test

In 2006, Masia et al. proposed a new testing procedure based on the same principle as used by other researchers for describing the shear strength of a soil specimen, (Masia, et al., 2006). In the test arrangement shown in Figure 2.9, a specimen consisting of two annular bricks connected by a mortar joint is subjected to combined normal and torsion loads. The unique shaped specimen is glued, by means of epoxy, between two plates in which one plate is fully fixed and the other one is used to induce the loads. Such a load and support arrangement was also utilized by Khalaf, as discussed above. The authors reported that the preparation of the specimen with the annular section is the most time-consuming and challenging part of the test setup (Masia, et al., 2010). In their tests, the authors attempted to obtain additional information beyond bond shear strength, τ_0, and coefficient of friction, μ, such as shear stiffness, shear fracture energy, post cracking coefficient of friction, and the dilatancy. These additional properties are required to

characterize the shear behaviour of a mortar joint for finite element analyses (FEA) at the micro-level. The FE-analyses conducted indicate that the test method produces an approximately uniform normal and shear stress distribution across the mortar joint. However, the FE-analyses also indicate that the distribution of shear stress varies with the radius (Masia, et al., 2006). Similar results were also observed later in a 3D-finite element analysis conducted by Hansen & Pedersen (2009). This is not surprising, since all three test methods mentioned here apply the theory of torsion to determine the ultimate shear strength. It should be noted that variation of shear stress with the radius is typical for torsion theory.

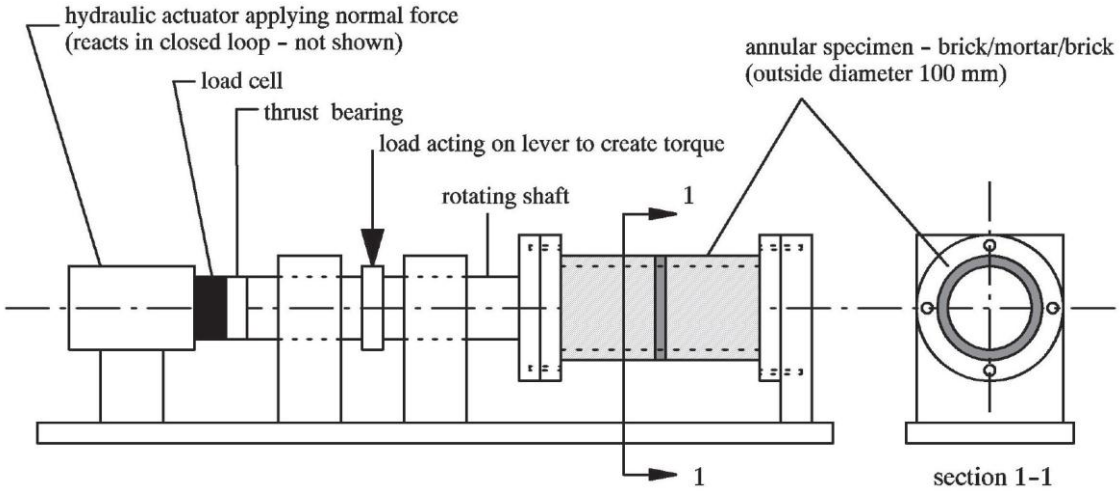

Figure 2.9: Torsion test method (Masia, et al., 2010)

In general, from the research reported in the literature, it can be concluded that the torsion test methods are not suitable for specimens constructed of weak bricks and strong mortar, particularly when subjected to high levels of normal compressive stress (Samarasinghe & Lawrence, 1994; Hansen & Pedersen, 2009; Masia, et al., 2010). In addition, all specimens used in the existing torsion test methods require additional effort

for their preparation, except the one used by Hansen & Pedersen (2009). Further, in the case of specimens constructed with perforated bricks, the torsion tests are incapable of producing reasonable results. Beyond that, the torsion tests might be helpful to predict the torsional shear capacity of a bed joint. However, the torsional shear capacity is only needed when a stretcher bonded masonry wall is subjected to flexure about an axis normal to the bed joints which is seldom the case in reality.

2.3 Factors affecting masonry shear strength

The shear strength of a masonry wall as well as of a mortar bed joint is affected by many different factors. For example, the properties of the unit (such as compressive strength, anisotropy, size and aspect ratio, absorption properties, condition of the units during the laying), mortar, and grout as well as the properties of the unit/mortar bond, and workmanship, (Sutcliffe, et al., 2001). In addition, the shear strength of a mortar bed joint obtained from a shear test is affected by the presence of normal compressive stress as well as by the arrangement of the shearing force.

2.3.1 The effect of compressive stress

In 1979, Hamid et al. conducted a research program with 46 specimens constructed from one type of concrete block and two mortar types (Type S and N), in which some of the specimens were grouted and some of them not. They observed that pre-applied normal compressive stress has a significant effect on the results obtained from a shear test (Hamid, et al., 1979). Similar observations were also made by other researchers (Pook, et al., 1986; Hofmann & Stöckl, 1986; Hansen, et al., 1998), when they subjected specimens to combined shear and normal loads using the triplet, and

Hofmann & Stöckl tests, respectively. The above mentioned investigations, as well as the one conducted by Ghazali & Riddington (1986), conclude that the shear strength of a mortar joint increases linearly with the level of normal compressive stress. This linear relationship, however, exists only up to a normal compressive stress of about $2\ N/mm^2$, (Riddington & Ghazali, 1987). A normal compressive stress higher than $2\ N/mm^2$ starts to reduce the rate of increase in shear strength, (Hamid & Drysdale, 1982; Riddington & Ghazali, 1990). Therefore, in general, it is accepted that the ultimate shear strength, τ_u, of a mortar bed joint subjected to normal compressive stress ($\sigma_c \leq 2\ N/mm^2$), follows a Coulomb relationship (Hamid, et al., 1979; Ghazali & Riddington, 1986; Riddington, et al., 1997):

$$\tau_u = \tau_0 + \mu * \sigma_c \qquad \textbf{(1)}$$

where τ_0 is the initial bond shear strength or the shear strength at zero normal compressive stress, and μ is the coefficient of internal friction at the interface between the mortar and the unit.

2.3.2 The effect of brick and mortar properties

The effect of brick and mortar properties on the shear behaviour of a mortar bed joint is controversial in the literature. In 1979, Hamid et al. concluded that shear strength of a mortar joint is a function of mortar properties as well as of the physical properties of the block such as surface roughness and initial rate of absorption (Hamid, et al., 1979). A similar conclusion was reported by Hofmann & Stöckl in 1986. They observed an increase in ultimate shear stress due to increased compressive strength of clay brick and

mortar strength. The increase due to the clay brick strength was related to surface roughness, condition at laying (i.e. wet or dry), and the corresponding suction capacity of the bricks (Hofmann & Stöckl, 1986). However, in 1997, Khalaf concluded that an increase in mortar strength has an effect to a certain extent on the bond shear strength, and that the type of brick has no significant effect on the bond shear strength (Khalaf & Naysmith, 1997). The limited effect of an increase in mortar strength was also observed by Hansen, et al. (1998). In contrast, Vermeltfoort observed an increase in initial shear strength while the mortar compressive strength was decreased. Therefore, additional research is suggested to examine the effect of mortar compressive strength on shear strength (Vermeltfoort, 2010).

2.3.3 The effect of unit aspect ratio and load arrangement

The effect of unit aspect ratio and load arrangement was demonstrated by researchers who modelled the triplet test with specimens having various unit aspect ratios, and were subjected to different load and support arrangements. It was concluded from the analyses that both high and low unit aspect ratios affect the stress distribution along the mortar joint, and thereby the results of shear strength obtained using the triplet test. A high unit aspect ratio leads to increased bending in the specimen and a low aspect ratio leads to concentration of shear stress in the end of the specimen. Further, it was observed that the load arrangement can lead either to increased or decreased bending in the specimen depending on the eccentricity of the applied load, (Riddington, et al., 1991; Bouzeghoub, et al., 1995). The results of a numerical evaluation carried out by the author for the proposed test method are presented in Chapter 3. The effect of unit aspect ratio

was also studied in this case and the results indicate that the stress distribution varies with the unit aspect ratio. Therefore, it can be concluded that the effect is not specific to any test method.

2.4 Mode of Failure

In general, the three modes of joint failure at the micro-level, for the specimens reported in the literature, are shown in Figure 2.10. Independent of the test method used, the failure can be either a total slip along the lower/upper interface of the specimen, or a slip starting at the upper interface followed by a diagonal crack (varying between 45 and 90 degrees) through the mortar joint and continuing with slip along the lower interface, or a failure of the unit itself. A failure of the units is most likely to occur when weak units are combined with a strong mortar, particularly if also subjected to a high normal compressive stress. Failure of the specimen can also occur as a result of the anisotropy of the units if the strength capacity of the units in the longitudinal direction is exceeded by the complex stress combination induced in the specimen during the test.

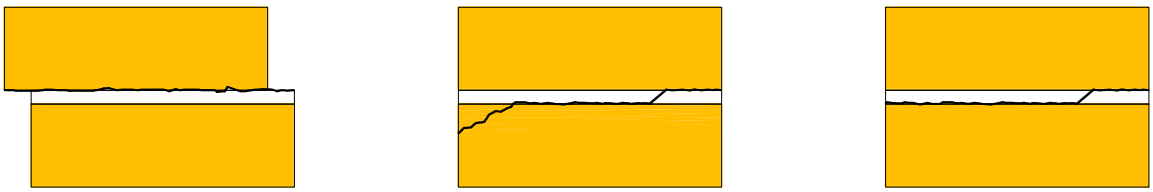

Figure 2.10: Mode of failure in a couplet

2.5 Summary

Over the last few decades, several test arrangements were devised and utilized by researchers to examine the shear strength of a mortar bed joint at the micro-level. Reviews and numerical evaluation of the test methods show that only the Hofmann &

Stöckl and triplet tests produce reasonable results in term of meeting the criteria as specified in Chapter 1. The Hofmann & Stöckl test produces the most uniformly distributed normal and shear stresses along the bed joint, but because it requires very complex equipment, it is unlikely that the test will be accepted as a standard test method. Thus, the triplet test is more suitable as a standard test and is more commonly used although the resulting stress distributions are not ideal. While the Hofmann & Stöckl test produces the best results and the triplet test is simpler to perform, the challenge remains to devise a test method that is able to combine the advantages of both test methods. A new test method has therefore been devised which aims to combine the advantages of the Hofmann & Stöckl and the triplet test. In the next chapter, the new test method is analyzed using finite element analyses.

CHAPTER 3: **NUMERICAL EVALUATION**

3.1 Introduction

The results of numerical analyses of mortar joint shear tests reported in the literature in the last 20 years indicates that the Hofmann & Stöckl and triplet test are most capable of producing the most desirable results with respect to criteria specified by Riddington et al. (1997). The main purpose of the numerical evaluations described in this chapter is to gain insight into the state of stress distribution imposed in the mortar joint by the proposed test method, and to compare the distribution with the stress distributions imposed by the two existing joint shear test methods (triplet and Hofmann & Stöckl tests). Therefore, the results of numerical analyses of the two existing test methods in addition to the one proposed in this chapter are discussed.

3.2 Material Properties

The brick chosen for the analyses of each test method are assumed to be solid clay brick with typical dimensions used in North America ($L\ x\ H\ x\ W$): $190\ x\ 57\ x\ 90\ mm$ (Model 1), and those used in an earlier study by Hofmann & Stöckl (1986): $240\ x\ 115\ x\ 113\ mm$ (Model 2). This step enables the comparison between the results of the original Hofmann & Stöckl test and the proposed one, and it also indicates to what extent the brick dimensions affect the test results.

The basic properties of the brick as well as of the mortar, assumed for the FEM analyses, are based on the existing literature, and are summarized in Table 3.1.

Table 3.1: Assumed Material Properties

Material	Modulus of Elasticity (N/mm^2)	Poison's ratio, ν
Brick	25500	0.13
Mortar	8500	0.18
Steel	200000	0.30

3.3 Modelling Strategy

A two-dimensional finite element model of the test methods based on linear stress-strain behaviour of material was deemed to be sufficient to gain insight into the state of stress distribution imposed in the mortar bed joints. The non-linearity of the mortar does not affect the mode of initial failure or the corresponding load, and only affects the stress distribution along the joint at a high level of pre-compression, (Bouzeghoub, et al., 1995).

For the numerical evaluation, two case studies (Case Study 1 and 2) were conducted using the commercial software package SAP2000 version 14. In Case Study 1, the numerical results reported in the literature were first reproduced by using the same elements, loads and boundary conditions as used in the original numerical evaluations. This step allows comparison of the results obtained for the proposed test method with the numerical results reported in the literature for the two existing tests, and validates the results obtained in the current analyses, especially the results of the proposed test method. In Case Study 2, a few modifications were made to account for the actual boundary conditions in the tests as explained in Section 3.3.2. Furthermore, a mesh sensitivity analysis was carried out by examining the results using various mesh sizes. The use of 8 node elements was also considered for Case Study 2, however convergence for mesh

sizes 10, 5, and 2.5 mm was not possible due to mesh size limitations in the software for 8 node elements. Therefore, elements with 4 nodes but half of the size (5, 2.5, and 1.25 mm) of the elements with 8 nodes were used. Table 3.2 shows that the 4 node elements utilized produce results with a difference less than 3% when comparing the X, Y, Z deformations (U_1, U_2, U_3) at an arbitrarily chosen node.

Table 3.2: Mesh refinement

	8 Node elements		4 Node elements		Difference	
	10 mm	5 mm	5 mm	2.5 mm		
U_1	0.116	0.0804	0.113	0.0791	2.5%	1.6%
U_2	0	0	0	0	0%	0%
U_3	-0.0114	-0.0094	-0.0114	-0.0092	0%	2.1%

In Figure 3.1, the results for the displacement obtained using 4 node elements with different mesh sizes (10, 5, 2.5, and 1.25 mm) are plotted versus the number of mesh elements, from left to right respectively. It can be seen that convergence starts at a mesh size of 5 mm. Therefore, it was concluded that a mesh size of 5 mm or lower provides results that are accurate enough for the purpose of this study.

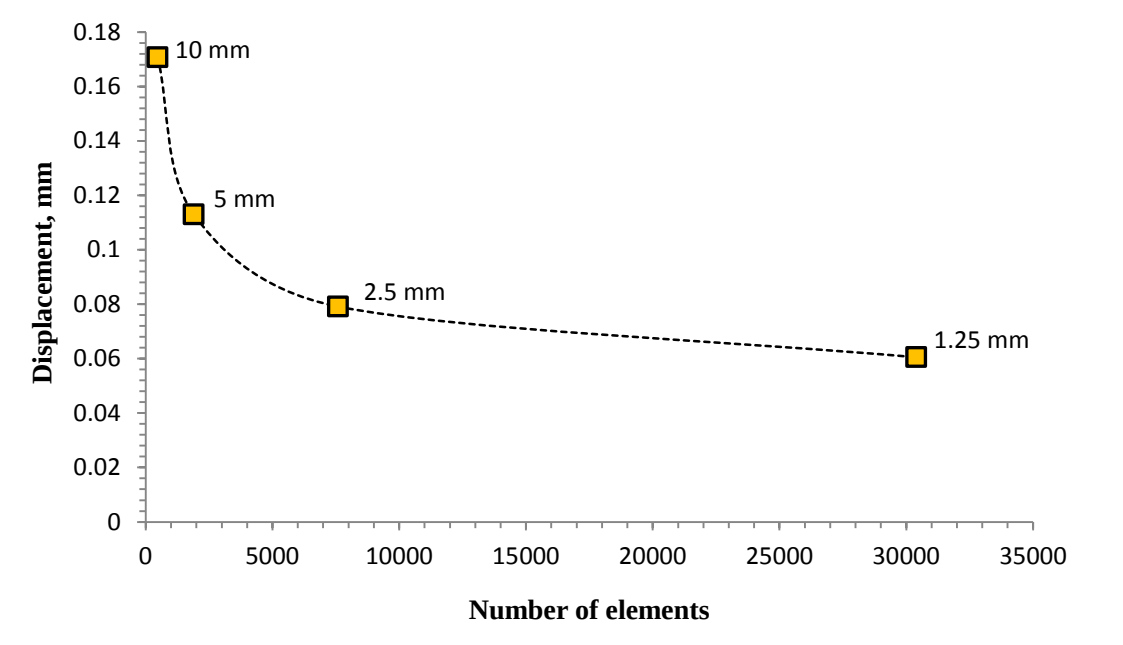

Figure 3.1: Mesh convergence

Hence, for the numerical analyses of the joint shear tests, elements with 4 nodes and isotropic behaviour are used for the brick, mortar, and steel by assuming plane stress. In both case studies, the applied horizontal loads should cause, depending on the bed joint area of each specimen, an average shear stress with a magnitude of $\tau = 1\ N/mm^2$ along the mortar joint. No external load, normal to the bed joint, is applied to the specimens, except in the Hofmann & Stöckl test, since this test can be performed only in the presence of pre-compression.

3.3.1 Case Study 1

In the following, the finite element models for the triplet, Hofmann & Stöckl, and the proposed test method are described, analyzed, and the corresponding results are discussed.

3.3.1.1 Triplet Test

The triplet test without pre-compression was proposed by the European Committee for Standardization (CEN) as a standard test for measuring the bond shear strength of masonry.

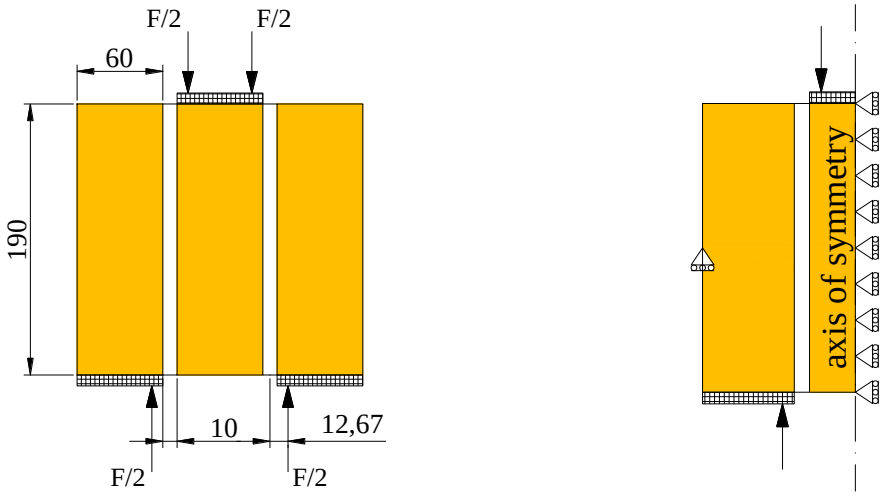

Figure 3.2: Triplet test- Loading arrangement (left) and model of half triplet specimen (right)

The symmetrical arrangement of the triplet test is utilised for the finite element modelling and the test is modelled as shown in Figure 3.2 on the right hand side. The vertical load on the specimen is applied through a steel block. The point of application of the force is determined according to the joint length, $l/15$. The particular load arrangement of the test, as shown in Figure 3.2 on the left hand side, was suggested by Bouzeghoub et al. (1995). In the finite element model, the specimen is supported on the right hand side by rollers providing only horizontal support to the model. On the left hand side the model was supported by one roller, in the vertical direction, to ensure a stable system. This has no effect on stress distributions along the joint and the vertical reaction at the support is equal to zero. In addition, the brick sizes were modified from

$190x57x90\ mm$ to $190x60x90\ mm$ and from $240x115x113$ to $240x120x120\ mm$ in order to utilise an integer mesh size of 5 *mm*. This, however, does not apply to the mortar joint. Thus, the half triplet specimen is meshed, as shown in Figure 3.3, using $12\ x\ 38$, $3\ x\ 38$ and $6\ x\ 38$ elements (Model 1) and $24\ x\ 48, 3\ x\ 48$ and $12\ x\ 48$ (Model 2) for the full unit, mortar joint, and half unit (left to right), respectively.

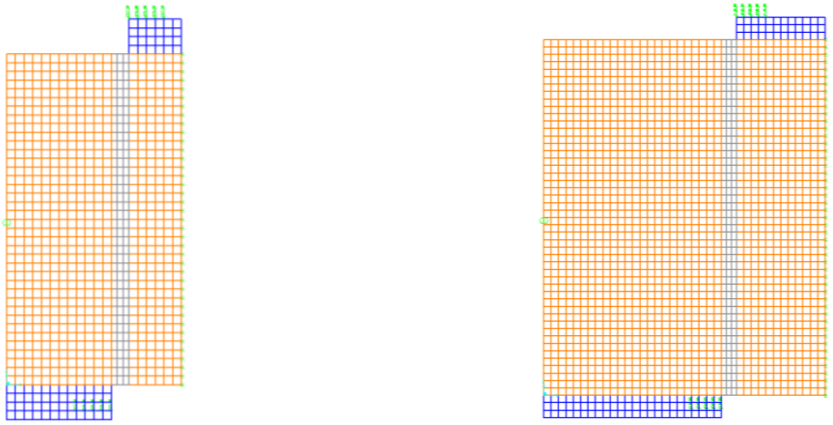

Figure 3.3: Case Study 1, meshing of triplet test- Model 1 (left), Model 2 (right)

The resulting normal and shear stress distributions in the specimen are illustrated in Figure 3.4 and Figure 3.5, respectively. The normal stress distribution shows that the mortar bed joint in both cases (Models 1 and 2) is subjected to varied normal stress, which is likely to affect the bond shear strength at the mortar joint due to the presence of normal tensile stress. The distribution of shear stress along the mortar joint also varies considerably.

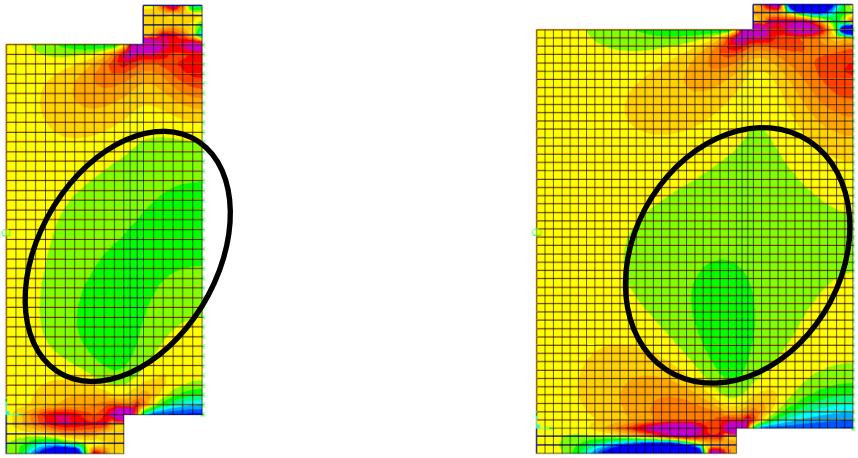

Figure 3.4: Case Study 1,
Normal stress distribution Model 1 (left), Model 2 (right)

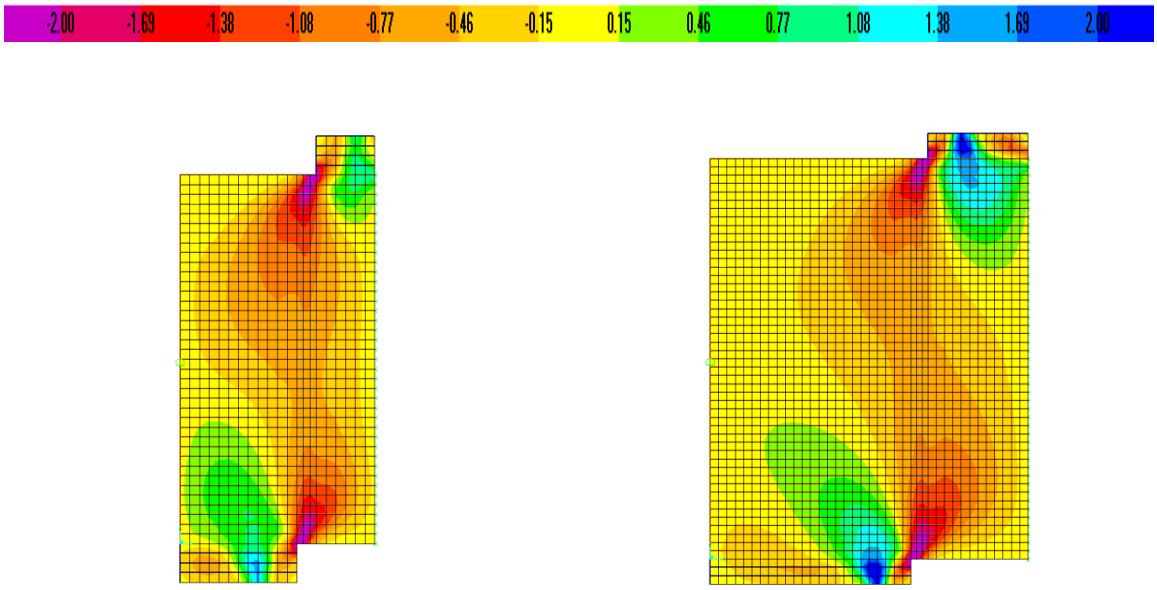

Figure 3.5: Case Study 1,
Shear stress distribution Model 1 (left), Model 2 (right)

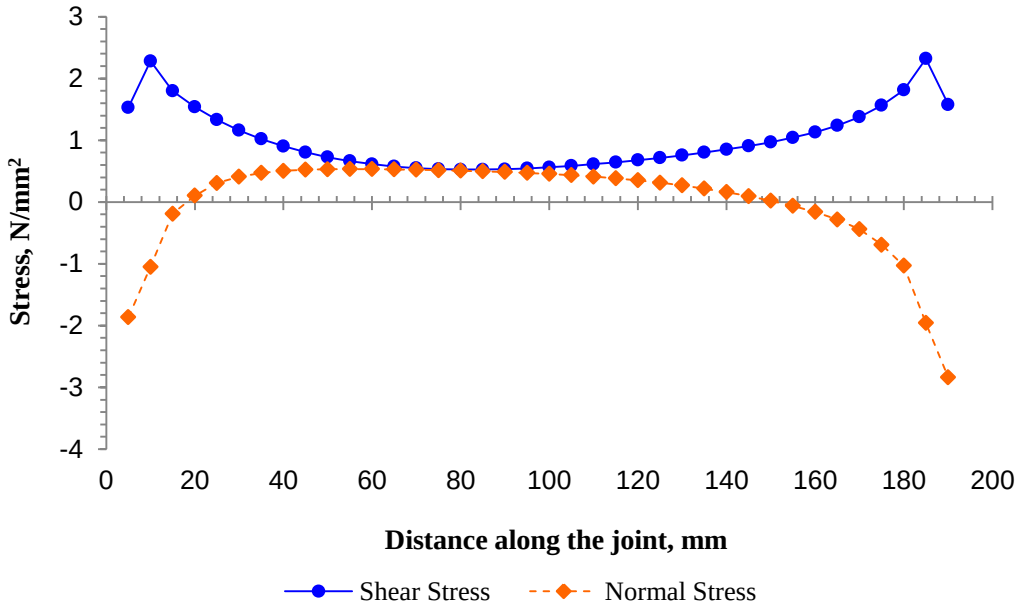

Figure 3.6: Case Study 1, stress distributions along the middle of the mortar bed joint (Model 1), Triplet test

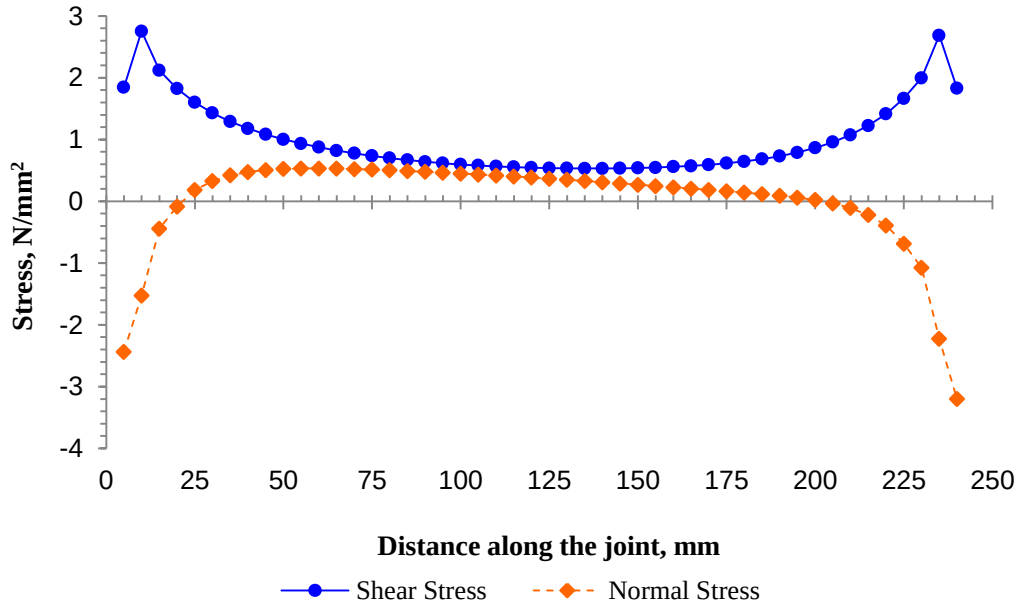

Figure 3.7: Case Study 1, stress distributions along the middle of the mortar bed joint (Model 2), Triplet test

The magnitude of the normal and shear stresses along the length at the mid-height of the joint are illustrated in Figure 3.6 and Figure 3.7. The shear stress deviates from the average imposed shear stress of $\tau = 1.0\ N/mm^2$ by more than 200% at the ends and up to 50% at the mid-length of the joint. This state of shear stress combined with the likewise varied normal stress leads to uncertainty whether the failure of the specimen is a result of the shear stress or of normal tensile stress, and whether the obtained results for bond shear strength represent the actual bond shear strength of the mortar joint or not.

3.3.1.2 Hofmann and Stöckl Test

The test was published by Hofmann & Stöckl (1986). A schematic sketch of the test is shown in Figure 3.9. As mentioned in Chapter 2, the bed joint is subjected to a moment of magnitude $M_H = F * a$, due to the two horizontal forces, F. In order to compensate for the induced moment, the specimen is subjected to two additional vertical forces, V_1 and V_2, which create an opposing moment with a magnitude of $M_V = V * b'$. The applied vertical loads are automatically adjusted in such a manner that M_V is always equal to M_H.

The lever arm of the horizontal couple, a, is dictated by the dimensions of the units and equals $135\ mm$ for the units used by Hofmann & Stöckl. Further, the resultant force, V, should not move beyond the left-hand end of the upper unit. This limits the lever arm, b, to a maximum of $180\ mm$, with respect to the mid-length of the bed joint, and a maximum b' of $360\ mm$.

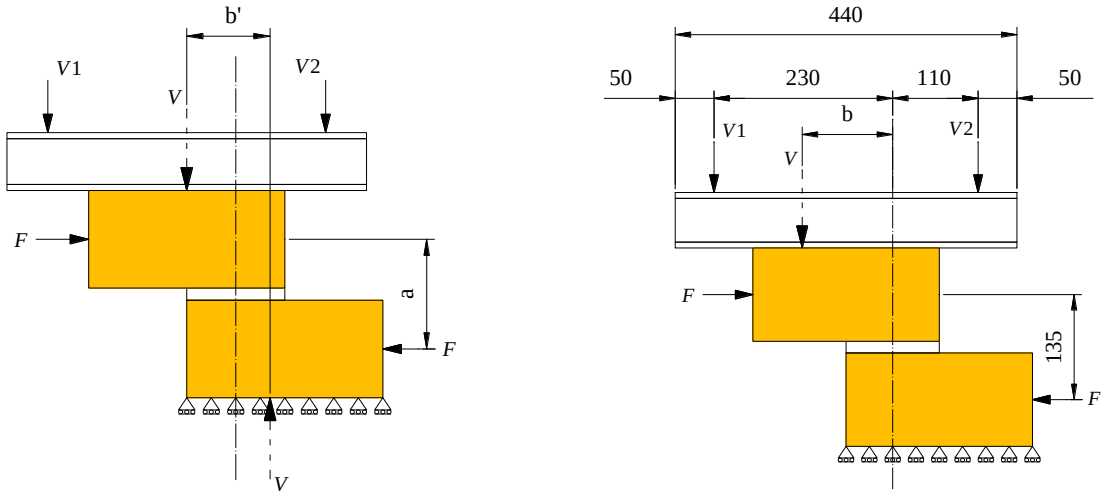

Figure 3.8: Hofmann and Stöckl Test

In Case Study 1, the finite element analyses for Models 1 and 2 are conducted in nearly the same manner as was done originally by Stöckl & Hofmann (1990), as shown in Figure 3.9, except that the factor for the vertical linear load (P_2') is modified and adjusted. It was determined that the factor presented by Stöckl & Hofmann (1990) for the vertical linear load (P_2') caused a moment greater than that imposed by the horizontal load (P) and leads to overturning of the specimen. Therefore, in the case of Model 2, the factor (P_2') is modified as shown in Eq. (2) and in case of Model 1, the factor is adjusted to the different unit and joint sizes, as shown in Eq. (3).

$$P_2' = \frac{12\ cm * (12\ cm + 1.5\ cm) * 3}{(24\ cm)^2} * P \quad \textbf{(2)}$$

$$P_1' = \frac{6\ cm * (6\ cm + 1.0\ cm) * 3}{(19\ cm)^2} * P \quad \textbf{(3)}$$

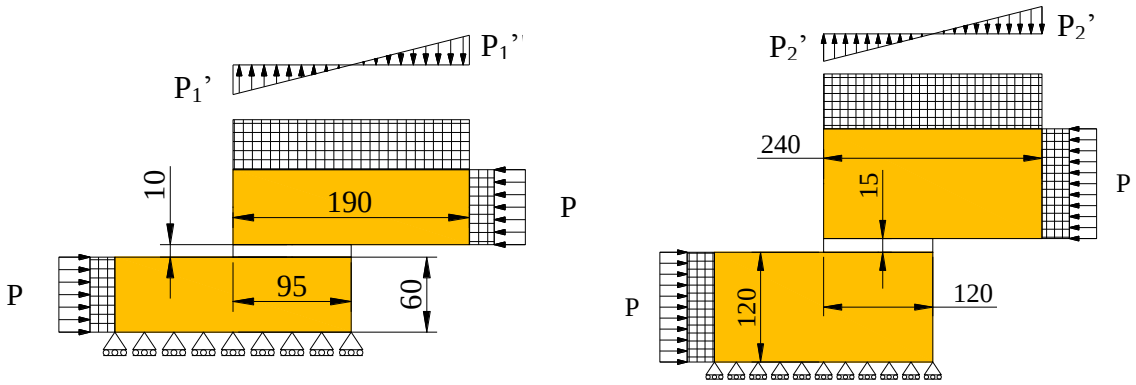

Figure 3.9: Hofmann and Stöckl Test - Model 1 (left), Model 2 (right)

Figure 3.10 presents the finite element models used for the analyses. In the two models shown, all nodes in the bottom are supported by rollers in the vertical direction, except the last one on the right hand side. This one is declared as a pin to ensure a stable system. Its reaction in the horizontal direction is equal to zero and has no effect on the stress distribution. The couplet itself is subjected to horizontal load as well as to vertical load. Both the vertical and horizontal loads are applied through a steel block. Except for the mortar joint in Model 1, square elements with a size of $5\,mm$ were used to mesh Models 1 and 2. For the mortar joint in Model 1 rectangular elements with a size of $3.\bar{3}\,x\,5\,mm$ $(H\,x\,L)$ were used. Thus, the units and joints are divided into $38\,x\,12$, $19\,x\,3$ and $38\,x\,12$ elements (Model 1) and $48\,x\,24$, $24\,x\,3$ and $48\,x\,24$ elements (Model 2), for the lower brick, joint, and upper brick, respectively.

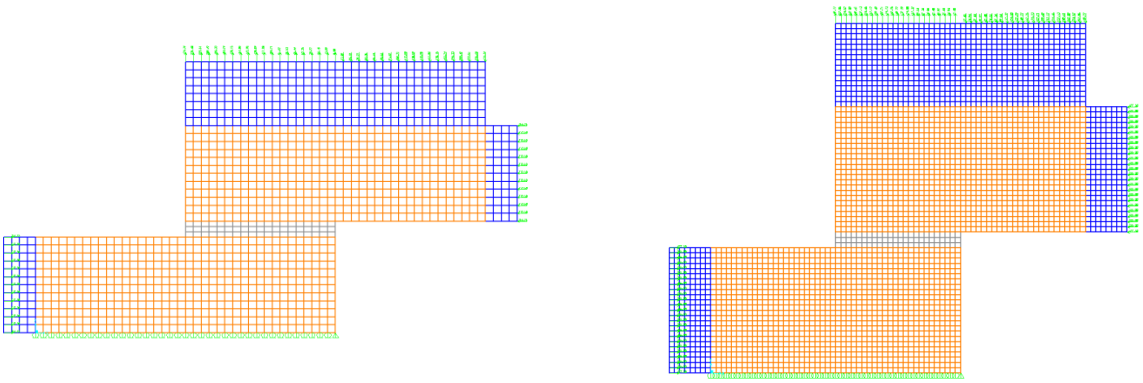

Figure 3.10: Case Study 1, FE models of Hofmann and Stöckl test- Model 1 (left), Model 2 (right)

The resulting distribution of normal stress in Figure 3.11 indicates that the normal tensile stress, induced in the bricks as well as in the mortar joint, results from the applied linear vertical load. Although the vertical load is applied through a steel block, because of the assumed perfect bond between the steel block and the bricks, the effect of the vertical load is transferred into the bricks and into the mortar joint, as shown in the encircled area in Figure 3.11. Therefore, it will be of interest to analyse a finite element model in which the bonds between the specimen and steel block are interrupted, as discussed in Section 3.3.2.1. The resulting distributions of shear stress are presented in Figure 3.12.

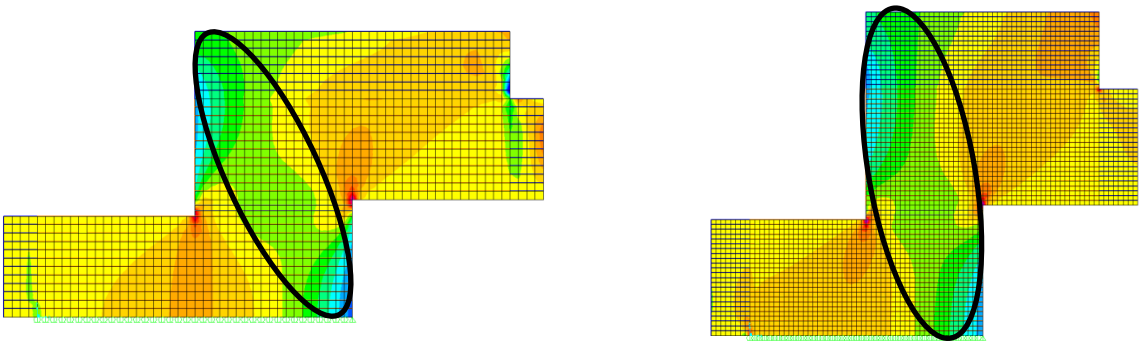

Figure 3.11: Case Study 1, normal stress distribution Model 1 (left), Model 2 (right)

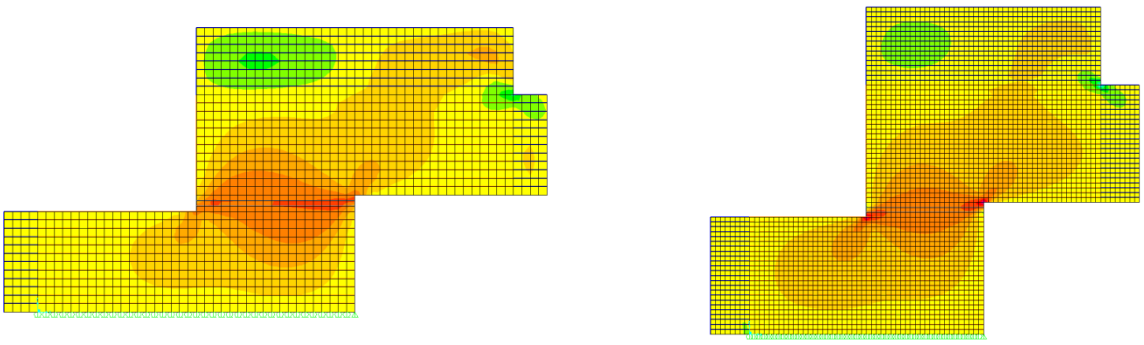

Figure 3.12: Case Study 1, shear stress distribution
Model 1 (left), Model 2 (right)

In Figure 3.13 and Figure 3.14, the magnitude of normal and shear stress at mid-height of the joint are illustrated along the length of the mortar bed joint in N/mm^2. As expected, the distributions of the shear and normal stresses in the Hofmann and Stöckl test are more uniform than in the triplet test. The different distributions of normal and shear stress in Models 1 and 2 indicate that the results of Hofmann & Stöckl test are affected by the unit size.

The results of Model 2 determined in the current analysis by using the modified factor for the vertical load, P_2', are identical to those obtained originally (Stöckl & Hofmann, 1990; Riddington, et al., 1997).

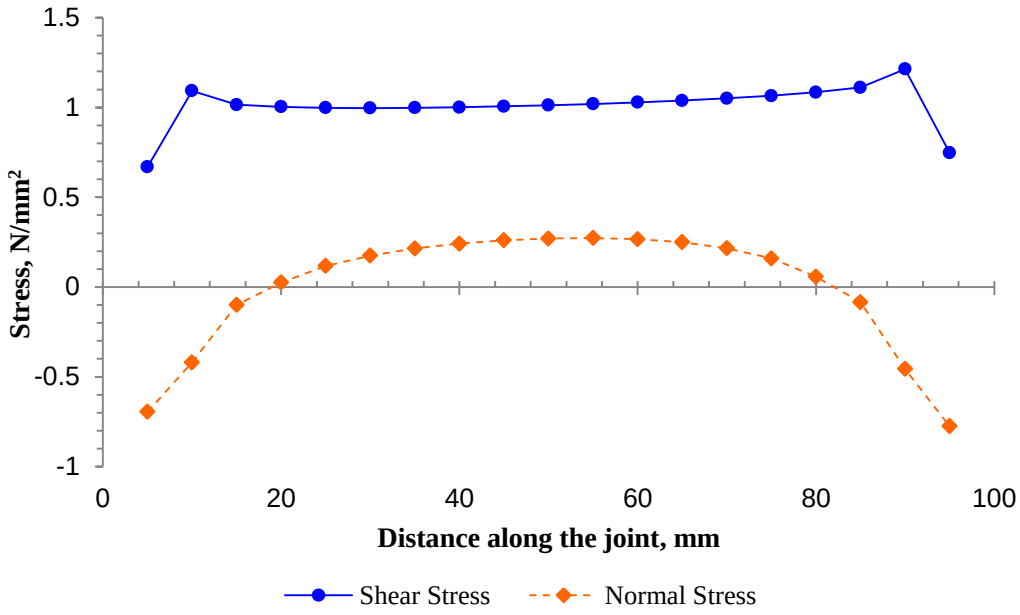

Figure 3.13: Case Study 1, stress distribution in the Hofmann and Stöckl test (Model 1)

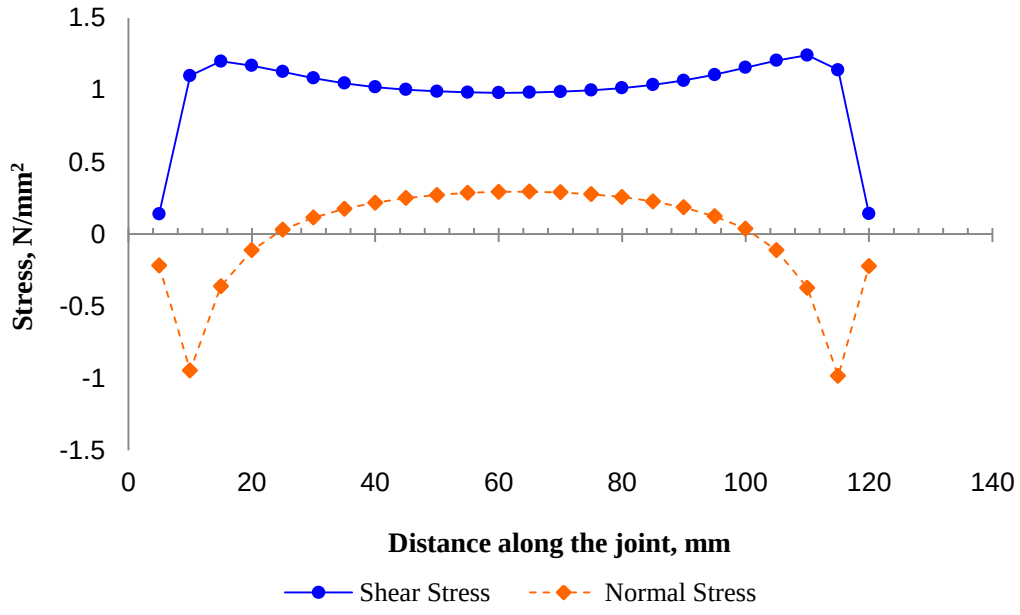

Figure 3.14: Case Study 1, stress distribution in the Hofmann and Stöckl test (Model 2)

3.3.1.3 Proposed Test Method

The proposed test method consists of one couplet bonded by a mortar joint over its entire length. Additional units are placed at the ends of the bricks, one at each end as shown in Figure 3.15. For the finite element model in Case Study 1, the bond between the two additional units and couplet is assumed to be perfect. As shown in Figure 3.15, the bricks are supported on their outer surface only in the vertical direction, and all nodes at the outer surface of the brick are supported by rollers except one at the bottom right, which is made a pin in order to ensure a stable system.

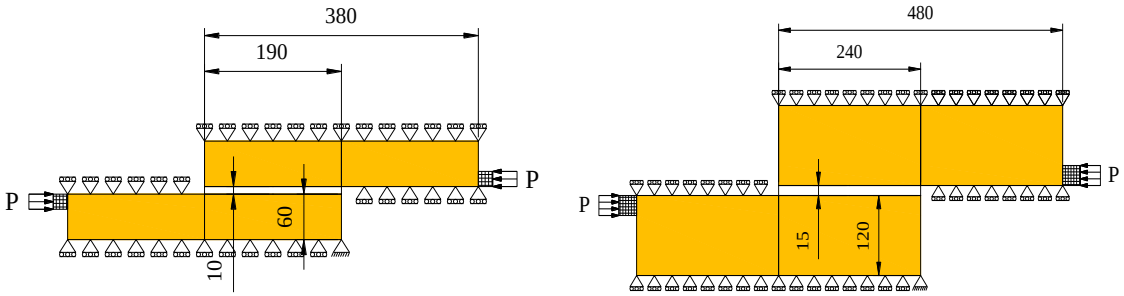

Figure 3.15: Case study 1, proposed test method- Model 1 (left), Model 2 (right)

The numerical analyses for the proposed test method are conducted in the same manner as for the triplet and Hofmann & Stöckl tests discussed above. The mesh pattern, for the lower brick, joint, and upper brick, consists of $76\,x\,12$, $38\,x\,3$ and $76\,x\,12$ elements (Model 1) and $96\,x\,24$, $48\,x\,3$ and $96\,x\,24$ elements (Model 2), respectively. Figure 3.16 shows the mesh and load arrangement of the finite element models. The horizontal load applied to both Models 1 and 2 should cause an average shear stress of $\tau = 1\,N/mm^2$ in the bed joint with respect to the cross sectional area of each mortar joint.

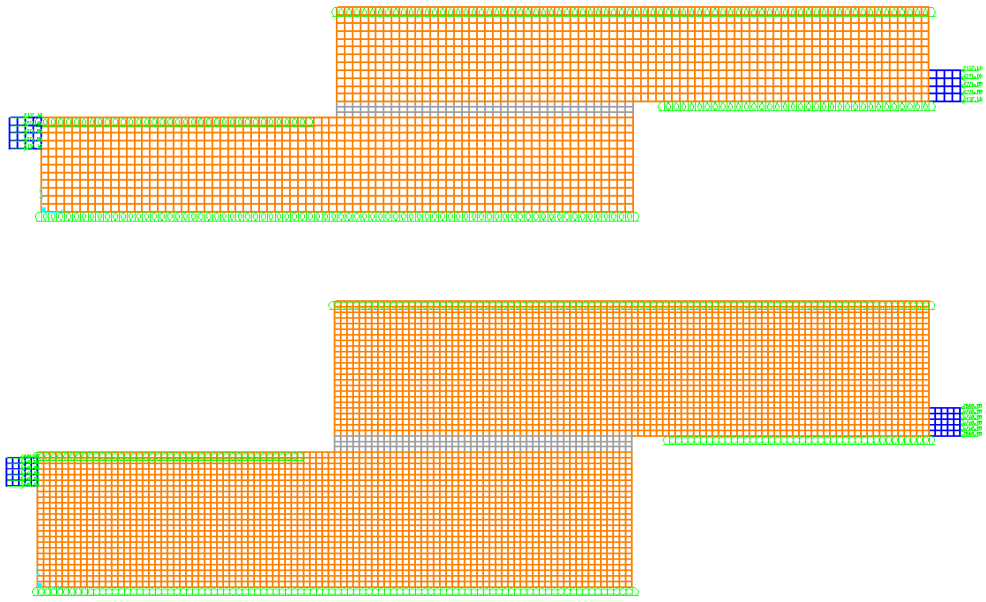

Figure 3.16: Case Study 1, finite element Model 1 and 2 of proposed test method

The distributions of normal and shear stress resulting from the finite element analyses are presented in Figure 3.17 and Figure 3.18. In the case of Model 1, the normal stress is distributed nearly uniformly over the entire mortar joint, and in the case of Model 2, the normal stress in the center of the mortar joint is close to zero. In both cases the normal and shear stresses are distributed symmetrically over the specimen.

In Figure 3.19 and Figure 3.20, the magnitudes of normal and shear stress at mid-height of the joint are illustrated along the length of the mortar joint in N/mm^2. The results indicate a nearly uniform shear stress along the bed joint, especially in Model 2, which has units of the same dimension as the Hofmann & Stöckl test. Further, in Model 2, the shear stress reflects a nearly constant value at the intended level of $\tau = 1\,N/mm^2$. Even though no external compression stress was applied to the system, the normal stress along the bed joint is only a normal compressive stress, unlike in the triplet and Hofmann & Stöckl tests where the mortar joint is subjected to both normal compressive and normal

tensile stresses. Compared to the Hofmann & Stöckl test, the proposed test method is able to produce similar distributions of normal and shear stresses along the mortar bed joint.

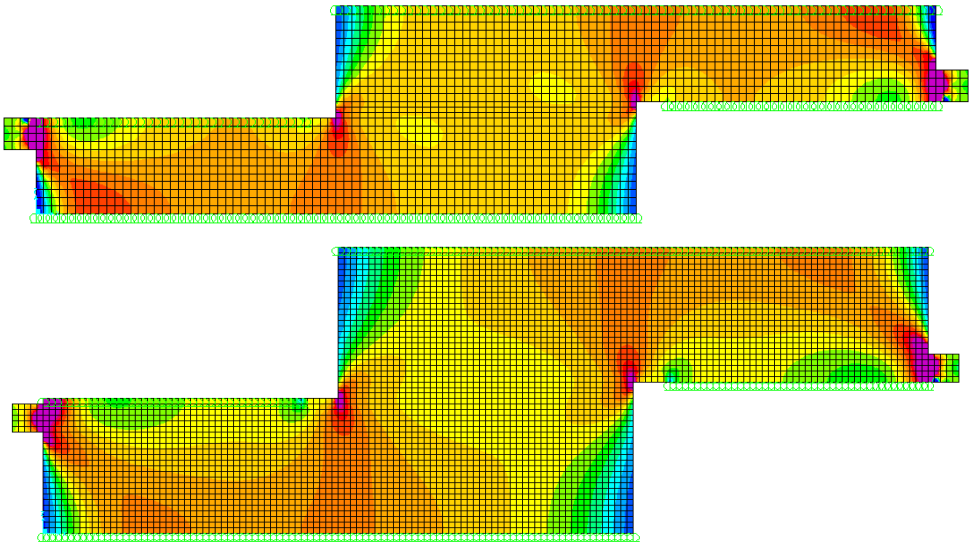

Figure 3.17: Case Study 1, normal stress distribution – Model 1 (top) and 2 (bottom)

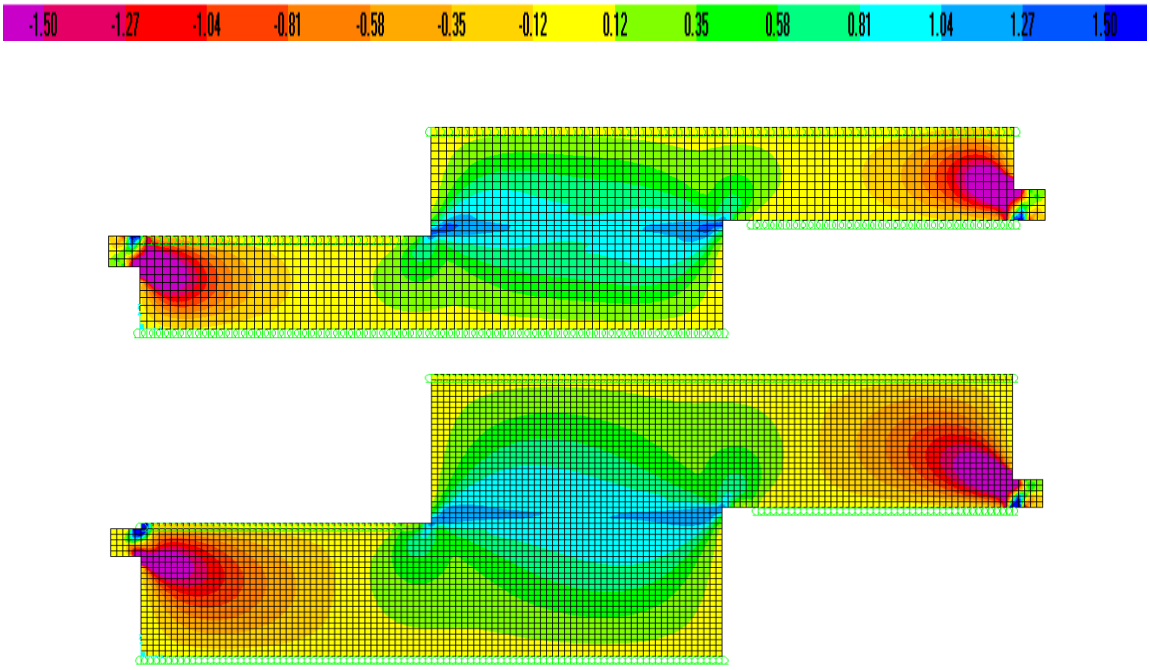

Figure 3.18: Case Study 1, shear stress distribution – Model 1 (top) and 2 (bottom)

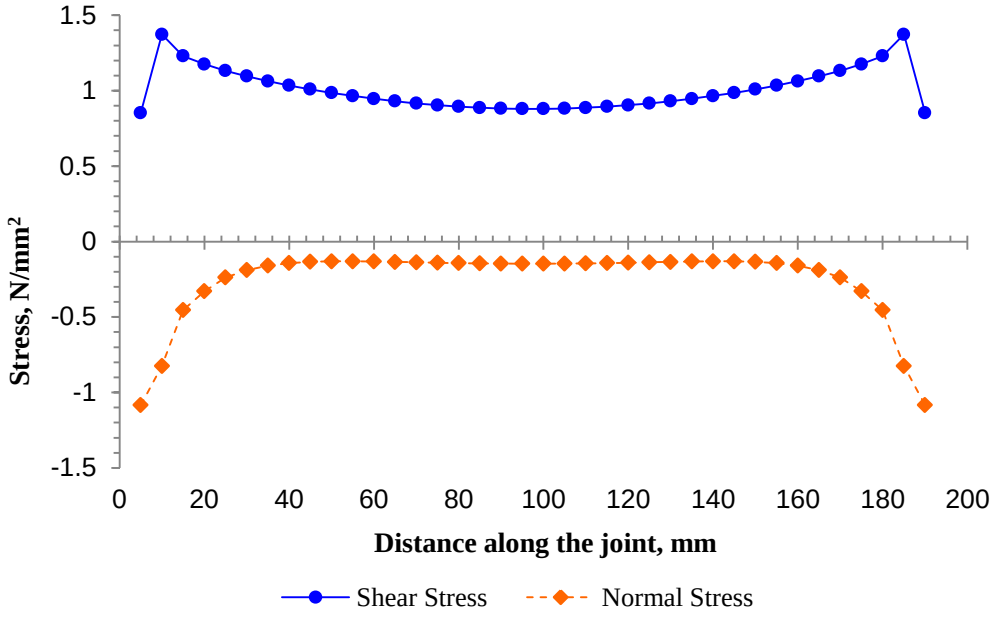

Figure 3.19: Case Study 1, stress distribution in the proposed test method (Model 1)

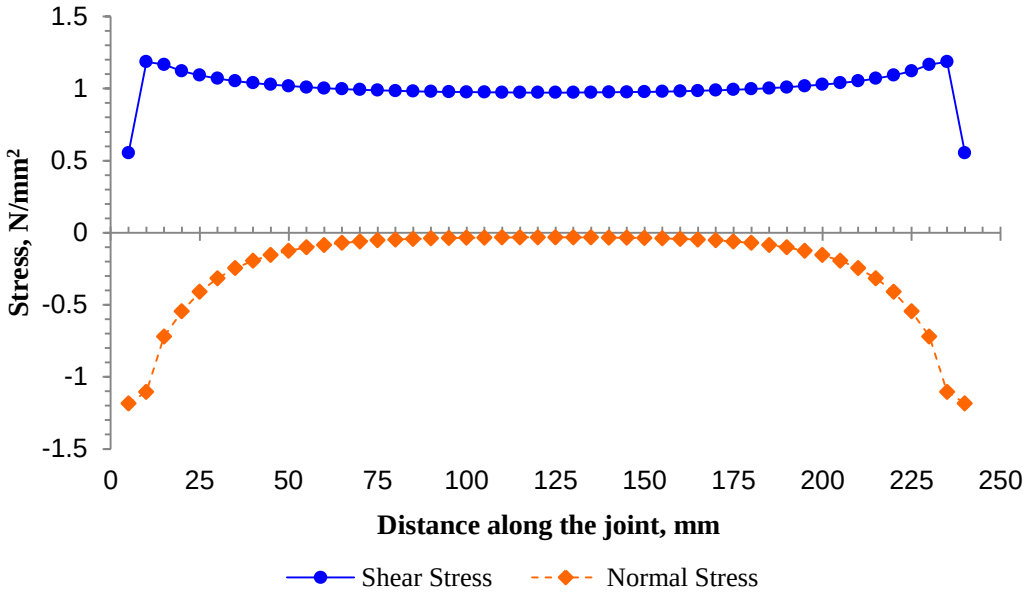

Figure 3.20: Case Study 1, stress distribution in the proposed test method (Model 2)

The difference between Models 1 and 2 in the distributions of normal and shear stresses reveals that the results of the proposed test method are affected by the dimensions of the units. Therefore, three additional analyses using Models 3, 4 and 5 were conducted. In the first additional analysis (Model 3), the dimension of the brick is modified to $190\ x\ 95\ x\ 90\ mm$ $(L\ x\ H\ x\ W)$, in order to study the effect of aspect ratio (height/length) of the brick. In the second additional analysis (Model 4), the original specimen used by Hofmann & Stöckl is subjected to the boundary conditions of the proposed test method, and in the third additional model (Model 5), the dimensions of the specimen of Model 4 are modified from $240\ x\ 120\ x\ 120\ mm$ to $190\ x\ 60\ x\ 90\ mm$. The latter two analyses, Models 4 and 5, are carried out to determine the response of the proposed test method to different shapes of specimen and different slopes of the theoretical load path between the two points of load application. All three additional finite element analyses were performed similarly to the previous ones, and the additional finite element models were meshed, for the lower brick, joint, and upper brick, with $76\ x\ 19$, $38\ x\ 3$ and $76\ x\ 19$ elements (Model 3), $48\ x\ 24$, $24\ x\ 3$ and $48\ x\ 24$ elements (Model 4) and $38\ x\ 12$, $19\ x\ 3$ and $38\ x\ 12$ elements (Model 5), respectively. A square mesh size of $5\ mm$ was used for the bricks and mortar in case of Model 4, and a rectangular mesh size of $3.\overline{3}\ x\ 5\ mm$ was used in the case of Models 3 and 5.

The analyses using Models 3, 4 and 5, for the proposed test method, were performed with varied points of load application. From these analyses, it was noticed that the change in the theoretical slope of the load path between the two points of load application did not have a significant effect on the distribution of normal and shear

stresses. However, the change in the aspect ratio of the brick affects the results, as can be seen by comparing Model 1 and 3 in Figure 3.21. Further, it was noticed that despite the different length of mortar joint, the results for the proposed test method and a particular unit aspect ratio are constant. For example, the height to length ratio of the units utilized in Model 2 $(240\ x\ 120\ x\ 120)$ as well as in Model 3 $(190\ x\ 95\ x\ 90)$ is equal to 2. The distribution of normal and shear stresses in both cases are exactly the same, as seen in Figure 3.22.

Comparison of the original Hofmann & Stöckl test (Model 2) analyses to the proposed test method in Model 4 shows that the proposed test method is capable of producing similar, if not better, results. The distribution of shear stress, as shown in Figure 3.23, is identical to the one produced in Model 2 of the Hofmann & Stöckl test. The normal stress along the mortar joint in Model 4 is offset such that the mortar joint is subjected only to normal compressive stress. However, the distribution is similar to the one produced in Model 2 of the Hofmann & Stöckl test. Comparison of the results from the Hofmann & Stöckl test with modified unit size (Model 1), to the results of Model 5, are shown in Figure 3.24. Again, it is clear that the proposed test method is capable of producing results at least as good as the Hofmann & Stöckl test.

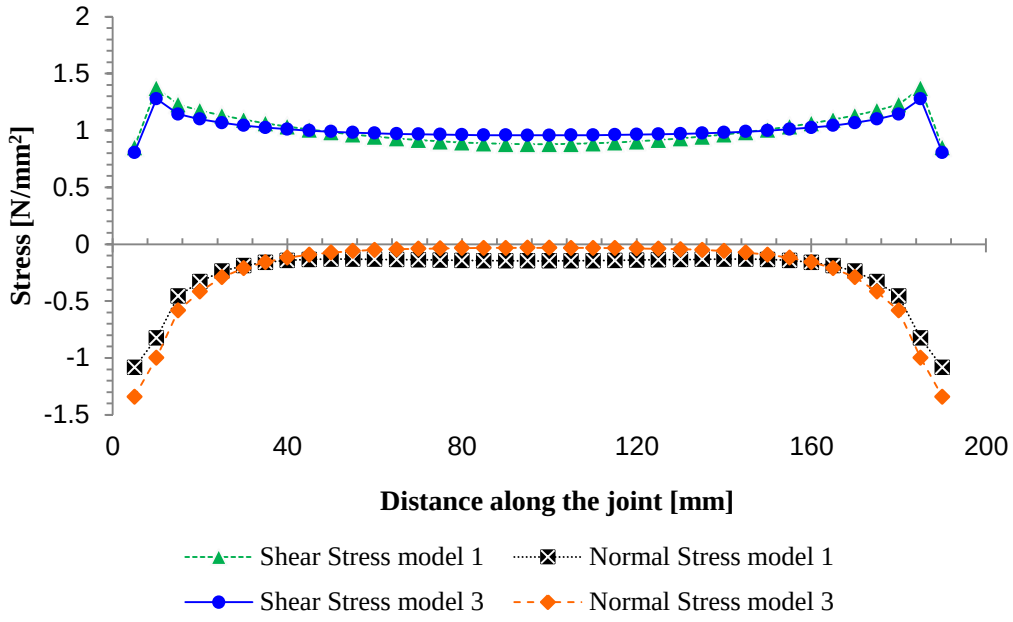

Figure 3.21: Case Study 1, stress distribution along the mortar bed joint in the proposed test method (Model 1 vs. 3)

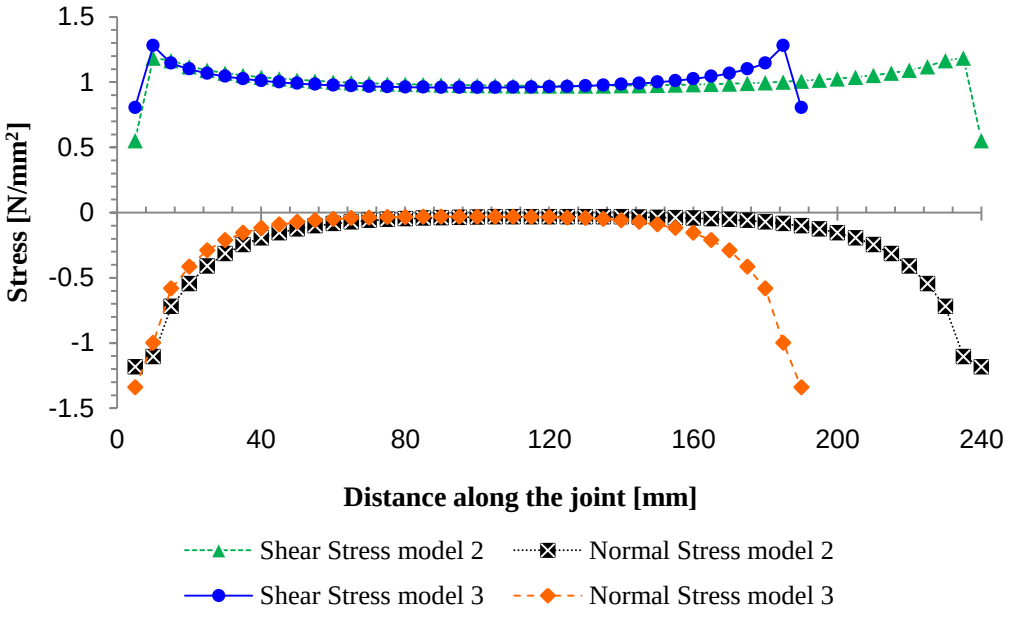

Figure 3.22: Case Study 1, stress distribution along the mortar bed joint in the proposed test method (Model 2 vs. 3)

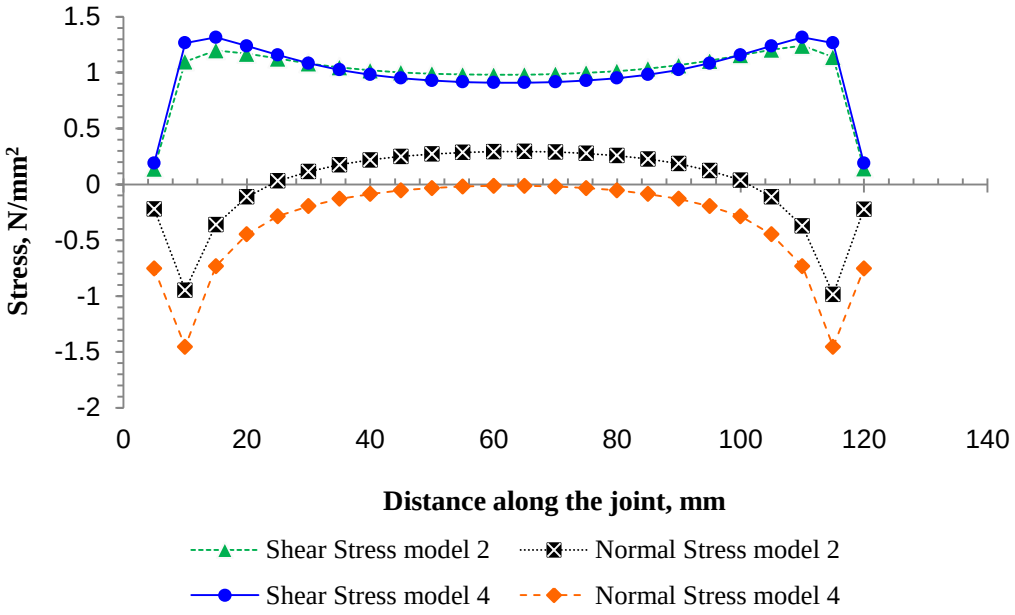

Figure 3.23: Case Study 1, stress distribution along the mortar bed joint, proposed method (Model 4) vs. Hofmann & Stöckl (Model 2)

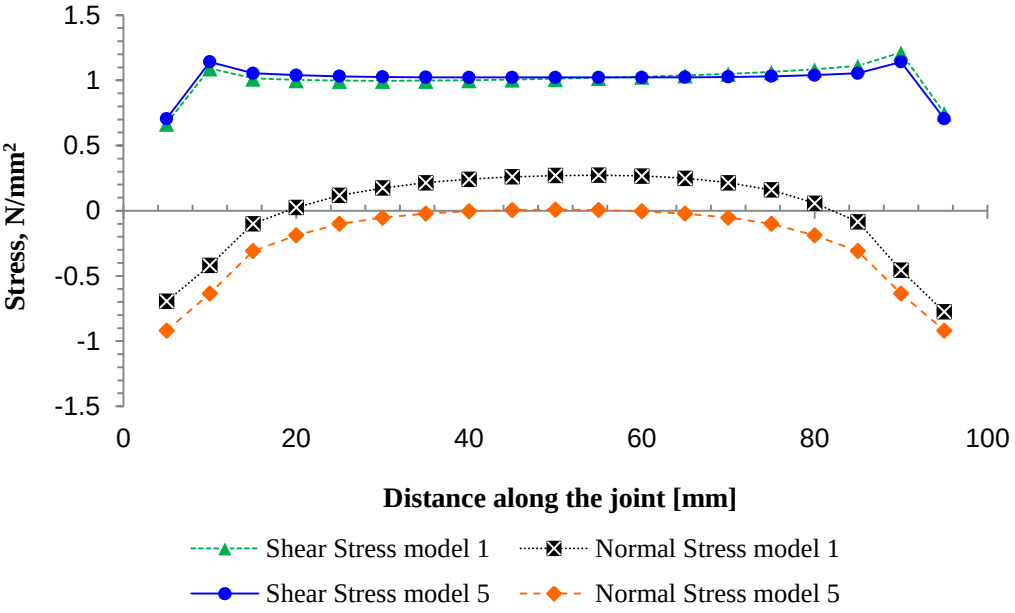

Figure 3.24: Case Study 1, stress distribution along the mortar bed joint, proposed method (Model 5) vs. Hofmann & Stöckl (Model 1)

3.3.2 Case Study 2

In Case Study 1, the proposed test method was compared with the triplet and the Hofmann & Stöckl tests by assuming a perfect bond between the specimen and the steel plates. Here, in Case Study 2, contact elements (GAP-elements) are placed between the specimen and the steel plates, as shown in Figure 3.26 and Figure 3.30, to assure more realistic conditions. The GAP-elements are only able to resist a vertical compressive force, and provide zero resistance against a vertical tensile force. The GAP-elements are used to ensure that the results of normal tension stress along the bed joint for the Hofmann & Stöckl test, as presented in Stöckl & Hofmann (1990) and Riddington, et al. (1997), are not a result of missing contact elements between the specimen and steel plates. However in both case studies, no interface elements or GAP-elements were placed between the units and mortar bed joint, since it was irrelevant for the purpose of the study. In addition to GAP-elements, the condition for the vertically applied load (Section 3.3.1.2) in the Hofmann and Stöckl Test3.3.2.1, was modified as well (see Section 3.3.2.1). Furthermore, in Case Study 2 the results for shear and normal stress distribution along the interface are presented in addition to the results along the mid-height of the joint. The stress distributions along the mid-height of the joint are presented for the sake of comparison with the results obtained in Case Study 1, and the results along the joint interface are presented to gain insight into the state of stress along the interface, where failure usually occurs in practice.

The results from Case Study 1 showed that the proposed test method produces better results than the triplet test, and similar results to the Hofmann & Stöckl test.

Therefore in Case Study 2, the proposed test method is compared only to the Hofmann & Stöckl test. Further, Case Study 2 is only conducted with Model 1 for the proposed test method and with Model 2 for the Hofmann & Stöckl test.

3.3.2.1 Hofmann and Stöckl Test

For the finite element analyses, the mortar bed joint is subjected to a shear stress of 1 N/mm^2, which requires a horizontal load of $F = 14400\ N$ with respect to the cross-sectional area of the mortar joint. The corresponding moment induced in the specimen is $M_H = 1944000\ Nmm$. Knowing that $M_H = M_V$, and combined with the assumption that the vertical loads, V_1 and V_2, are applied as shown in Figure 3.8, allows calculation of the required vertical loads for the above mentioned horizontal load, F. In Figure 3.25, the vertical loads, V_1 and V_2, as well as the corresponding resultant force, V, are presented for different lever arms b'. It is quite evident that the greater the lever arm between V_1 and V_2, the lower the required vertical loads to compensate for the moment due to horizontal load, and also, the lower the compressive stress along the mortar bed joint. Therefore, for the current finite element analyses, the maximum lever arm $b' = 360\ mm$, or $b = 180\ mm$, is assumed. In so doing, the required vertical loads are $V_1 = 4606\ N$ and $V_2 = 794\ N$, and the corresponding resultant force $V = 5400\ N$.

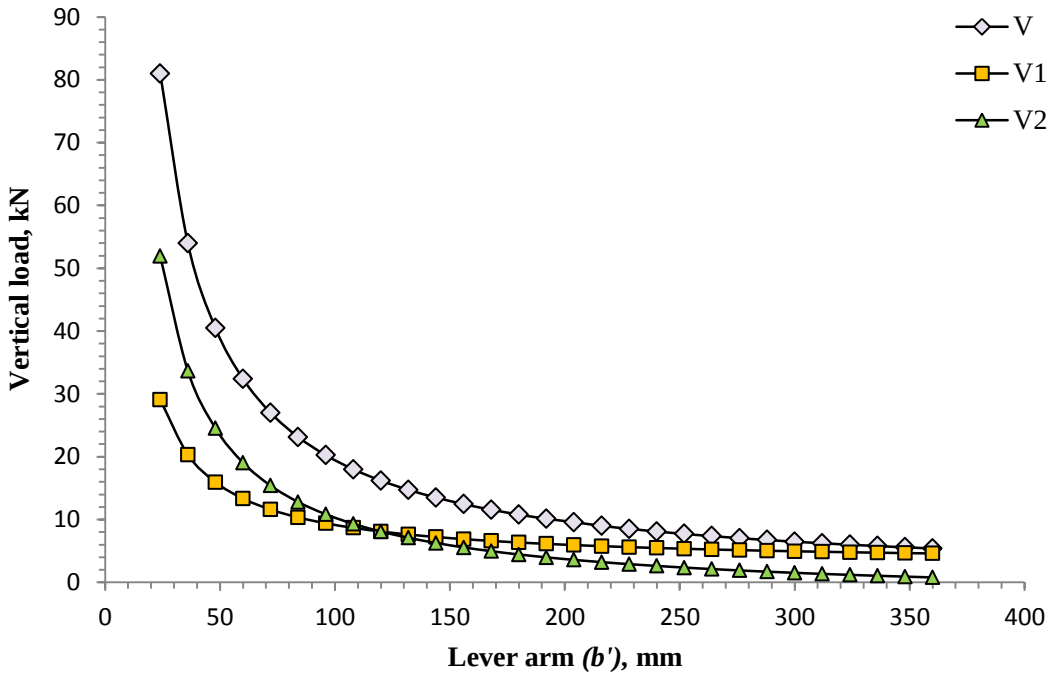

Figure 3.25: Vertical loads and the corresponding lever arms

The finite element model of Case Study 2 for the Hofmann & Stöckl test is presented in Figure 3.26. As mentioned above, the interface between the bricks and the steel plates are defined by using GAP-elements. The lower brick of the couplet is supported in the vertical direction by using rollers, but in combination with the GAP-elements the rollers provide only resistance against the compressive force. Further, the support of the upper brick on the left hand side, in combination with the GAP-elements, provides resistance only against a compressive horizontal force.

In Figure 3.26, the deflected shape of the finite element model is presented. It shows that the I-section, used to apply the vertical loads, lifts up on the right hand side from its original position by about $1.6\,mm$. If the interface between the specimen and steel plates was not defined by the GAP-elements, the specimen, as well as the mortar

joint would be subjected to a normal tensile stress due to this deformation. However, in Case Study 2 the specimen and the steel plates are separated by using GAP-elements, therefore no tensile stress is induced to the specimen, see Figure 3.27. The circled area in Figure 3.27 indicates the state of stress due to the resultant vertical force couple, V, which creates the compensating moment. The distribution of shear stress, also shown in Figure 3.27, is similar to the distribution of shear stress in Case Study 1. This similarity between Case Study 1 and 2 indicates that the use of GAP-elements and differently applied vertical load has no effect on the distribution of shear stress. The results of normal and shear stresses at mid-height of the joint are shown in Figure 3.28. In comparison to the results of Case Study 1, only a short length of the mortar joint is subjected to a normal tensile stress with a maximum of $0.023\ N/mm^2$ which is $92\ \%$ less than the level of normal tensile stress in Case Study 1. The shear stress along the bed joint also varies less than in Case Study 1, but unlike Case Study 1, the distributions of normal and shear stresses are asymmetrical. In Figure 3.29, the shear and normal stress distributions along the interface are presented. The shear stress distribution along the interface is more uniform than at the mid-height of the joint. The distribution of the normal compressive stress along the interface is non-uniform. The higher negative value for the normal compressive stress on the left hand side and the positive value on the right hand side, are a result of the deflection of the upper brick. The upper brick is pushed down due to the vertical resultant force at the upper left. Thereby, it causes a stress concentration at the upper left edge of the mortar joint, and tensile stress at the upper right edge of the mortar joint. However, Case Study 2 indicates that the level of normal tensile stress along the

mortar joint, at the mid-height as well as at the interface, is not as high as reported in the literature.

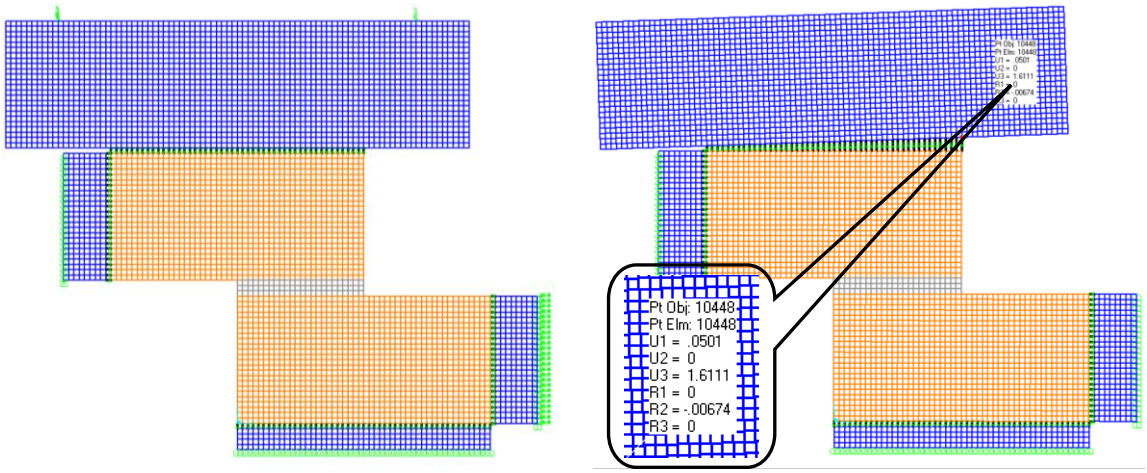

Figure 3.26: Case Study 2, finite element model and the corresponding deflected shape of Hofmann & Stöckl test

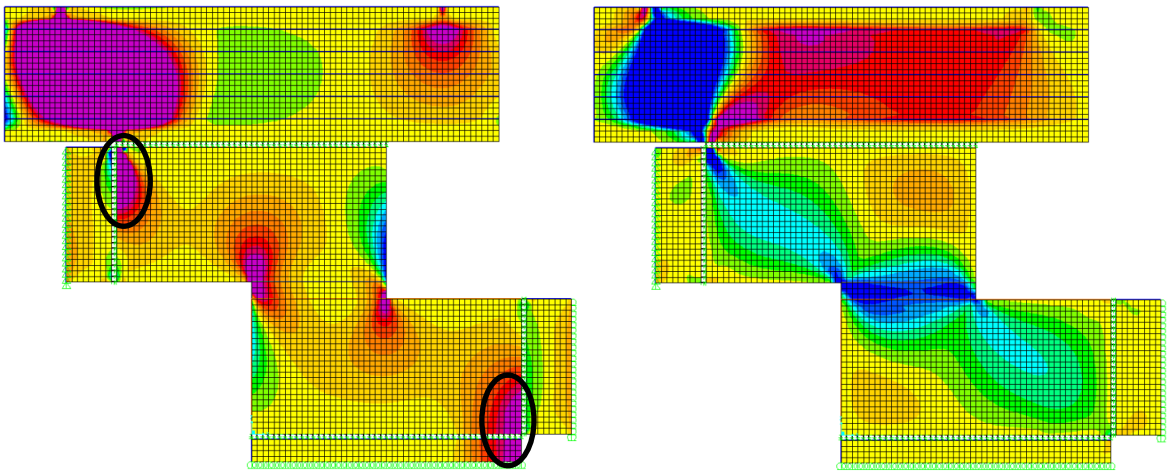

Figure 3.27: Case Study 2, normal and shear stress distribution, Hofmann & Stöckl test

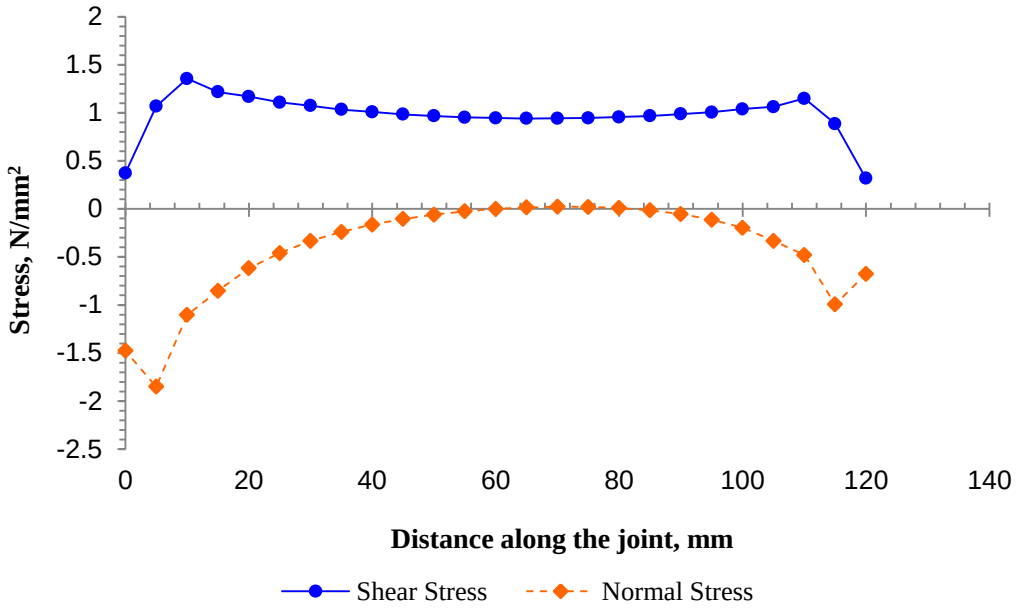

Figure 3.28: Case Study 2, stress distribution along the mortar bed joint at the mid-height, Hofmann & Stöckl Test (Model 2)

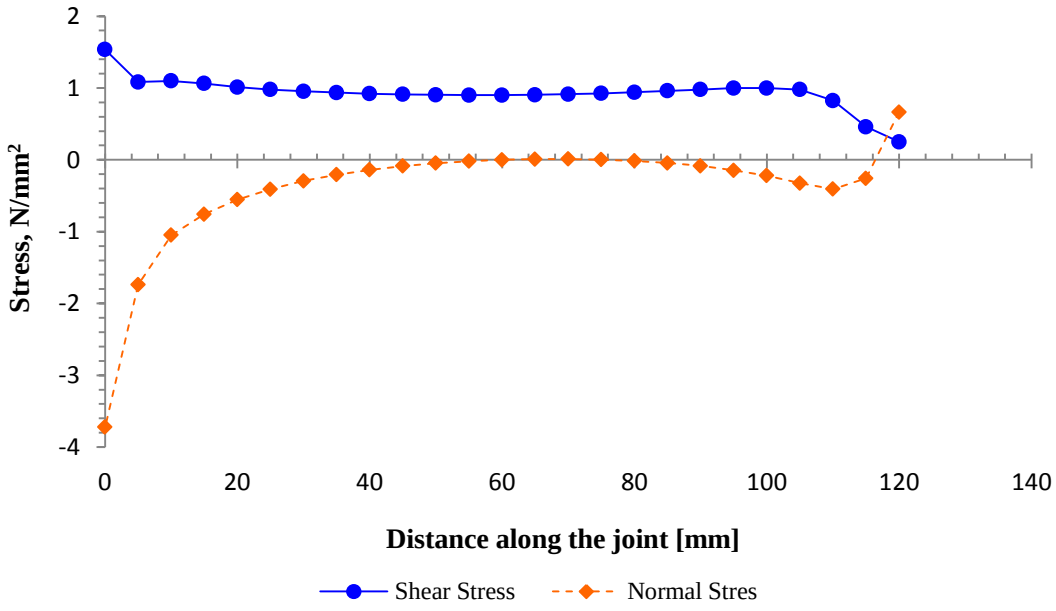

Figure 3.29: Case Study 2, stress distribution along the mortar bed joint at the interface, Hofmann & Stöckl Test (Model 2)

3.3.2.2 Proposed Test Method

In Case Study 2, the finite element model of the proposed test is modified by using GAP-elements and steel plates of thickness $t = 10\,mm$, as shown in Figure 3.30. The steel plates are placed on the top and bottom of the bricks, and are supported in the vertical direction by means of rollers. The interface between the bricks and steel plates are defined by using GAP-elements. GAP-elements are also placed in the head joints between the specimen (the couplet) and the additional bricks that are placed at the opposite ends of the couplet. On the left hand side, the horizontal load is applied to the brick through a steel block, and on the right hand side, the brick is supported against the horizontal movement by a steel block. Both steel blocks have dimensions of $20\ x\ 20\ x\ 90\ mm\ (L\ x\ H\ x\ W)$.

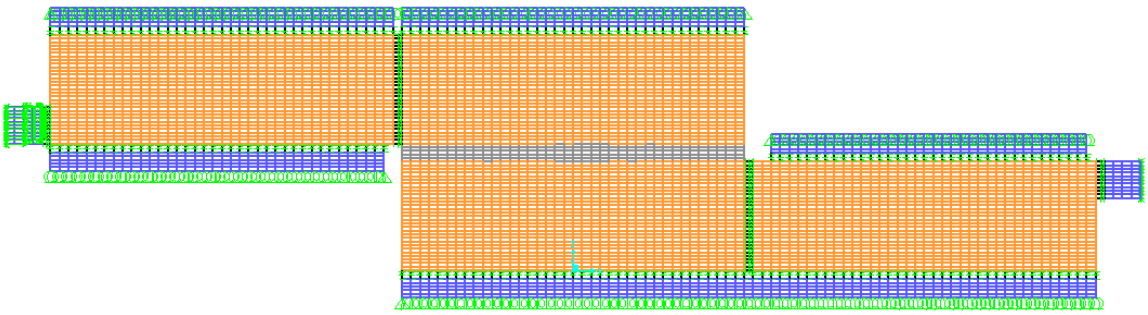

Figure 3.30: Case Study 2 - Finite element model of the proposed test method

The distribution of normal stress in Figure 3.31 shows a concentration of normal stress at the top left and bottom right of the couplet (circled area). These normal stress concentrations result from the steel plates that are supported in the vertical direction preventing overturning of the couplet. The resultants of the reacting forces form a couple which generates a compensating moment opposing the one induced in the specimen by

the horizontal load. A similar reaction is achieved in the Hofmann & Stöckl test by using complex equipment.

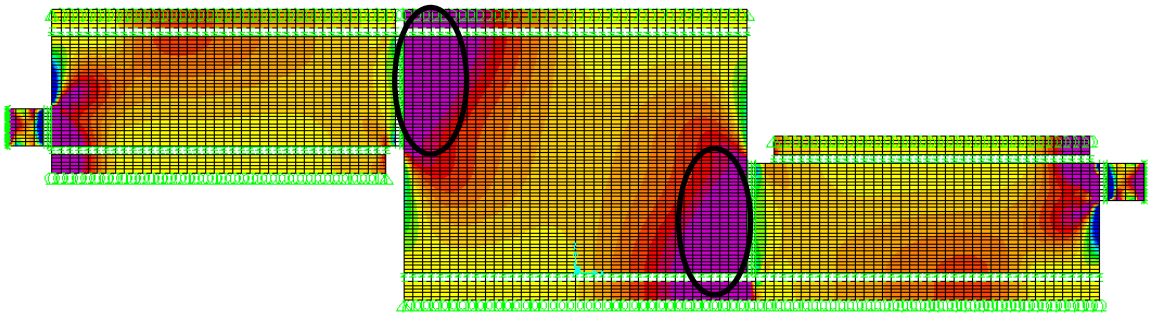

Figure 3.31: Case Study 2-Normal stress distribution of the proposed test method

Figure 3.32 illustrates the state of shear stress in the couplet. It indicates that the distribution of shear stress is concentrated around the joint, especially in the center of the couplet. This concentration of shear stress could cause a failure in the middle of the mortar joint, far away from the edges. Further, it shows that the mortar joint is subjected to a nearly constant shear stress which means that most of the joint will be close to failure.

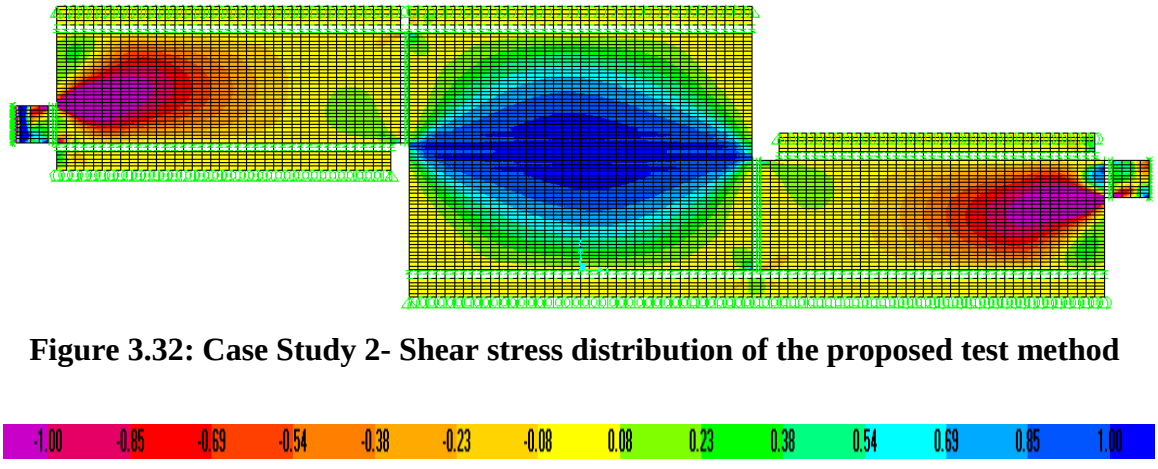

Figure 3.32: Case Study 2- Shear stress distribution of the proposed test method

The resulting stress distributions at mid-height of the joint are presented in Figure 3.33. In contrast with the Hofmann & Stöckl test, the first thing to note is that the normal stress as well as the shear stress is distributed symmetrically along the mortar joint. Further, 90% of the mortar joint is subjected to a nearly uniform shear stress, and the value of the shear stress is the intended level of $\tau = 1\,N/mm^2$. The distribution of normal stress deviates along the mortar joint which is a result of the eccentrically applied horizontal load with respect to mid-height of the joint. As long as the horizontal load is induced to the specimen eccentrically, achieving uniformly distributed normal stress will remain a challenge, because the eccentricity produces a moment. However, in comparison to the Hofmann & Stöckl test, no tensile stress is imposed to the mortar joint, and the variability of the normal stress is reduced, as shown in Figure 3.34. Further, in Figure 3.35 the stress distributions along the mortar joint at the interface are presented. The results obtained indicate more uniform stress distributions than the Hofmann & Stöckl test.

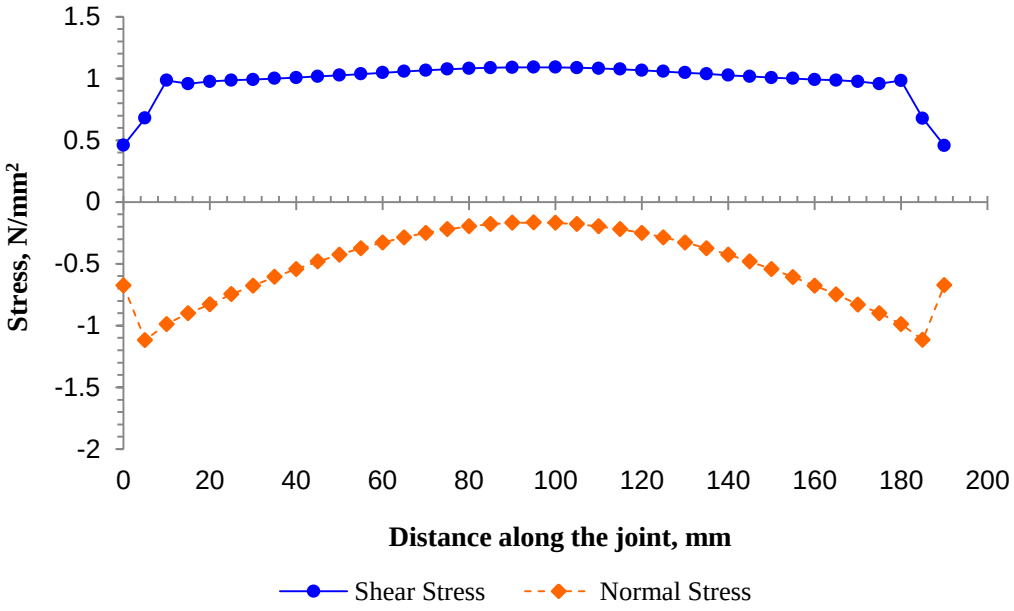

Figure 3.33: Case Study 2, stress distribution along the mortar bed joint at the mid-height, proposed test method (Model 1)

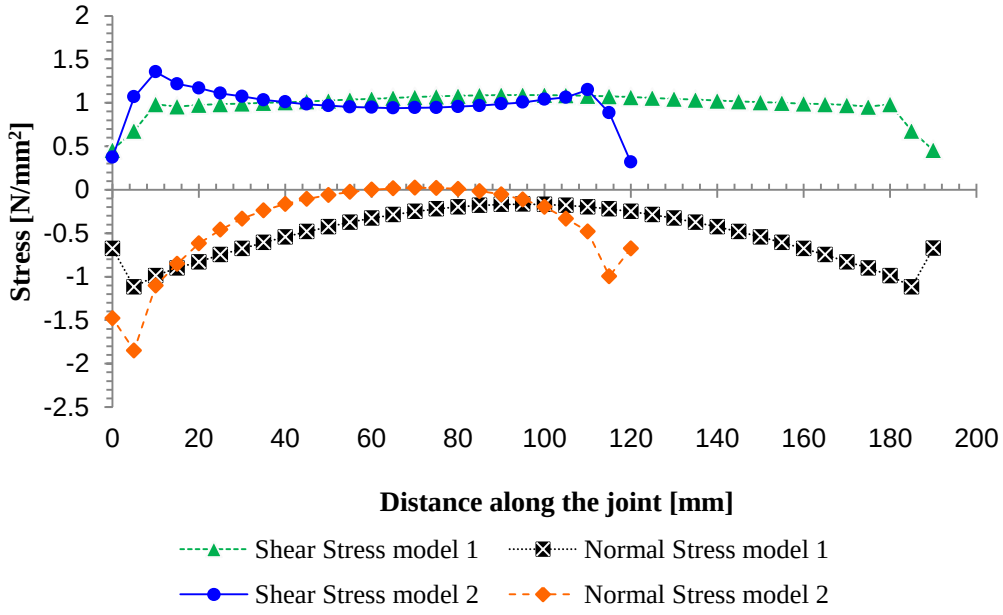

Figure 3.34: Case Study 2, stress distribution along the mortar bed joint, Proposed Method (Model 1) vs Hofmann & Stöckl (Model 2)

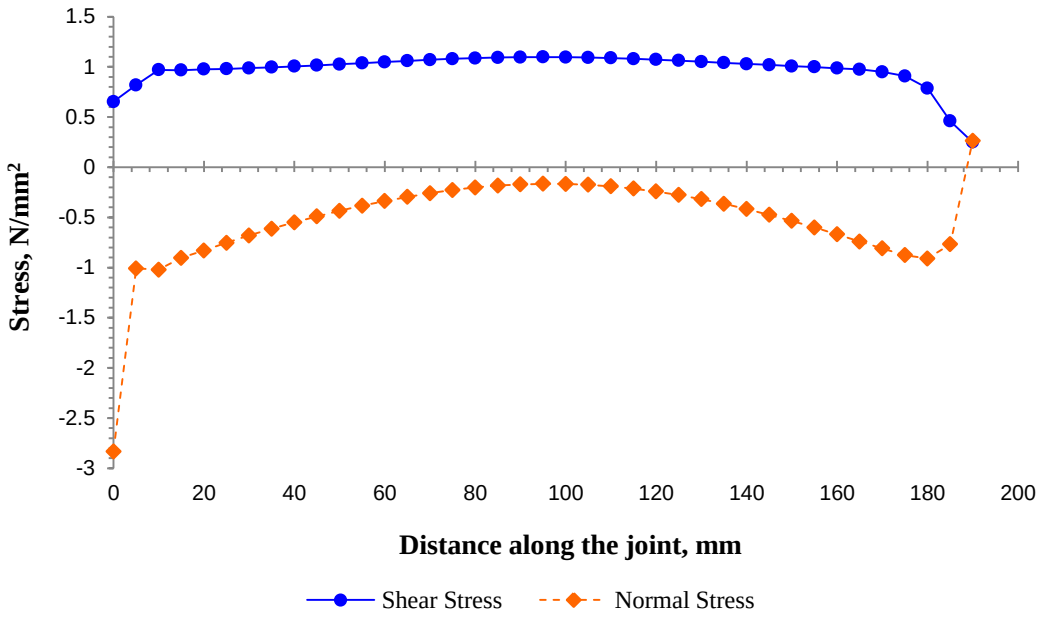

Figure 3.35: Case Study 2, stress distribution along the mortar bed joint at the interface, proposed test method (Model 1)

3.4 Summary

In this chapter the proposed test method was compared with the triplet and Hofmann & Stöckl tests using numerical analyses. Different boundary conditions, Case Study 1 and 2, were considered to compare the state of stress distribution along the mortar bed joint in each test method. In Case Study 1, no contact elements (GAP-elements) were placed between the specimen and the steel plates. In Case Study 2, the interface between the bricks and steel plates were defined by using GAP-elements. In both cases, however, a perfect bond was assumed between the mortar joint and the bricks. The numerical analyses were conducted by modeling a two-dimensional finite element model in SAP2000 version 14. The results obtained were based on assumed linear stress-strain behaviour of material. The applied horizontal load, in each case, was determined

with respect to the bed joint area of each specimen to produce an average shear stress of $\tau = 1\ N/mm^2$.

Based on the numerical evaluations, it can be concluded that the proposed test method is capable of producing desirable results for nearly uniform shear stress in a mortar joint. Compared to the triplet test, the resulting distributions of normal and shear stress in the proposed test method are more uniform, and are based only on one mortar joint, rather than two as in the triplet test. Further, unlike the case of the triplet test, no tensile stress is induced in the bed joint. Compared to the Hofmann & Stöckl test, the distribution of shear stress in the proposed test method is similar; however, the mortar bed joint is subjected only to normal compressive stress. In Case Study 2, however, it was demonstrated that by using GAP-elements and differently applied vertical load, the magnitude of the normal tensile stress in the Hofmann & Stöckl test is not as high as that reported in the literature.

By using units of different dimensions in the numerical analyses, it was shown that the results of the Hofmann & Stöckl test as well as the proposed test method are affected by the length to height ratio of the bricks.

CHAPTER 4: **EXPERIMENTAL STUDY**

4.1 Introduction

The purpose of the numerical evaluation, described in Chapter 3, was to gain insight into the state of stresses imposed in the mortar bed joint and to compare the proposed test method with the existing triplet and Hofmann & Stöckl tests. The evaluation conducted indicates that the proposed test method provides more uniform distribution for normal and shear stress along the mortar bed joint than the triplet test and similar results to the Hofmann & Stöckl test.

This chapter provides a detailed description of the proposed test method utilized for the experimental program, which was intended to verify the results of the numerical analyses in terms of the state of stress induced in the joint. A description of the materials, the specimens, and the equipment used for measuring purposes as well as the experimental program itself is provided here.

4.2 Experimental Program

The purpose of the experimental program was to:

1. Investigate the level of normal and shear stresses induced in the specimen using the proposed test method.

2. Investigate the consistency of the results obtained using the proposed test method.

The experimental program was conducted using couplet specimens, constructed using two bricks in stack bond. The specimens were constructed using two types of brick and one type of mortar. Each combination of brick and mortar was used to produce 25 specimens. During the test procedure, each specimen was subjected to a horizontal load and to one of the predefined levels of normal compressive stress. In total, four different levels of pre-compressive stress were combined with the applied horizontal load; and each combination was tested with five repetitions. Twenty specimens of each combination were used to investigate the reproducibility of the results using the new test arrangement. The remaining five specimens of each combination were used in combination with a digital imaging measurement system to investigate the level of stresses induced in the specimens in the new test method.

4.3 Development of the Proposed Test Method

The proposed test method is the result of an attempt to combine the advantages of two existing test methods, namely: the triplet and the Hofmann & Stöckl test. In order to do so, the proposed test method should utilize simple equipment as in the triplet test, and it should provide results as good as the Hofmann & Stöckl test (i.e. uniform stresses in the joint). To fulfill the objectives, a test setup was devised and analyzed by using the finite element method. The initial numerical analyses of the first test arrangement and the corresponding results were presented in Popal & Lissel (2010). The first version of the proposed test arrangement is shown in Figure 4.1.

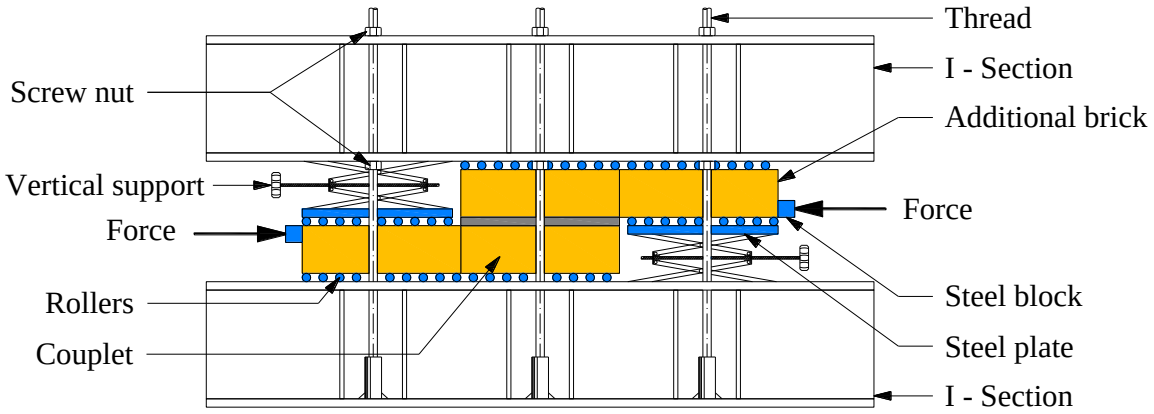

Figure 4.1: First Version of the Proposed Test Arrangement (Popal & Lissel, 2010)

Here, in the first version of the test arrangement, the couplet is placed between two sets of rollers which are in turn supported by the beams placed on the top and bottom of the couplet. The two beams can be moved relative to each other by using the threaded rods and screw nuts. The rollers are used to minimize the friction between the bricks and the beam surfaces as well as to distribute the normal compressive force as uniformly as possible. The lower beam provides a plane level surface for the rollers and the upper beam provides support to the couplet in the vertical direction as well as allows the application of normal compressive stress, if desired. If it is desired to avoid any compressive stress normal to the specimen, i.e. if the test is to be conducted without any pre-compression, the weight of the upper beam can be supported by using the six screw nuts (3 on each side), arranged at the bottom of the upper beam. Otherwise, the nuts at the bottom may be loosened and the pre-compression can be applied by means of torque using the six screw nuts arranged at the top of the beam combined with the arranged threaded rods (turn-of-nut method). It was intended to weld the threaded rods to the lower flange of the bottom beam with holes in the upper flange of the bottom beam as well as in the lower and upper flanges of the top beam.

The horizontal force would be applied to the couplet by means of two hydraulic jacks via the steel block and the additional brick units that are placed between the hydraulic jacks and the couplet on each side. The additional bricks are intended to avoid load concentration in the couplet and reduce the angle of the load path thereby reducing the variation in stress along the joint. In order to ensure an absolutely horizontal movement of the two additional brick units, the brick on the left hand side is supported in the vertical direction on the top and the brick on the right hand side at the bottom with the apparatus as shown in Figure 4.1. As in the case of the couplet, the friction between the brick units and the supporting apparatus is minimized by using rollers.

During the initial phase of the testing program, it was determined that application of the normal compressive stress by means of torque, using the threaded rods combined with the screw nuts, is very arduous and time intensive. Further, due to the uneven surface of the bricks, the rollers in contact with the surface of the brick would cause load concentrations which could lead to brick failure. In addition, smooth movement of the rollers in the horizontal direction was inhibited which affects the magnitude of the applied horizontal load. The top and bottom steel beams also did not provide the perfectly plane, level surface assumed for the roller and application of the shearing force using two hydraulic jacks is also more complex than desired. Therefore, modifications to the test arrangement were made resulting in version two. A schematic sketch of the modified version is shown in Figure 4.2. Figure 4.3 shows the test setup as constructed.

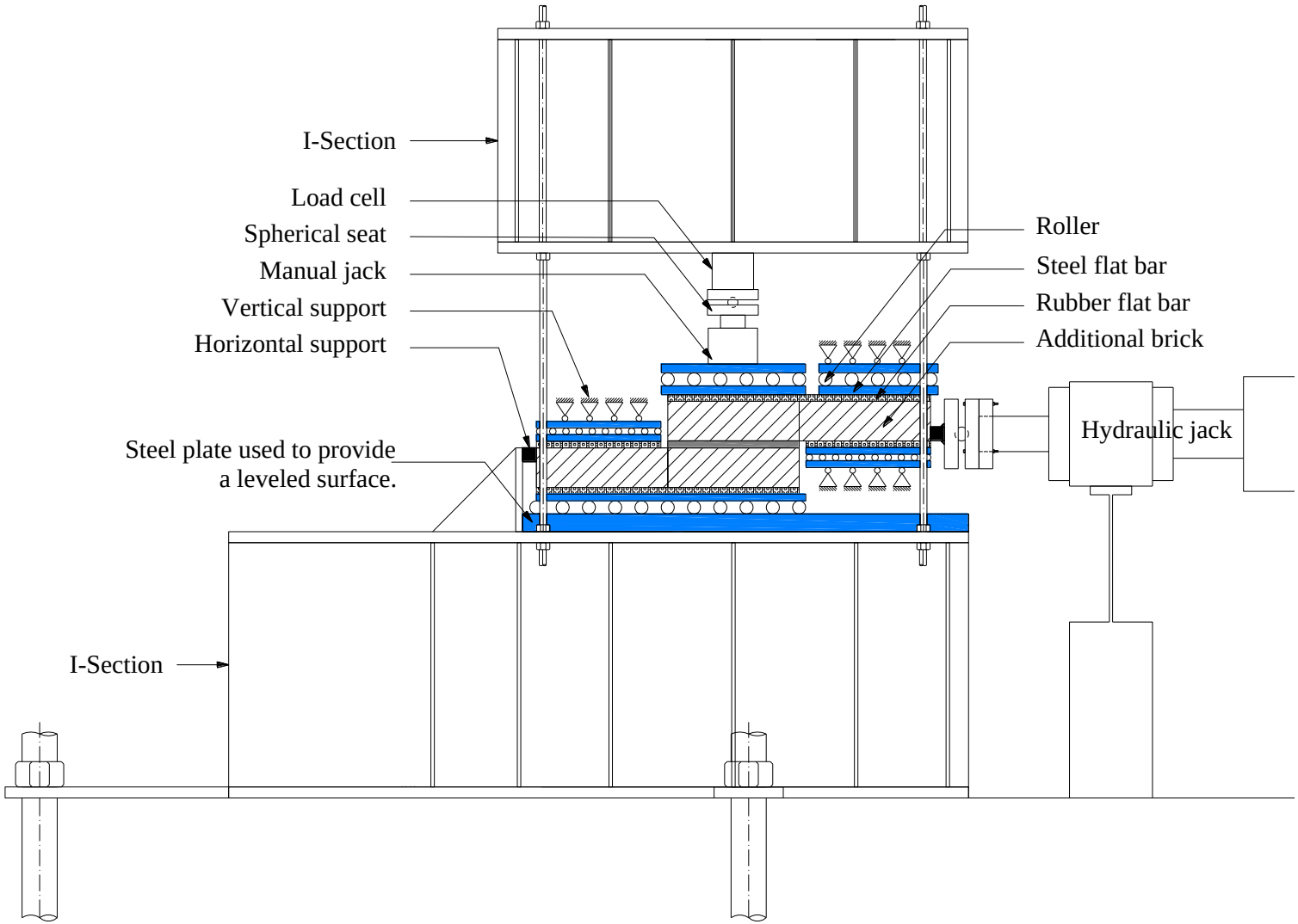

Figure 4.2: Schematic of the new test arrangement (version 2)

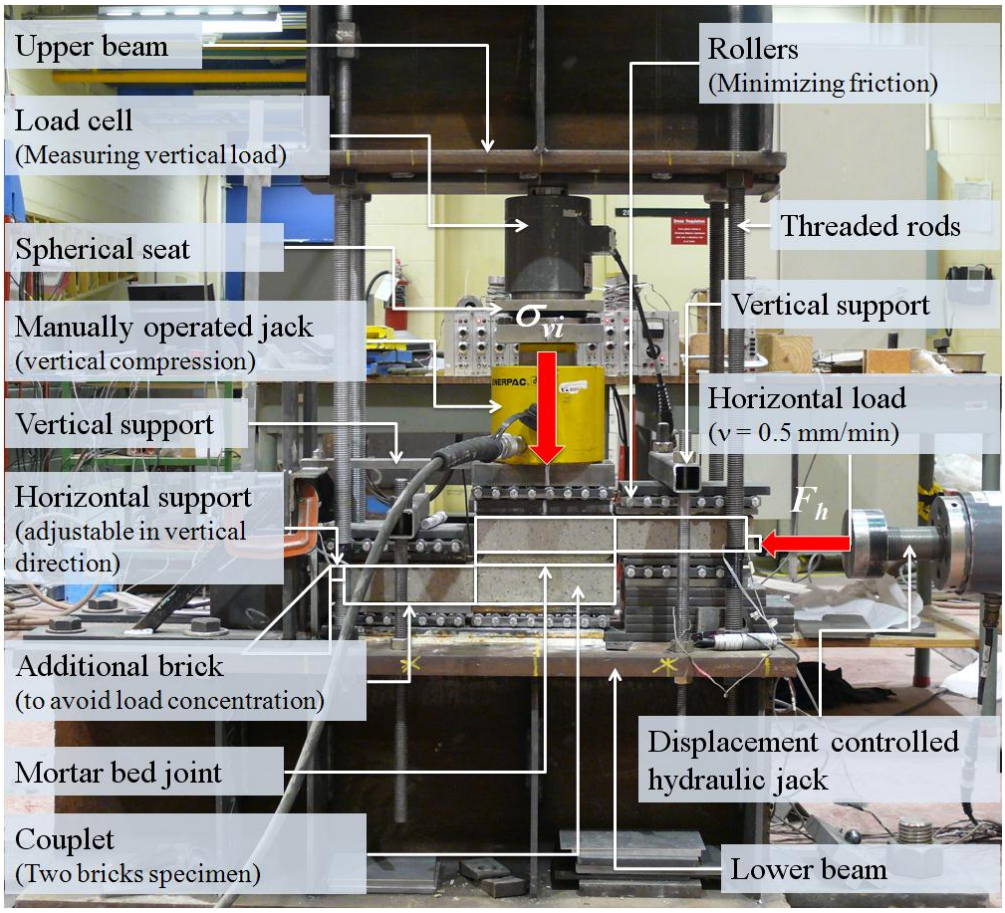

Figure 4.3: Test arrangement for version 2 of the proposed test method

Here, a plane, level surface for the rollers is provided by means of a steel plate with smoothed surface and dimensions of $500\ x\ 25\ x\ 200\ mm$. The steel plate is bedded on the top of the lower beam by means of leveling grout (plaster of Paris). In addition to the steel plate, a horizontal support is welded on top of the lower beam, and thereby one of the hydraulic jacks is replaced. The reaction load at the horizontal support is transferred by the lower beam to the floor by fixing the beam to the floor. This ensures that the results obtained due to the horizontal load are not affected by load circulation in the test setup. Further, the normal compressive stress is applied to the specimen by using a manually operated jack instead of torqueing the screw nuts on the threaded rods. The

normal compressive force is measured by a load cell placed on top of a spherical seat between the upper beam and manually operated jack. The equivalent vertical load for each level of intended compressive stress was determined based on the nominal area of the gross bedded area of the units. In this modified test arrangement, the upper beam provides a rigid surface in the vertical direction and support for the manually operated jack, and the lower beam, as before, is fixed to the floor and provides a level, plane surface as well as support in the horizontal direction.

During this redesign phase, the use of Teflon sheets instead of rollers was also considered. The recommended product is composed of two Teflon sheets (each with a thickness of $t = 0.25\,mm$ and a coefficient of friction of $\mu = 0.032$) and two rubber sheets (each with a thickness of $t = 2.0\,mm$), and is manufactured in the Netherlands. The layers are stacked as follows: One layer rubber followed by two layers of Teflon sheet and an additional layer of rubber on the top of it. However, the material could not be shipped outside Europe and an equivalent material was not available in North America. Therefore the idea was replaced by using an assembly composed of one sheet of rubber, $t = 0.5\,mm$, one steel plate ($t = 12.5\,mm$), and one roller with repeating steel plate and rubber sheet on the top of it. The rubber sheets are used to accommodate the unevenness of the surface of the bricks and the steel plates are used to allow smooth movement of the rollers. The steel plates arranged at the top and bottom of the couplet are not connected to the plates arranged at the top and bottom of the additional bricks, so that the couplet and the additional brick can move independently.

In the redesigned test arrangement, the couplet can be subjected to a horizontal load or to a combination of horizontal and vertical load. While the vertical load is applied by means of a manually operated jack, the horizontal load is applied by means of a displacement controlled hydraulic jack with a capacity of $150\ kN$.

4.4 Materials

For the experimental program, two types of perforated clay brick and one type of mortar (Type S) were utilized to construct two-brick, one-mortar joint specimens (couplets). The choice of the material for the purpose of this research project is irrelevant, since it is intended to investigate the variation in normal and shear stresses along the mortar joint, and the consistency of the results using the new test method. The actual joint shear strength, and the effect of the materials used or applied loads, was not being studied.

4.4.1 Brick units

The two types of brick utilized for the experimental work, are three-cored clay bricks provided by IXL Masonry Supplies Ltd., as shown in Figure 4.4.

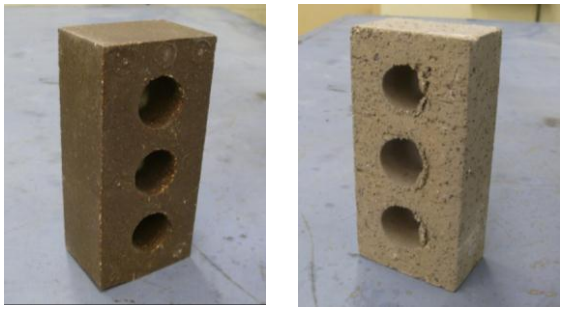

Figure 4.4: IXL Sable Titans Brick, left, and Interstate Platinum Brick, right

The IXL Sable Titans brick (IXL-STB) is a dry pressed clay brick with nominal dimensions of $190\ x\ 63\ x\ 90\ mm$, and the Interstate Platinum brick (IPB) is an extruded wire cut clay brick with dimensions of $195\ x\ 57\ x\ 93.5\ mm$, (length *x* height *x* width). The bricks are approximately 80% solid by area and their selection was mainly based on the compressive strength. The compressive strengths of the bricks were determined according to CSA A82-06, (2006) and are listed with their coefficient of variation (COV) in Table 4.1. The average values of the compressive strength are based on the nominal bed face area of the corresponding bricks. In the case of the IXL-STB, ten random full-size bricks were selected from the pallet and were tested for compressive strength. In the case of the IPB, because of the low COV, only five random full-size bricks were tested. Each brick was placed between two boards of plywood with dimensions $205\ x\ 6\ x\ 100\ mm$ and subjected to a load applied normal to the bed face of the bricks.

Table 4.1: Mean compressive strength of brick units

	Brick Types	$f_{c\ unit}$ (N/mm^2)	COV %	Weight (kg)	Dimensions (mm)
1	IXL Brick Sable (IXL-STB) Dry Pressed Brick	42	18.5	1.90	190x63x90
2	Interstate Platinum Brick (IPB) Extruded Brick	64	4.5	1.70	195x57x93.5

4.4.2 Mortar

The bricks utilized in the experimental study were joined together by means of premixed mortar of Type S provided by Spec Mix. The premixed Type S mortar consists of Portland cement, lime, and sand with a mix-ratio of $1.0 : 0.5 : 4.5$ by volume, respectively.

For the purpose of the experimental work, the premixed mortar was combined with water in small batches. In each batch, 7 kg mortar was mixed with 1.5 liters of water using the same mixing procedure under the same environmental conditions in which the specimens were manufactured and stored. The flow of the mortar of each batch was measured on a standard flow table, and the average value and the corresponding COV are given in Table 4.2. Further, in Table 4.2 the values for the compressive strength of the mortar are listed. In order to determine the compressive strength of the mortar, 24 cubes with a side length of $a = 50.8\,mm$ were cast. Twelve cubes were air cured in the same room as the specimens were stored, and the remaining twelve cubes were stored according to the requirements of CSA A179-04 (2004). Six cubes from each curing condition were tested at ages of 30 and 90 days. The cubes were subjected to a compressive load, and the corresponding compressive strength was obtained according to CSA A179-04. The difference in the compressive strength between the ages of 30 and 90 days, was approximately $3.5\,N/mm^2$in the case of the cubes stored according to CSA A179-04, and was insignificant for the air cured cubes.

Table 4.2: Compressive strength of mortar Type S

	$f_{c\,mortar}$ (N/mm^2)							
	30 days				90 days			
Mortar Type S	Wet	COV	Dry	COV	Wet	COV.	Dry	COV
1.0:0.5:4.5	12.5	7.97 %	9.90	4.34 %	16.0	1.80 %	9.50	6.15 %

4.5 Preparation of Specimens

The masonry specimens used in the experimental work were built of two bricks and one mortar joint to form couplets, as shown in Figure 4.5.

Figure 4.5: Masonry specimens, left (IXL-STB) and right (IPB)

The couplets were manufactured by using a simple jig that was designed and used in an earlier research project at the University of Calgary. Using this simple apparatus ensures proper alignment of the units and a $10\,mm$ thick mortar joint through all the couplets. The simple jig consists of four right angled wooden pieces each furnished with an $M6$ hex screw (screw head diameter $=\ 9.8\,mm$) that is embedded in the middle of the right angled wooden pieces, and is held in place by an $M6$ hex nut. In each corner of the lower brick, one of the wooden pieces was placed and the screw head was set on the bed face of the brick. All four corner pieces were held together initially, by a heavy-duty elastic band and, later by a hose clamp, as shown in Figure 4.6.

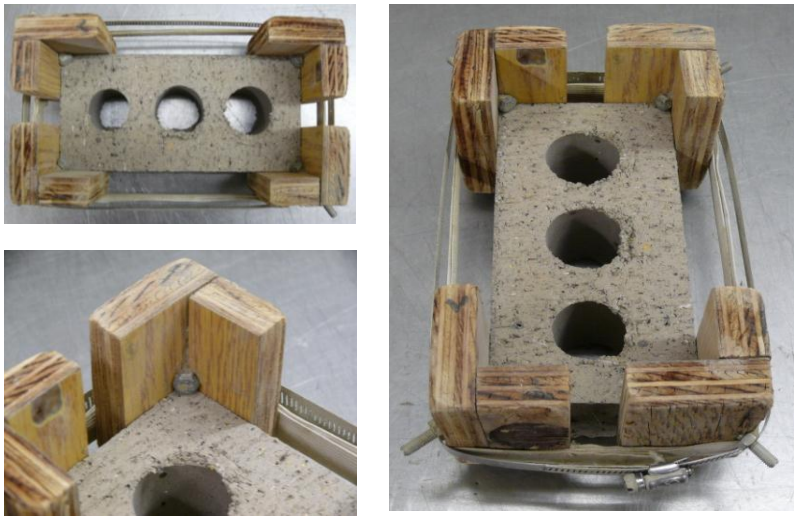

Figure 4.6: The simple jig for constructing the couplets

Once the lower brick was prepared as shown, a full bed of mortar was placed on top of the lower brick and then the upper brick was added and tapped down to the required level. Afterward, when the couplet was completed, the hose clamp and the heavy duty elastic were removed, and the wood pieces at the corner were pulled out. The manufactured specimens were air cured and stored in laboratory conditions at a temperature of 20 to 24 ℃ until testing. During the manufacturing process, a large amount of mortar flowed into the cores of the lower and upper bricks. As a result, the specimens were more or less fully mortared couplets.

4.6 Measurement Equipment

For acquisition of data, a load cell was used to measure the manually applied vertical load, and the hydraulically controlled horizontal actuator includes its own load cell and displacement transducer. To measure displacements, different types of measuring instruments were utilized. The measuring instruments are:

1. Linear Strain Converters (LSCs) to measure displacement
2. 10 Megapixel Digital Camera combined with Geo-Particle Image Velocimetry (Geo-PIV)

The LSCs were used to measure the relative displacement between two points on the couplet. The Geo-PIV was used to gain insight into the stress condition along the mortar bed joint. In the following, the LSCs, the camera, and the Geo-PIV are explained in detail.

4.6.1 Linear Strain Converters

The LSCs utilized for measuring the relative displacement sense the spindle displacement by using a fully activated 350Ω strain-gauge bridge, and covered a displacement range of $10\,mm$. After calibration in the Civil Engineering lab of the University of Calgary, the LSCs measure with an accuracy of ± 0.02 to $0.04\,mm$.

The relative displacement of two points, located on the upper and lower bricks of the couplet, was measured both in-plane, as well as out-of-plane. The relative displacement data were recorded along with the horizontally applied load. In total, three LSCs were used as shown in Figure 4.7. One of the LSCs was attached parallel to the applied horizontal load (i.e. in Y-direction) to the left lower corner of the upper brick, and its corresponding target, a small steel angle with dimensions $50x50x2\,mm$, was attached to the right upper corner of the lower brick. The other two LSCs were arranged normal to the surface of the couplets (i.e. in X-direction) to measure any relative out-of-plane displacement between the upper and lower bricks of the couplets. The LSC measurements were recorded every second, and stored in a computer which also recorded the data (displacement and force) from the horizontal hydraulic jack and the load cell.

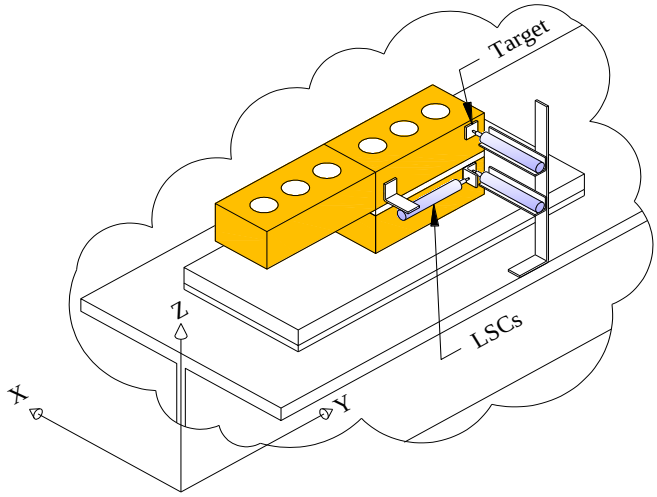

Figure 4.7: Arrangement of LSCs on the specimens

4.6.2 Particle Image Velocimetry and GeoPIV

A Particle Image Velocimety (PIV) system of measurement uses images of particles to measure the flow velocity. The technique was originally developed in the field of fluid mechanics, and was utilized for measuring flow field in a fluid (Adrian, 1991). In the PIV technique, this is done by tracking patches placed in an area of interest through a series of digitally captured images. Later, once a series of digital images is captured, the area of interest in the initial image can be divided in a mesh of PIV test patches. Each patch possesses a unique texture and specific coordinates in image 1 at the time $= t_1$, (u_1, v_1). To locate the specific coordinates of a patch from image 1 within a corresponding pre-defined larger search patch in image 2, the correlation between the two patches is evaluated. The location with the highest correlation within the search patch indicates the specific coordinates of the initial patch at time$= t_2$ in image 2, (u_2, v_2). This procedure, as illustrated in Figure 4.8, is repeated for the entire mesh of patches within an image, and then repeated for each image within the series, to determine the displacement vector of each test patch (White & Take, 2002).

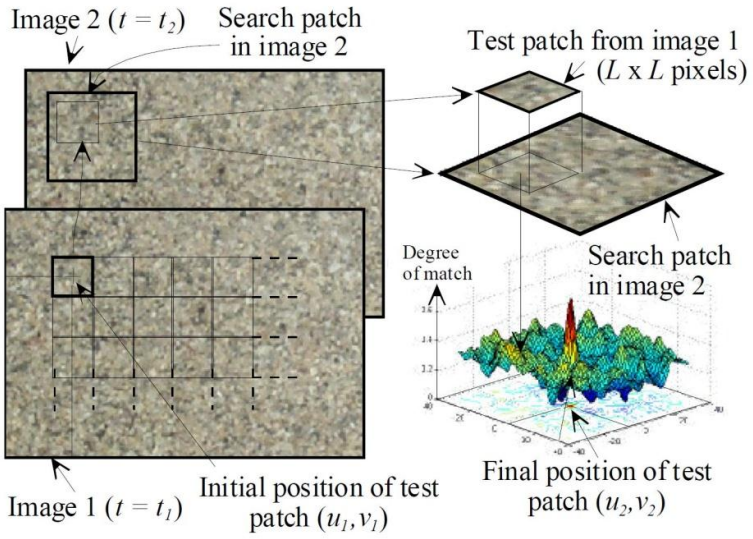

Figure 4.8: Principles of PIV analysis (White & Take, 2002)

The principle of PIV has also been utilized in the field of geomechanics to measure the deformation of soil, which is considered to be a low-velocity flow process, (White, et al., 2001a) and (White, et al., 2001b). For this application, the principles of PIV analysis were adapted for the purpose of geotechnical tests by writing a MATLAB module named GeoPIV (White & Take, 2002). The GeoPIV MATLAB module is a non-contact, two-dimensional displacement measurement system which proceeds in three steps as shown in the flow chart in Figure 4.9. Step one involves the preparation of a series of digital images as well as of two ASCII input files (GeoPIV7_luncher.txt and GeoPIV7_mesh.txt). In step two, the PIV analysis is conducted within the MATLAB module. The last step involves the calibration of digital images and calculation of strains (White & Take, 2002). The calibration between image-space and object-space can be accomplished with a relation between the actual dimensions of the specimen and the number of pixels within the corresponding digital image.

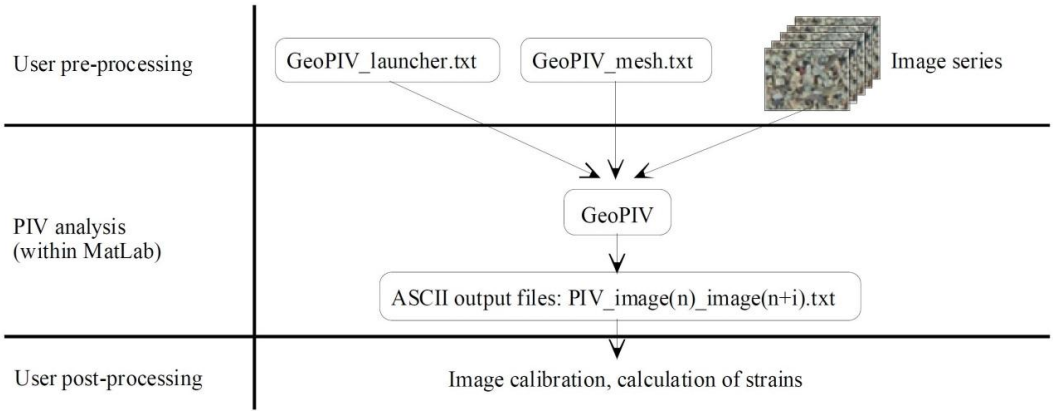

Figure 4.9: GeoPIV image processing system (White & Take, 2002)

The GeoPIV MATLAB module has also been applied to measure strains in structural elements. Bisby and Take (2009) applied the technique in their experimental work to measure the hoop and axial strain of concrete cylinders confined with FRP. The experimental program conducted showed that the GeoPIV measurement technique is capable of providing accurate measurements of both hoop and axial strains (Bisby, et al., 2007) and (Bisby & Take, 2009).

For the current research, GeoPIV has been applied to measure the in-plane deformations of couplets tested using the proposed test method. The advantage of using GeoPIV in comparison to a contact system, such as linear strain converters (LSCs), is the possibility of being able to observe the movement of an entire area of interest, while the contact system measures only the relative displacement between two points and is limited to the number of instruments used. GeoPIV also offers advantages over traditional strain measurement instruments, such as strain gauges, since the latter can also only measure the strain at the specific location where it is attached.

4.6.2.1 Preparation of Specimen for Geo-PIV

As mentioned above, the PIV technique measures the velocity of a point by tracking a test patch of texture, specified in the initial digital image, through a series of digital images. For this reason, the couplets used in the current research project were painted white and then speckled with black paint, as shown in Figure 4.10. The three LSCs shown in Figure 4.7 were mounted on the unpainted side of the couplets. The results obtained from LSCs are used to validate the results obtained by using GeoPIV.

Figure 4.10: Painted specimen, left, speckled specimen, right

4.6.3 Setup of camera for the digital images

The GeoPIV measurement system requires a series of digital images for the analysis that capture the reaction of a specimen during a test phase. To document the reaction of the specimens in the current study, a digital camera with an aspect ratio of 4: 3 and a picture size of $3648\,x\,2736$ $(10M)$ pixels was utilized. The digital camera was placed on a tripod at a distance of $l = 3.00\,m$ from the specimen. The height of the camera, or rather the height of the center point of the lens, was adjusted to the height of the center point of the mortar bed joint. Further, the body of the camera was leveled, so that the line of sight of the camera was perpendicular to the area of interest (i.e. the surface of the couplet). Once the location, height, and line of sight of the camera were

adjusted, then the field of view was adjusted onto the specimen using the camera zoom, as shown in Figure 4.11. In addition to the zoomed view of the specimen, Figure 4.11 also shows a plan view of the setup. In order to avoid any extraneous causes of movement, the camera was operated by using a remote trigger.

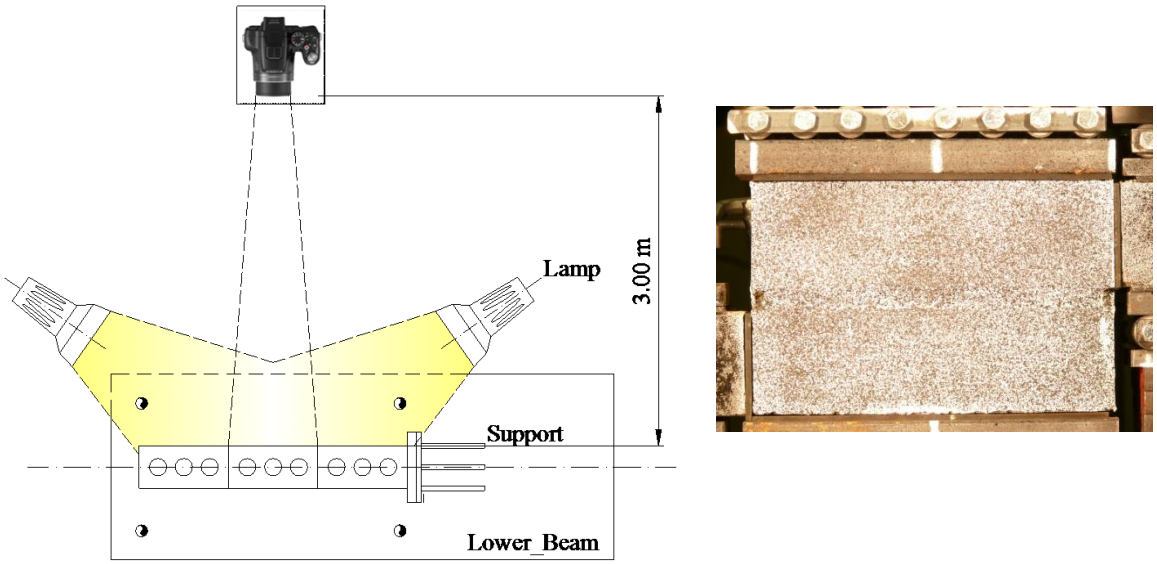

Figure 4.11: Camera and Light setup (left); the actual field of view (right)

During the testing phase, the specimen is illuminated by two lamps placed at the right and left hand side of the specimen, and the digital camera is activated simultaneously with the hydraulic jack (i.e. when the testing phase started) and deactivated at the end of the testing phase. The time for each test was measured using a stopwatch with an accuracy of $\pm 1/100\ sec$. In order to relate the timing of the digital images to the timing of the horizontal applied load and the corresponding movement, an additional LSC was connected to the data acquisition system. The additional LSC was not attached to the specimen and activated only at the beginning and the end of the testing phase by applying a displacement equal to the capacity of the LSC simultaneously with the start and end of

the testing phase. These two measurements mark the exact time of the testing phase in the recorded data produced by the hydraulic jack.

4.7 Summary

This chapter describes the experimental program, the materials utilized, the specimens, the measurement equipment, and the arrangement of the proposed test method. Two types of clay brick (dry-pressed and extruded) and one type of mortar (Type S) were combined to construct two-brick, one-mortar joint specimens. After curing, the specimens were tested by using the proposed test method. During the testing phase, the specimens were subjected to horizontal and vertical loads using a hydraulic displacement controlled actuator and a manually operated jack, respectively. In total, 50 specimens, 25 for each brick type, were tested at four different levels of pre-compressive stress normal to the bed joint. The relative displacement between the upper and lower bricks of the specimen was measured with Linear Strain Converters (LSCs). In addition to the LSCs, a measurement system based on Particle Images Velocimetry (PIV) was utilized to gain insight into the state of stresses along the mortar joint and to measure the displacement of an entire area of interest. The recorded data are summarized, analyzed, and discussed in Chapter 5.

CHAPTER 5: **RESULTS AND DISCUSSION**

5.1 Introduction

A new test method was proposed, constructed, and used to test 50 couplets constructed of two types of brick and one type of mortar. The tests conducted were divided into eight series with varying levels of pre-compression (Series I to Series VIII). The specimens, test setup and the experimental program with the corresponding load condition were described in Chapter 4.

In this chapter, the results obtained using conventional Linear Strain Converters (LSCs), as well as the particle image velocimetry measurement system, GeoPIV, are presented and discussed. The results obtained using the LSCs were recorded automatically into a computer every second, and the images for use in the Geo-PIV software were recorded at a rate of approximately two digital images per second. First, the load-displacement behaviour observed using the LSCs is presented, followed by the results from the GeoPIV analysis. The results of the first 40 tests were measured with the LSCs (Appendix A), and were used to evaluate the reproducibility of results using the proposed test method. Ten additional tests were carried out with the GeoPIV measurement system, in addition to the LSCs, and were used to gain insight into the state of normal and shear stress that is induced in the mortar bed joint using the proposed test method.

5.2 Measurements using Linear Strain Converters

5.2.1 Results

5.2.1.1 IXL-STB (Dry Pressed Brick)

Twenty couplets were divided into four series where a different level of normal compressive stress ($0.03; 0.25; 0.375; and\ 0.50\ N/mm^2$) was applied for each series, with each series consisting of five specimens. To induce the desired level of normal compressive stress, in Series # I, the specimens were subjected to a normal compressive load of $0.5\ kN$, in Series # II to a normal compressive load of $4.3\ kN$, in Series # III to a normal compressive load of $6.4\ kN$, and Series # IV to a normal compressive load of $8.6\ kN$. Following application of the normal compressive load, the displacement controlled horizontal load was applied with a speed of $v = 0.5\ mm/min$. For all specimens, the horizontal load was applied until failure occurred and until a clear tendency of the residual strength was observed. The normal compressive force, the horizontal load, and the relative shearing displacement between the upper and lower bricks were measured and recorded continuously and automatically once per second.

During the testing, all twenty specimens, subjected to the above mentioned loading conditions, experienced a small rotation which led to an uplift of about $2\ mm$ at the heel of the specimens. No cracking of the mortar joint or debonding of the interface between the mortar joint and the bricks was observed at the time that the overturning of the specimens occurred. However, with increasing horizontal load the cracking process started at the upper interface between the mortar joint and the upper brick at the side where the horizontal load was applied. The initiated crack continued to propagate along

the interface up to either approximately one quarter or three-quarters of the length of the mortar joint followed by a diagonal crack through the mortar joint and then cracking along the interface between the mortar joint and the lower brick of the specimens. In the case of the specimens in Series # I, the diagonal crack through the mortar joint was a 45 degree crack, in Series # II, 60 degrees, and in Series # III and IV the cracks were between 60 and 90 degrees. In some of the tests two diagonal cracks were observed. Figure 5.1 shows typical cracks observed during the tests in Series # I through IV. In all specimens the failure occurred in the mortar bed joint, except for the specimens in Series # IV. In Series # IV, the failure occurred in the mortar bed joint as well as in the bricks of the specimens.

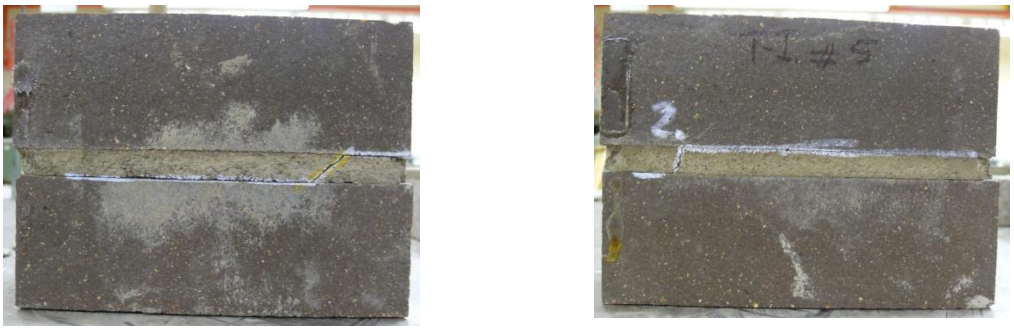

Figure 5.1: Typical cracks observed for Series # I through IV

The load-displacement results were plotted for each series and are discussed below. The results were normalized by first dividing the applied horizontal load by the ultimate recorded horizontal load for each specimen, and then averaging the corresponding values of the relative shear displacement, plotted along the X-axis. The error bars represent the variation between the 5 specimens.

The results of Series # I, as presented in Figure 5.2, indicate that the horizontal load increases linearly as a function of relative displacement until it reaches the peak. After the peak, a partial loss of energy occurs, and the horizontal load increases again until the second peak is reached. The magnitude of the second peak, for the tests in Series # I, was lower than the magnitude of the first peak, except in the case of Test # 3.

The average load at first peak for Series # I was $F_{mean} = 9.5\,kN$ at an average relative displacement of $\delta_{mean} = 0.50\,mm$. The scatter is relatively low for the load at first peak as evident by the coefficient of variation (COV) of 12% which, when compared to the variation expected for masonry, indicates a consistent response in the proposed test setup.

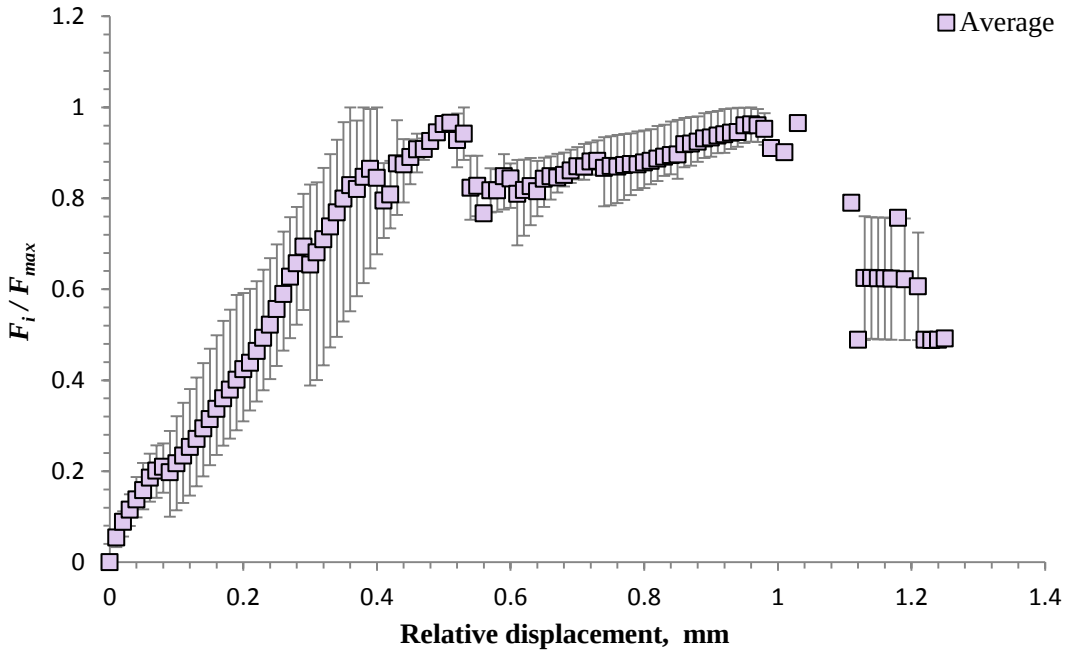

Figure 5.2: Results for Series # I, σ = 0.03 N/mm^2

The results of Series # II, as presented in Figure 5.3, exhibit a nearly vertical increase in the horizontal load initially, and then a linear increase until the first load peak is reached. The initial vertical increase in the horizontal load is the amount of load necessary to overcome the normal compressive load and the resulting friction between the steel plates and rollers. In an ideal case this load should equal zero.

Before the first peak, the shape of the normalized load-displacement curves for all 5 specimens is identical. After the first peak, however, the results showed no consistency in the failure behaviour of the specimens in Series # II which differs considerably from the specimens in Series # I. Further, unlike Series # I, the magnitude of the second peak is always greater than the first peak.

The minimum horizontal load at first peak was measured for specimen 2 ($F_{min} = 9.2\ kN$) and the maximum for Specimen 5 ($F_{max} = 14.2\ kN$). The average load at first peak is $F_{mean} = 12.0\ kN$ at an average relative displacement of $\delta_{mean} = 0.64\ mm$. The scatter of the load at first peak is higher compared to the specimens in Series # 1 with a COV of 18%, however the variation is still in an acceptable range relative to the variability of the materials themselves.

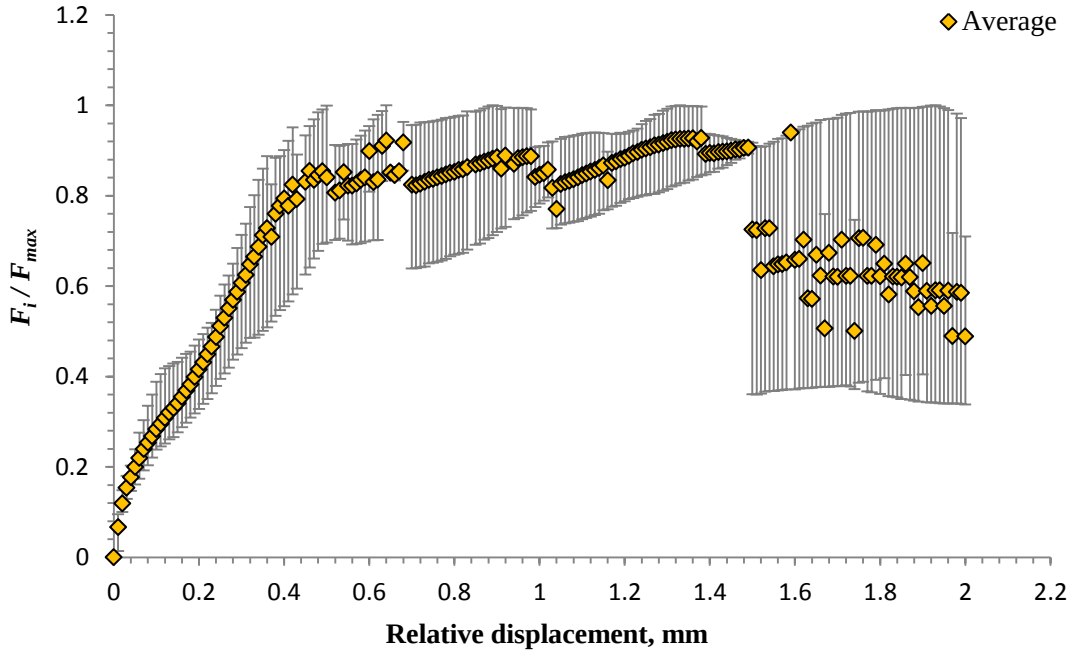

Figure 5.3: Results for Series # II, σ = 0.25 N/mm^2

In Series # III, as shown in Figure 5.4, the horizontal load increases nearly vertically at first, and then linearly as a function of relative displacement until failure begins. Once failure starts, the results exhibit random behaviour between specimens. In Specimens 1, 4, and 5, the applied horizontal load increases again after the first peak and reaches a second peak which is greater in magnitude than the first. In Specimens 2 and 3, it is not possible to distinguish between the first and second peaks. Therefore, the first drop in the magnitude of horizontal load was considered as the first peak.

The minimum horizontal load at first peak was measured for Specimen 2 ($F_{min} = 13.5\ kN$) and the maximum for Specimen 5 ($F_{max} = 17.1\ kN$). The average horizontal load at first peak was $F_{mean} = 15.9\ kN$ at an average relative displacement of $\delta_{mean} = 0.66\ mm$. The consistency of the load at first peak is evident by the relatively low COV of 11%.

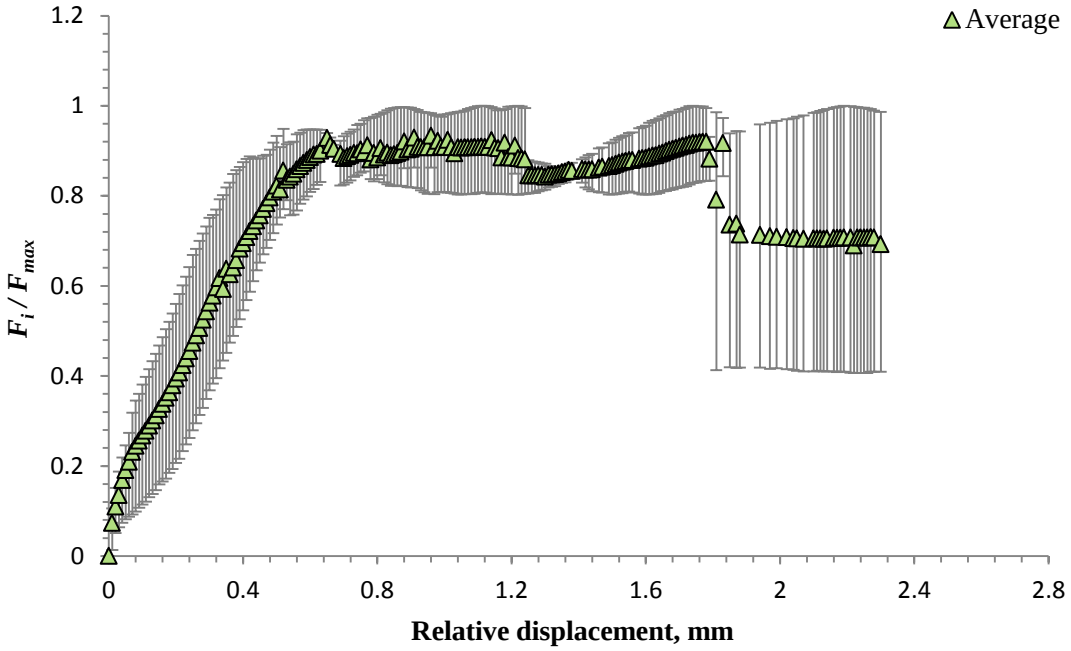

Figure 5.4: Results for Series # III, σ = 0.375 N/mm^2

In Series # IV, as shown in Figure 5.5, there is initially a nearly vertical increase in the horizontal load, followed by a linear increase as a function of relative displacement until the first peak. After the first peak, no significant decrease in the horizontal load was observed, except for Specimen 3. Therefore, once a relative displacement of approximately 4 mm was reached, the test was stopped. Unlike the previous series, all five specimens in Series # IV experienced brick failure.

The minimum horizontal load at first peak was measured for Specimen 2 ($F_{min} = 13.0\ kN$) and the maximum for specimen 3 ($F_{max} = 15.2\ kN$). The average horizontal load at first peak was $F_{mean} = 14.6\ kN$ at an average relative displacement of $\delta_{mean} = 0.50\ mm$. There is low scatter for the load at first peak as evident by the low coefficient of variation (COV) of 6%.

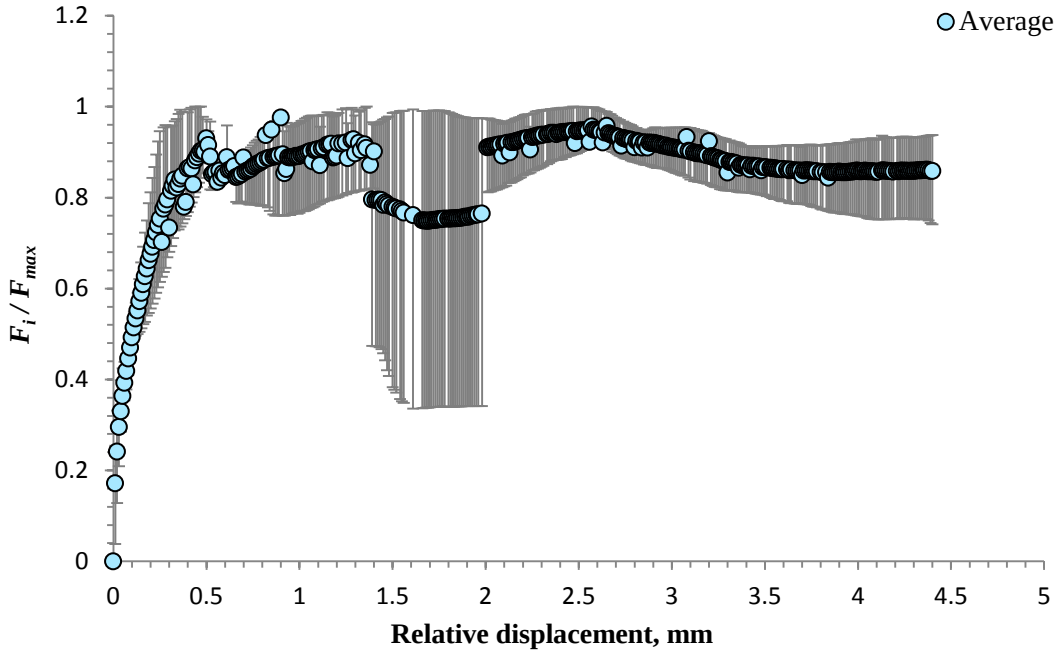

Figure 5.5: Results for Series # IV, σ = 0.50 N/mm^2

5.2.1.2 IPB (Extruded Brick)

Twenty couplets constructed from extruded bricks were divided into four further series (Series # V, VI, VII, and VIII) which were subjected to the same four levels of normal compressive stress as Series # I to IV. Each level of normal compressive stress (i.e. each series) consisted of five specimens. Series # V, VI, VII and VIII were subjected to normal compressive loads of approximately $0.55\,kN$, $4.6\,kN$, $6.8\,kN$, and $9.1\,kN$, respectively, prior to application of the displacement controlled horizontal load at a velocity of $v = 0.5\,mm/min$. As before, the normal compressive force, the horizontal load, and the relative displacement between upper and lower bricks were continuously recorded, and the data acquisition occurred once per second automatically.

During the testing, all twenty specimens experienced a small rotation which led to an uplift of about $2\,mm$ of the heel of the specimens. No cracking of the mortar joint or

debonding of the interface was observed due to the overturning occurring, except in the case of Specimen 1 of Series # V. In this case, the overturning of the specimen led to a crack opening of approximately $0.5\,mm$. Since it was a one-time event it was presumed that the bond between the mortar joint and brick was not well developed.

In general, the joint failure for the extruded bricks started with the slow formation of an interface crack along the upper interface and continued with a diagonal crack through the mortar joint and subsequent shearing of the lower interface. In some tests, two or three diagonal cracks were observed. The observed diagonal cracks through the mortar joint had an angle between 60 and 90 degrees. Furthermore, failure without any diagonal cracks was also observed. Figure 5.6 shows typical cracks observed during the tests of Series # V through VIII. The observed failure occurred in the mortar joint as well as in the bricks of the specimens. All tests, except for Series # V, ended with mortar joint and brick failure.

Figure 5.6: Typical cracks observed for Series # V through VIII

The results for Series # V are shown in Figure 5.7. There is initially a nearly vertical increase of the horizontal load followed by a non-linear increase with relative displacement until the peak is reached which can be seen clearly in Specimens 2, 3, and

4. In Specimens 1 and 5, the horizontal load increases more or less linearly, up to the first peak. In general, after the first peak, the horizontal load increases again and reaches a second and, in some cases, a third peak. In Series # V, the magnitude of the third peak is always lower than the second one, and the second one is higher than the first, except for Specimen 1. However, once a crack is initiated, or part of the bond between the mortar joint and the bricks is lost, the results exhibit more random behaviour due to the progression of failure.

The minimum horizontal load at first peak was measured for Specimen 2 ($F_{min} = 6.6\,kN$) and the maximum for Specimen 1 ($F_{max} = 8.4\,kN$). The average value was $F_{mean} = 7.5\,kN$ at an average relative displacement of $\delta_{mean} = 1.13\,mm$. The relatively low COV of 9% indicates consistent results using the proposed test arrangement.

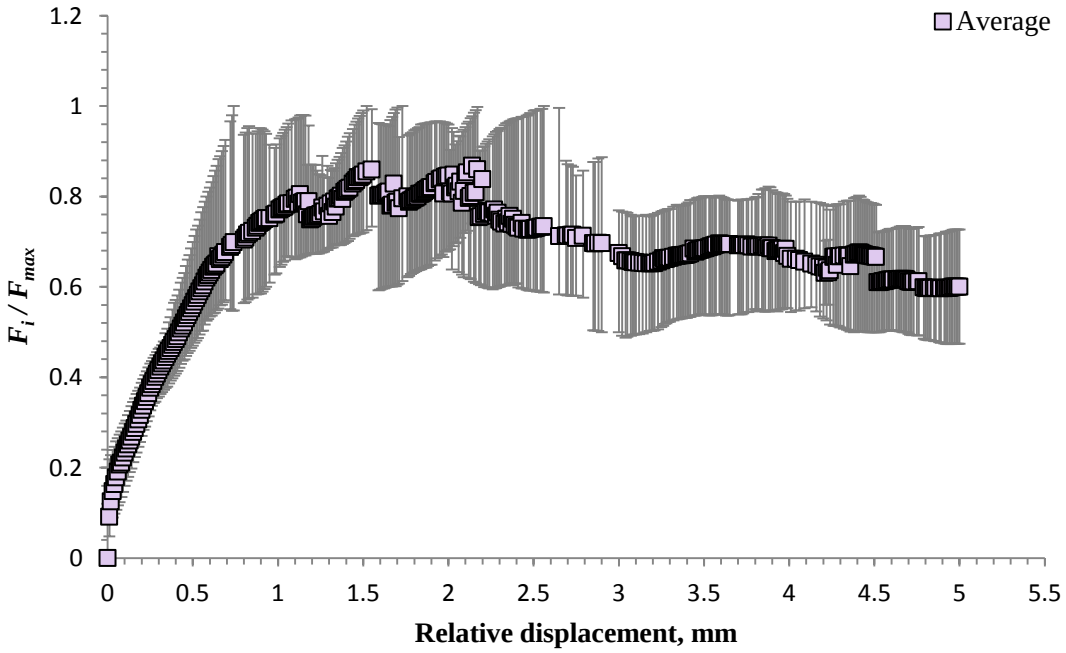

Figure 5.7: Results for Series # V, σ = 0.03 N/mm^2

The results of Series # VI, as shown in Figure 5.8, also exhibit a nearly vertical increase in the horizontal load followed by a non-linear increase until the first peak was reached. Prior to the first peak, Specimens 1, 3, and 4 exhibited different failure progression than Specimens 2 and 5. After the first peak, it was difficult to define the exact point of failure. Therefore, the testing of each specimen was stopped once a relative displacement between the upper and lower brick of approximately of 5 mm was reached. In Series # VI, failure occurred in the mortar bed joint as well as in the brick. It was unclear which one occurred first, therefore it was assumed that the first noticeable drop in the horizontal load was due to the failure of the mortar joint.

The minimum horizontal load at first peak was observed for Specimen 1 ($F_{min} = 13.1\ kN$) and the maximum for Specimen 3 ($F_{max} = 16.4\ kN$). The average value for the horizontal load at first peak was $F_{mean} = 14.4\ kN$ at an average relative displacement of $\delta_{mean} = 1.15\ mm$. The consistency of the load at first peak is evident by the low COV of 10% which is also an indicator of the reproducibility using this test arrangement.

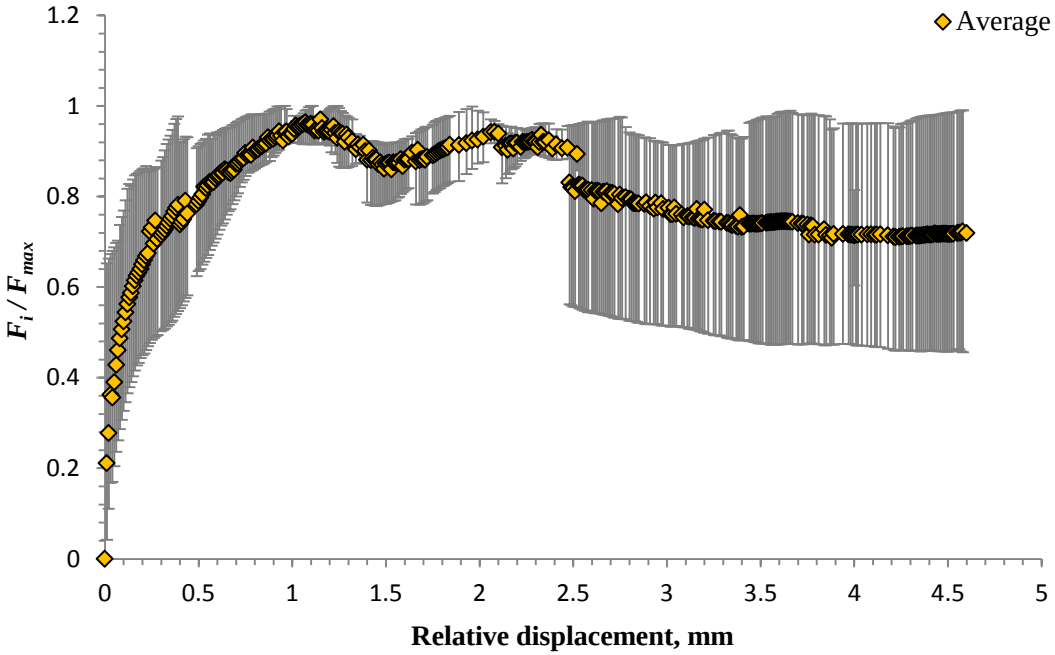

Figure 5.8: Results for Series # VI, σ = 0.25 N/ mm^2

The results for Series # VII, shown in Figure 5.9, also exhibit the initial vertical increase in the horizontal load, followed by a non-linear increase until the peak was reached. The shape of the normalized load-displacement curves for each specimen before the first peak is identical, especially for Specimens 1, 3, 4, and 5. In general, after the first peak the results do not provide a clear point of failure, therefore the test was stopped once a relative displacement between the upper and lower bricks of approximately $5\ mm$ was reached. In all tests in Series # VII the failure occurred in the mortar joint as well as in the bricks of the specimens, and it was unclear when exactly the mortar and when the brick failure occurred. Therefore, as in the case of Series # VI, the first drop in magnitude of the horizontal load was declared as the point at which the mortar joint failed.

The minimum horizontal load at first peak for the tests in Series # VII was measured for Specimen 1 ($F_{min} = 12.8\ kN$) and the maximum for Specimen 2 ($F_{max} =$

15.8 kN). The average value was $F_{mean} = 15.2\ kN$ at an average relative displacement of $\delta_{mean} = 0.89\ mm$. The scatter of the load at first peak is low with a COV 8%, again proving the consistency of the proposed test arrangement.

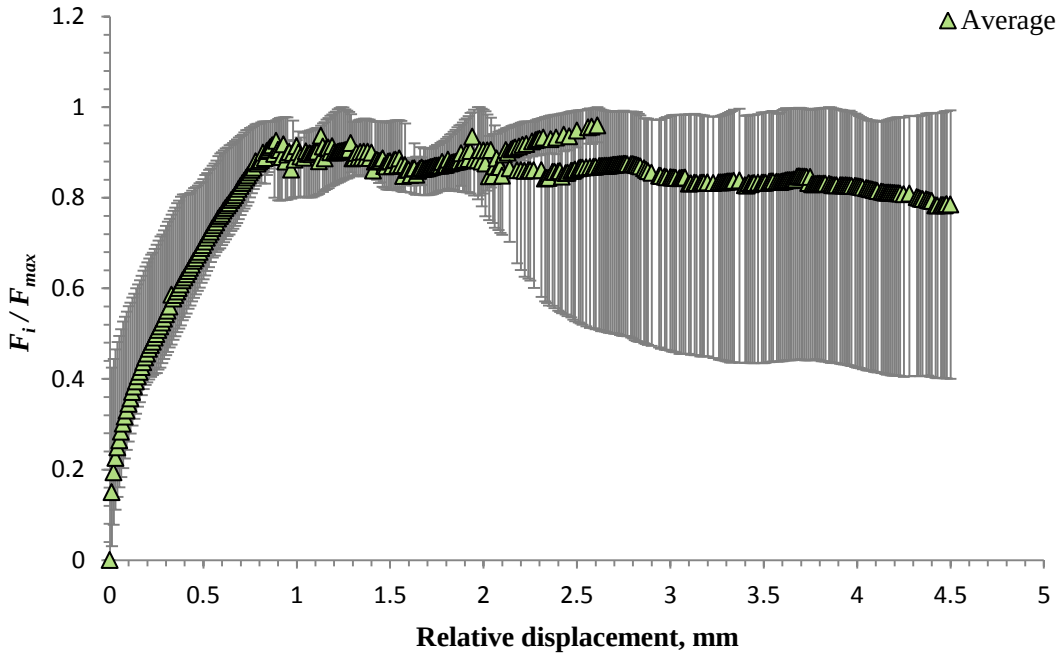

Figure 5.9: Results for Series # VII, σ = 0.375 N/mm^2

The results for Series # VIII are shown in Figure 5.10. A vertical increase in the horizontal load is observed initially, followed by a non-linear increase until the peak is reached. The shape of the normalized load-displacement curves before the first peak is identical for all the specimens. Once the peak load was reached, the applied horizontal load for specimens 1, 2, and 3, fluctuates within a fixed range until the test was stopped. Once again, the results do not provide a clear point of failure, therefore the testing of each specimen in Series # VIII was stopped when a relative displacement between the upper and lower bricks of approximately 6 mm was reached. Since all tests in Series # VIII ended with failure of the mortar joint as well as with failure of the bricks, the first drop in

magnitude of the applied horizontal load was declared as the point at which the mortar joint failed.

The minimum horizontal load at first peak for Series # VIII was observed for Specimen 2 ($F_{min} = 12.9\ kN$) and the maximum for Specimen 2 ($F_{max} = 14.9\ kN$). The average value was $F_{mean} = 14.0\ kN$ at an average relative displacement of $\delta_{mean} = 1.27\ mm$. The scatter of the load at first peak was quite low for this series, with a COV of 6%.

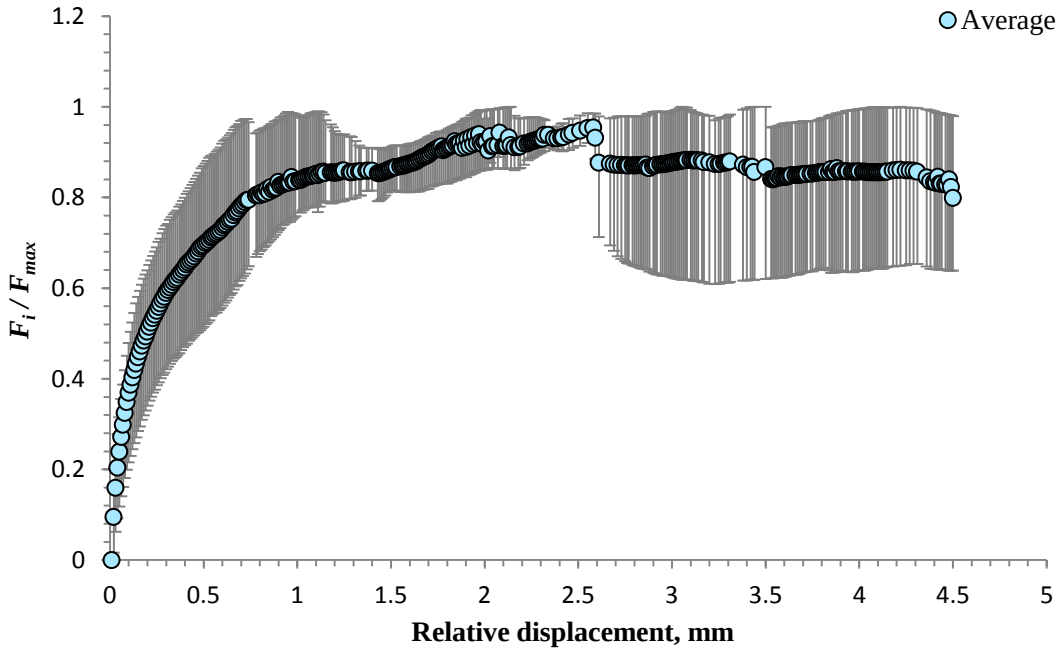

Figure 5.10: Results for Series # VIII, σ = 0.50 N/mm^2

The amount of scatter of the load at first peak, for Series # I to IV (Dry pressed Bricks), ranges within 6% and 18%, and for Series # V to VIII (Extruded Bricks) within 6% and 10%. These relatively low values lead to the conclusion that the proposed test method provides consistent results.

5.2.2 Discussion

The rotation observed in all specimens is the result of the eccentrically applied horizontal load. Figure 5.11 illustrates the difference between the line of action of the externally applied forces and the internal reaction forces which cause overturning of the specimens. The overturning of the specimens leads to areas of stress concentrations at the right (directly above the mortar joint in the lower area of the upper brick) and left (directly beneath the mortar joint in the upper area of the lower brick) ends of the specimens. Drawing an imaginary line between those two areas indicates the flow of the applied load between the action and reaction points, and thereby the existence of tensile force. Therefore, even though no cracking or debonding of the bond along the interface due to the overturning of the specimens was observed, it is presumed that the initiation of the crack was a result of the specimens being subjected to combined tension and shear at this stage of the testing. However, due to the observed failure mode in the mortar joint, it is presumed that once the crack was initiated, the crack propagation process was governed by the applied shear force. Furthermore, the overturning of the specimens leads to an increase in the pre-applied vertical load which was intended to counter the induced moment due to the applied horizontal load. Obviously, the increase of the pre-applied vertical load is not large enough to avoid the overturning of the specimens and therefore an improvement to the test arrangement is necessary.

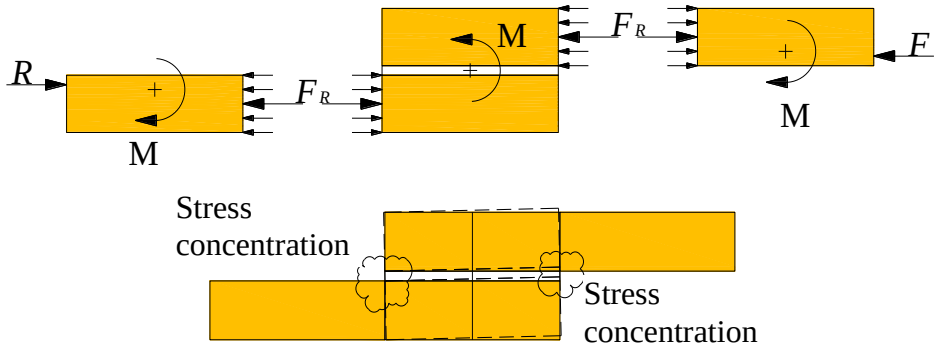

Figure 5.11: Moment and stress concentration due to eccentrically applied load

During the testing, a second peak in the applied horizontal load with a larger magnitude than the first one was often observed. The second peak in the horizontal load, could be due to the mechanical anchorage provided by the amount of mortar that flowed into the cores of the bricks during the manufacturing of the specimens. The bricks were connected to each other with a shape of mortar as shown in Figure 5.12, rather than a uniform mortar layer with a thickness of $t = 10\ mm$.

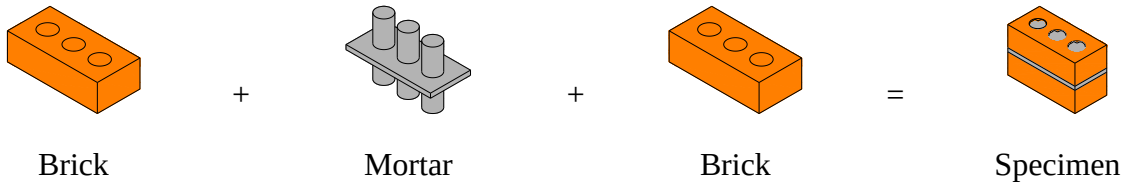

Figure 5.12: Test specimens

Shrinkage of the mortar may have caused a small gap between the interior surface of the brick core and the mortar cylinder, however, once the bond between the mortar joint and brick at the interface is lost, and a small displacement along the joint occurs, the mechanical anchorage of these mortar cylinders takes effect, and it is obvious that additional horizontal load will be required to shear through these three cylinders of mortar. Therefore, depending on diameter, height, density, and rigidity of these three

cylinders of mortar in each specimen, the magnitude of the second peak of the applied horizontal load was usually greater than the first peak load. Further, if no gap between the surface area of the cylinder and the brick cores was initially present, then the magnitude of the first peak could also be affected. In addition, these three cylinder of mortar, each with a diameter of $\emptyset \cong 35.5\, mm$, exert pressure on the webs between the holes, and thereby cause a stress distribution around the holes as shown in Figure 5.13.

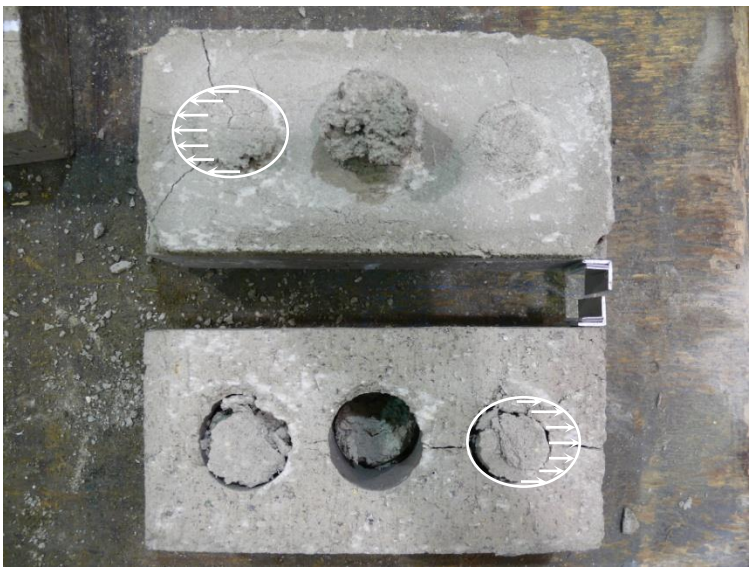

Figure 5.13: Stress concentration around the holes due to the mortar cylinders

As a result of the manufacturing process, bricks typically possess less compressive strength in the longitudinal direction than in the direction perpendicular to the bed face, and this effect is more significant for extruded bricks compared to dry-pressed bricks. Therefore, the pressure exerted could be the reason for the large number of brick failures observed during the testing, and the reason that fewer brick failures were observed for the dry pressed bricks than for the extruded bricks. Hence, it can be concluded that the observed brick failure is not necessarily a result of the proposed test

method, but rather of the test specimens. Figure 5.14 shows a typical example of failure observed for the extruded bricks.

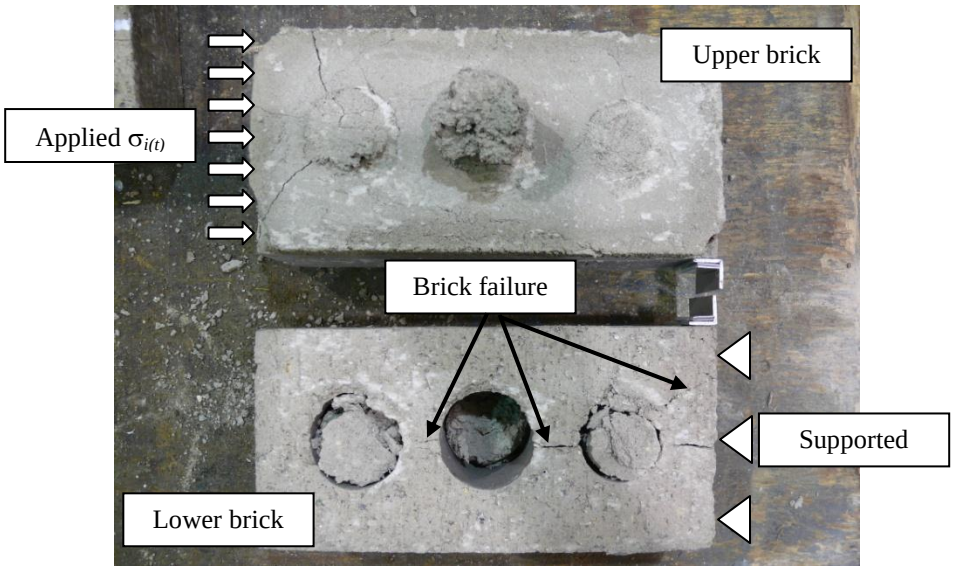

Figure 5.14: Typical example for the observed brick failure

The results obtained from the first part of the experimental work are summarized and presented in Table 5.1. In order to evaluate the effect of the normal compressive stress on the results, the means of two subsequent series were analysed by using the t-test. The P-values in Table 5.1 indicate that the differences in the results between Series III and IV, VI and VII, and VII and VIII are not governed by the change in normal compressive load (P > 10%), but most likely by the existence of the mortar cylinders. Therefore, a relationship between ultimate shear strength, τ_u, and normal compressive strength as formulated in Eq. (1) cannot be derived from the experimental results. It should be also noted that these are the series for which brick failure was observed in all the tests conducted. As mentioned above, the brick failure could be a result of stress

concentration caused by mortar cylinder. Hence, the observed brick failure cannot be related to the new test arrangement.

Table 5.1: Summary of experimental results

		Min. (kN)	Max. (kN)	Means (kN)	COV %	P-values %
Pressed Bricks (IXL-STB)	Series # I	7.3	10.0	9.5	12	6.9
	Series # II	9.2	14.2	12.1	18	1.0
	Series # III	13.5	17.2	15.9	11	26
	Series # IV	13.0	15.2	14.6	6	
Extruded Bricks (IPB)	Series # V	6.6	8.4	7.5	9	0.0
	Series # VI	13.1	16.4	14.4	10	57
	Series # VII	12.8	15.8	15.2	8	30
	Series # VIII	12.9	14.9	14.0	6	

5.3 Measurements using GeoPIV

The GeoPIV measurement system was utilized to measure the deformations along the mortar joint, from which the strains were calculated. Thereby, information was obtained about the state of stresses induced in the mortar joint using the new test arrangement. For this reason, five additional specimens of each brick-mortar combination were prepared as described in Chapter 4, and tested under the same applied normal stress as in Series # I and V (very low normal compressive stress). The additional tests are named: Series # IA and Series # VA. The specimen behaviour during the testing was documented by means of digital images. Every second, approximately two digital images were recorded. On average, depending on total duration, 1100 to 1300 digital images were recorded for each test. In addition, for the sake of validation, the relative

displacement between the upper and lower bricks was also recorded every second using LSCs.

5.3.1 Methodology of Analysis

The recorded digital images were analysed using a MATLAB module described in Chapter 4. Before applying the MATLAB module, a factor for converting coordinates from image-space to object-space was determined. To obtain the factor, the difference in pixels between two points was divided by the actual distance between the two points. For each specimen, this calculation was carried out for six pairs of points selected along the outer edges of the specimens, and an average factor of $0.06\,mm/pixel$ was obtained. The accuracy of this factor is evident by the very low COV of 0.35%.

In the analysis, 10 patches were selected along the length of the mortar joint with the aim to obtain the shear strain level in the mortar joint. In addition, 10 further patches were selected close to the mortar-brick interface with the intent to determine the shear strain distribution along the interfaces, as shown in Figure 5.15. In the figure, the small squares are the patches selected.

Figure 5.15: Meshed patches

From evaluation of the digital images, the MATLAB module produces text files which contain image-space coordinates of the patches for each evaluated digital image. The text files were first converted to MS Excel files, and then analysed using MS Excel. The analysis of the data included the conversion of image-space coordinates to object-space coordinates, in order to obtain the coordinates of the 20 patches in each image as well as the relative displacement between the neighbouring patches. To validate the results obtained using the GeoPIV measurement-system, the values of relative displacement between Patches # 5 and 6 were compared with the values obtained using LSCs. The relative displacement between these two patches corresponds to the displacement measured by the LSC on the back of the specimen. Figure 5.16 shows the typical results and that both measurements agree with each other very well.

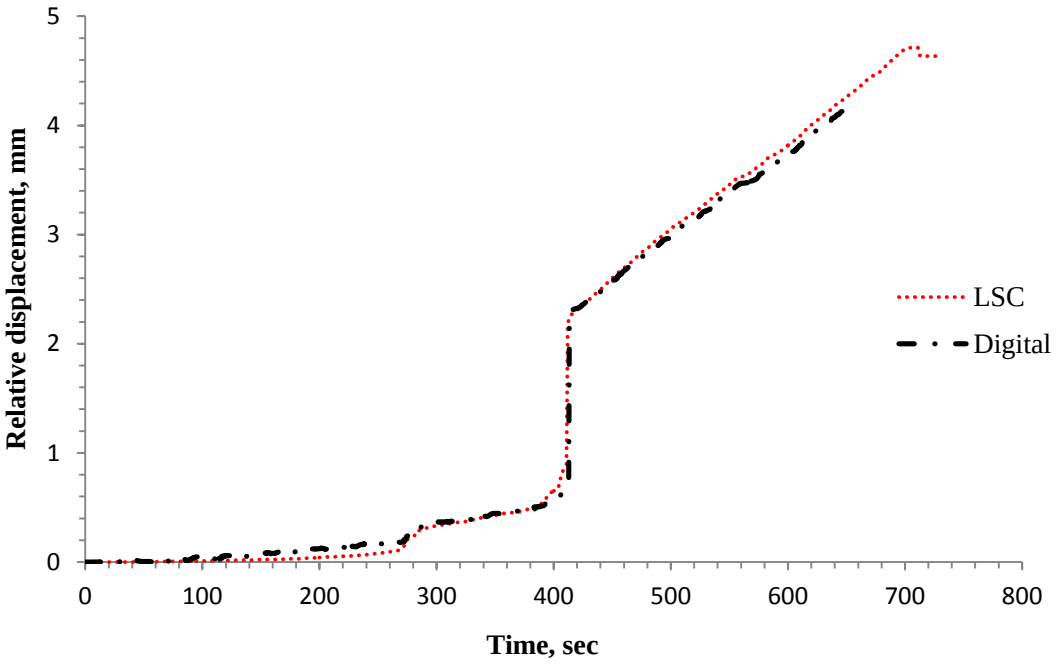

Figure 5.16: Comparison of LSC and Digital GeoPIV Displacement Measurements for Specimen # 2 in Series IA

Both the horizontal and vertical relative displacement between the neighbouring patches is required to obtain the shear strain for each rectangle bound by four patches, as shown in Figure 5.17. For the calculation of shear strain, only data from the earlier stages of testing, where the load-displacement relationship was continuous, linear-elastic, were considered. The shear strain ($\gamma_{\alpha\beta}$) was calculated using the GeoPIV measurements and shear strain theory as shown in Figure 5.18.

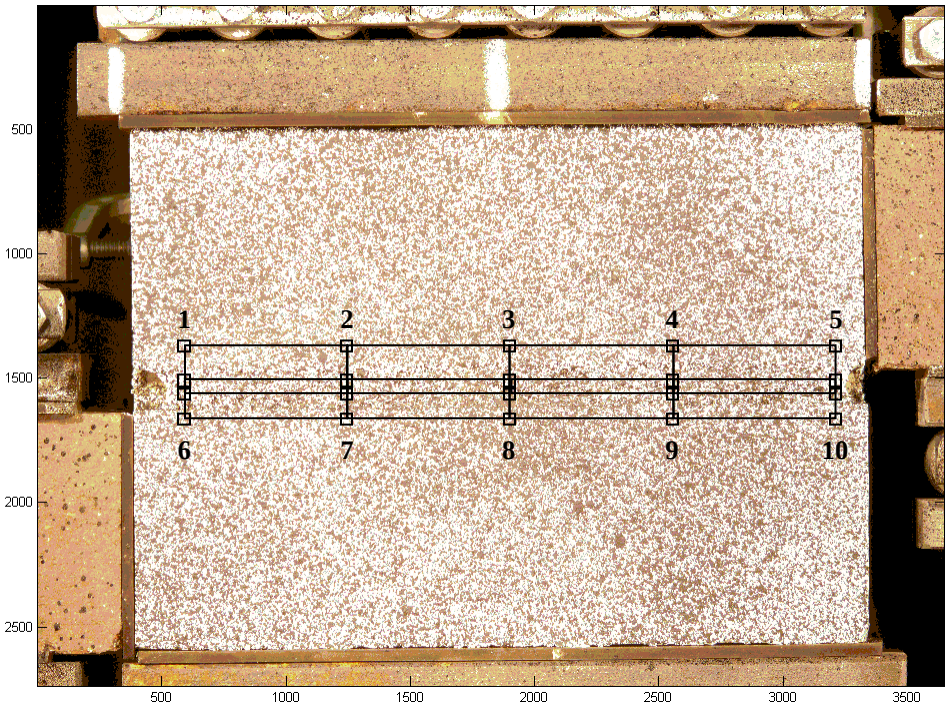

Figure 5.17: Rectangles used for shear strain calculations

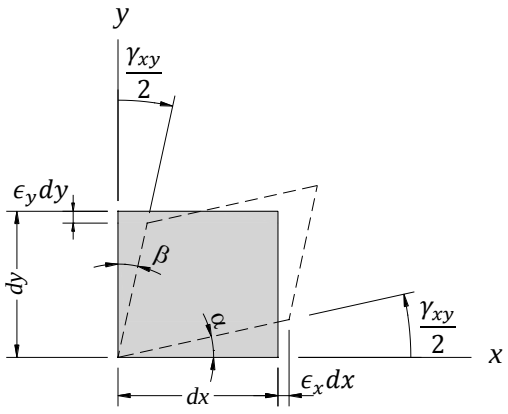

Figure 5.18: Shear strain

Using the patch coordinates, the shear strain for each of the rectangles is calculated as in the following example for rectangle 1,2,6,7:

$$\gamma_{\alpha,1267} = \frac{y_7 - y_6}{x_7 - x_6} \quad \textbf{(4)}$$

$$\gamma_{\beta,1267} = \frac{x_7 - x_2}{y_7 - y_2} \quad \textbf{(5)}$$

$$\gamma_{\alpha\beta,1267} = \gamma_{\alpha,1267} + \gamma_{b,1267} \quad \textbf{(6)}$$

5.3.2 Results & Discussion

Initially, the shear strain, $\gamma_{\alpha\beta}$, in the mortar joint was calculated using equations (4) through (6) from the relative displacement of the 10 patches in the mortar joint (unnumbered patches in Figure 5.17). The mean results are listed with the corresponding time frame, COV, and load in Table 5.2. Assuming a constant shear modulus, the shear stress along the mortar joint can be calculated from the shear strain using Eq. (7) and Eq.(8), where $\tau_{i,joint}$ is the shear stress along the mortar joint at time i, $\gamma_{\alpha\beta_i}$ is the calculated shear strain at time i, and G, E and υ are the Shear modulus, Young's modulus and the Poisson's ratio of the mortar, respectively.

$$\tau_{i,joint} = G * \gamma_{\alpha\beta_i} \quad \textbf{(7)}$$

$$G = \frac{E}{2 * (1 + \upsilon)} \quad \textbf{(8)}$$

Some important observations can be made from the results in Table 5.2. First of all, considering the magnitude of the corresponding loads, one would expect average shear stresses in the order of 0.10 to 0.50 N/mm^2. However, the calculated results for shear stress, $\tau_{i,joint}$ listed in Table 5.2, are much higher, which is unreasonable. The error in calculating the shear stresses could result from a variety of sources. First, the properties of the mortar given in Table 3.1, are selected from the literature, and therefore differ from the actual properties of the mortar used in this research program. Secondly,

Eq. (8) is based on the assumption that the material is isotropic, homogeneous and behaves in a linear-elastic manner. Although masonry is often assumed to be an isotropic and homogenous material, and this assumption may lead to reasonable results at the meso- and macro-level, at the micro-level, where the units and joints are considered separately, this assumption is questionable. The very nature of the constituent materials and the mixing and placing of the mortar make it nearly impossible to guarantee homogeneity of the mortar joint. In addition, Eq. (7) is derived for materials subjected to pure shear. This is not the case for the test method used in this research because the eccentrically applied load also produces a bending moment. Therefore, more research is necessary to obtain the properties of the mortar, and the knowledge obtained can then be used to determine the exact state of stress along the mortar joint.

Another important observation from Table 5.2 is that the shear strain values are very scattered indicating a non-uniform distribution of the shear strain in the mortar joint. The high variation in the strain could also result from a variety of sources including the mortar properties and the graphical resolution. With the 10 Megapixel camera utilized, a movement of one pixel represents a displacement of $0.06\,mm$ in reality. The effect of graphical resolution becomes particularly noticeable in the case of very small relative displacements (less than one pixel), and results in a higher amount of scatter as seen at the earlier stages of testing in Table 5.2. This is also the most likely explanation for the extremely high variation in the normal strain (also reported in Table 5.2). In addition, since the mortar is a granular material, the irregularity in the results of normal and shear strain in the middle of the joint may also be due to dilation that occurs when the fractured

surfaces slide past each other during the testing procedure. As noted, a movement of one pixel represents a displacement of only $0.06\,mm$ in reality. Hence, a very small displacement, either positive or negative, in the vertical direction will contribute to the irregularity of the results. Therefore, a digital camera with a graphical resolution of at least 15 Megapixels is recommended.

Since the results within the mortar joint were likely affected significantly by the graphical resolution, a larger area of analysis was chosen to try to minimize this effect. Therefore, additional patches (numbered 1 – 10 in Figure 5.17) were selected at the mortar-brick interface to obtain the strains over the entire joint.

In Table 5.3, the mean results for shear strain ($\gamma_{\alpha\beta}$) calculated from the relative displacement of the 10 patches at the mortar-brick interfaces are listed with the corresponding time frame, COV, and load. The low amount of scatter of the shear strain values leads to the conclusion that the distribution of the shear strain, and consequently the shear stress, along the joint is uniform. As discussed above, the shear modulus, *G*, for the mortar cannot be determined, thus, the average shear stress in the joint was calculated using Eq. (9):

$$\tau_{avg_i} = \frac{F_{t_i}}{A} \qquad \textbf{(9)}$$

where τ_{avg_i} is the average shear stress along the joint at time i, F_{t_i} is the measured applied horizontal load at time i, and A is the gross cross-sectional area at the interface. The results for shear stress obtained using Eq. (9) are also listed in Table 5.3. Unlike the

shear strain, the values of the normal strain, ε_y, (i.e. normal to the mortar joint) still indicate a non-uniform distribution as evident by the high value of COV. However, as mentioned above, the high COVs for the normal strains are most likely due to the very small displacements, either positive or negative, in the vertical direction and insufficient graphical resolution provided by the 10 Megapixel camera. Scatter in the normal strains may also be related to the bending moment that is induced by the eccentrically applied horizontal load (overturning did occur as evidenced by the uplift).

The results obtained from the FEM analysis in Chapter 3 indicated that the proposed test arrangement produces a more uniform stress distribution than the triplet test and the results are as good as, if not better than, the Hofmann & Stöckl test. However, in order to compare the state of strain/stress for the triplet and Hofmann & Stöckl tests, experiments using the GeoPIV measurement system would be necessary.

Table 5.2: Mean values for four rectangles selected within the mortar joint

	Time (sec)	$\gamma_{\alpha\beta}$	COV (%)	Load (N)	$\tau_{i,\,joint}$ (N/mm^2)	ε_y	COV (%)
Dry Pressed Bricks							
Specimen IA-1	117	0.0005	105	2000	1.8	0.001	128
	155	0.0013	49	3000	4.7	0.0006	311
	192	0.0015	64	4000	5.4	0.0008	226
	229	0.0018	42	5000	6.5	0.0009	233
Specimen IA-2	242	0.0014	139	4774	5.0	0.0005	158
	257	0.0017	137	5518	6.0	0.0006	197
	273	0.0023	170	6263	8.0	0.0009	203
	288	0.0030	188	7007	10.8	0.0018	207
Specimen IA-3	151	0.0005	90	3125	1.8	0.0001	303
	168	0.0008	89	3750	2.9	0.0002	392
	185	0.0015	127	4375	5.4	0.0007	211
	202	0.0031	143	5000	11.2	0.0010	189
Specimen IA-4	203	0.0008	45	3375	2.9	0.0002	125
	228	0.0005	67	4250	1.8	0.0001	162
	252	0.0007	70	5125	2.5	0.0001	170
	277	0.0006	81	6000	2.2	0.0002	112
Specimen IA-5	144	0.0007	113	3771	2.5	0.0012	125
	162	0.0014	91	4526	5.0	0.0012	160
	180	0.0006	72	5280	2.2	0.0014	137
	198	0.0018	93	6034	6.5	0.0015	167

Extruded Bricks							
Specimen VA-1	444	0.0015	154	5355	5.4	0.00004	430
	463	0.0013	156	6000	4.7	0.00004	797
	481	0.0024	171	6644	8.6	0.0001	173
	500	0.0021	107	7289	7.6	0.0002	93
Specimen VA-2	449	0.0006	85	3897	2.2	0.0001	429
	474	0.0007	30	4525	2.5	0.0003	141
	499	0.0007	43	5152	2.5	0.0002	317
	524	0.0013	76	5780	4.7	0.0001	168
Specimen VA-3	213	0.0005	41	1876	1.8	0.0001	217
	252	0.0009	78	2749	3.2	0.0002	226
	290	0.0008	79	3623	2.9	0.0002	95
	328	0.0015	86	4496	5.4	0.0001	442
Specimen VA-4	261	0.0006	137	1825	2.2	0.0001	203
	297	0.0005	69	2550	1.8	0.0001	227
	332	0.0006	40	3275	2.2	0.0002	86
	367	0.0012	74	4000	4.3	0.0001	298
Specimen VA-5	254	0.0004	82	1627	1.4	0.0001	249
	288	0.0005	38	2253	1.8	0.0003	213
	323	0.0015	67	2878	5.4	0.0002	246
	357	0.0013	40	3503	4.7	0.00008	642

Table 5.3: Mean values for four rectangles encompassing the mortar joint

	Time (sec)	$\gamma_{\alpha\beta}$	COV (%)	Load (N)	τ_{avgi} (N/mm^2)	ε_y	COV (%)
Dry Pressed Bricks							
Specimen IA-1	117	0.0004	59	2000	0.12	0.0002	194
	155	0.0002	46	3000	0.18	0.0001	561
	192	0.0002	36	4000	0.23	0.0001	150
	229	0.0007	54	5000	0.29	0.0001	207
Specimen IA-2	242	0.0029	14	4774	0.28	0.0037	78
	257	0.0078	4	5518	0.32	0.0070	86
	273	0.0095	3	6263	0.37	0.0086	85
	288	0.0116	2	7007	0.41	0.0107	85
Specimen IA-3	151	0.0015	21	3125	0.18	0.00002	379
	168	0.0035	6	3750	0.22	0.00009	339
	185	0.0053	2	4375	0.26	0.00024	180
	202	0.0068	5	5000	0.29	0.00073	86
Specimen IA-4	203	0.0041	7	3375	0.20	0.0004	87
	228	0.0058	3	4250	0.25	0.0006	130
	252	0.0094	4	5125	0.30	0.0006	153
	277	0.0113	3	6000	0.35	0.0008	133
Specimen IA-5	144	0.0015	8	3771	0.22	0.0008	62
	162	0.0026	14	4526	0.26	0.0015	68
	180	0.0036	3	5280	0.31	0.0023	47
	198	0.0050	10	6034	0.35	0.0014	51

Extruded Bricks							
Specimen VA-1	444	0.0025	12	5355	0.29	0.0001	103
	463	0.0036	10	6000	0.33	0.0001	155
	481	0.0059	12	6644	0.36	0.0001	32
	500	0.0078	10	7289	0.40	0.0001	51
Specimen VA-2	449	0.0006	85	3897	0.21	0.0001	121
	474	0.0007	30	4525	0.26	0.0002	82
	499	0.0007	43	5152	0.30	0.0001	89
	524	0.0013	76	5780	0.34	0.00003	292
Specimen VA-3	213	0.0002	40	1876	0.10	0.00004	51
	252	0.0003	32	2749	0.15	0.0001	69
	290	0.0002	121	3623	0.20	0.00001	444
	328	0.0006	14	4496	0.25	0.00005	117
Specimen VA-4	261	0.0004	57	1825	0.10	0.00004	192
	297	0.0003	29	2550	0.14	0.00004	119
	332	0.0004	66	3275	0.18	0.00005	107
	367	0.0003	58	4000	0.22	0.00005	40
Specimen VA-5	254	0.0003	74	1627	0.09	0.00001	74
	288	0.0003	37	2253	0.12	0.00005	58
	323	0.0003	56	2878	0.16	0.0001	33
	357	0.0002	90	3503	0.19	0.0001	99

In Figure 5.19, typical results for both the displaced and initial position of the patches are presented. The comparison confirms that the specimens experienced a small rotation as mentioned in 5.2.1.1 and 5.2.1.2. Nonetheless, the performance of the new test method, in terms of the reproducibility, and the uniform shear strain induced in the joint as determined from the GeoPIV measurements, is very good since the aim was to design a simple test that induces uniform shear in the joint. The main issue with the proposed

test arrangement is the overturning of the specimen caused by the eccentrically applied horizontal load. Therefore, an improvement in the test arrangement is necessary. A modified version of the test setup is presented in Chapter 6. However, as long as the horizontal load is eccentrically applied to the specimen; the specimen will be subjected to a bending moment.

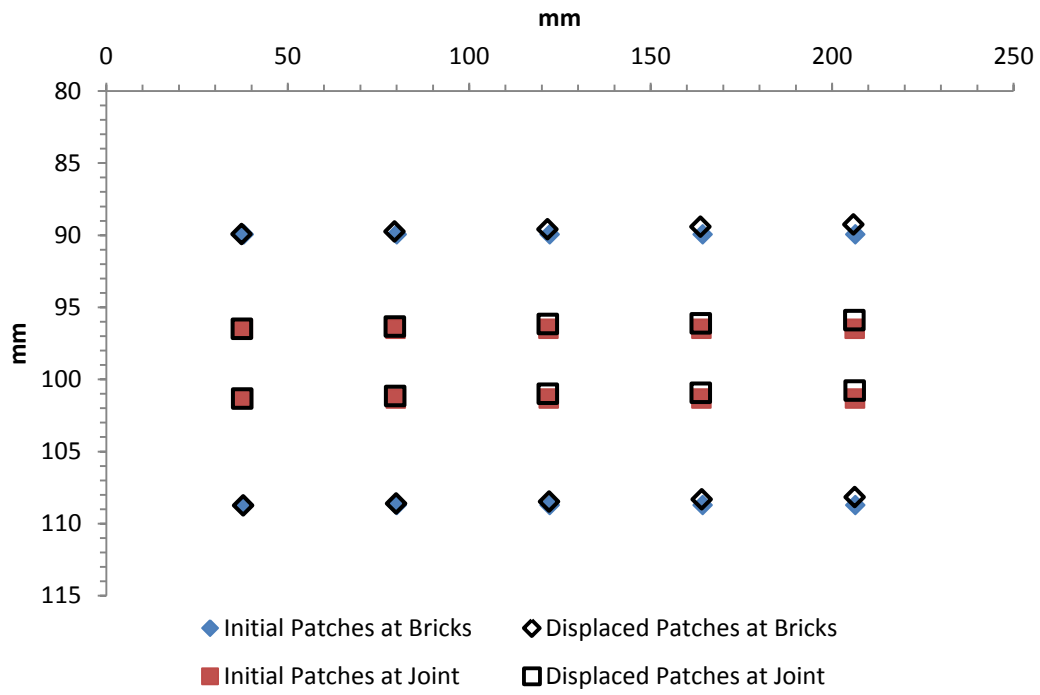

Figure 5.19: Typical displaced versus initial patches for Specimen 2 in Series IA

5.4 Summary

In total, 50 specimens were tested using the new test arrangement described in Chapter 4. The results of 40 specimens were obtained using LSCs, and were compared to confirm the reproducibility of the results using the new test method as summarized in Table 5.1.

Ten further tests were conducted using a digital imaging measurement technique which made it possible to calculate strains in the specimens. The digital images were evaluated using a MATLAB-module named GeoPIV. The results presented in Table 5.3 show that the new test method produces uniform shear strain along the joint.

The experimental work as well as the data analysis indicates that the main issue with the new test method is the small overturning of the specimens due to the eccentrically applied horizontal load. Therefore, a modification of the test method is necessary to minimize the overturning as much as possible.

CHAPTER 6: **CONCLUSIONS & RECOMMENDATIONS**

6.1 Summary

In a structure made of masonry, lateral loads, caused by wind or earthquake, are resisted by masonry shear walls. The shear strength of a masonry wall depends on many factors including the strength of units and the mortar bed joints. Therefore, over the last few decades, several test arrangements were devised and utilized by researchers to examine the shear strength of a mortar bed joint. The numerical analysis presented in this thesis shows that the Hofmann & Stöckl test produces nearly uniform normal and shear stresses along the bed joint, however it requires very complex equipment. On the other hand, the triplet test is simpler to perform, but the numerical analysis showed that it does not produce uniformly distributed stress.

The new test method described in this thesis was devised to combine the advantages of the Hofmann & Stöckl and the triplet tests. In the test arrangement designed, the couplet can be subjected to a horizontal load or to a combination of horizontal and vertical loads. The proposed test method was initially compared with the triplet and Hofmann & Stöckl tests using a two-dimensional finite element model in the commercial software package SAP2000. In addition to the FEM evaluation, an experimental program was conducted. Couplets constructed of two types of clay bricks (dry-pressed and extruded) and one type of mortar (Type S) were tested to evaluate the reproducibility of the results using the new test method. In total, 50 specimens, 25 for each brick type, were tested at four different levels of normal pre-compressive stress. The relative displacements between the upper and lower bricks of the specimen were

measured with linear strain converters (LSCs), and also a measurement system based on Particle Image Velocimetry (GeoPIV).

6.2 Conclusions

The conclusions below are derived from the results of the numerical evaluation and the results of the experimental program presented in Chapters 3 and 5, respectively.

6.2.1 Finite element model

The results obtained from Case Study 1 prove that the new test method is capable of producing desirable results for nearly uniform shear stress in a mortar joint, and that no tensile stress is induced in the bed joint. Compared to the triplet test, the resulting distributions of normal and shear stresses in the new test method are more uniform, and are based only on one mortar joint, rather than two as in the triplet test, which only provides results for the weakest one. Further, unlike the case of the triplet test, no tensile stress is induced in the bed joint. Compared to the Hofmann & Stöckl test, the distribution of shear stress in the proposed test method is similar.

Results obtained from Case Study 2 indicate that the magnitude of normal tensile stress along the mortar joint for the Hofmann & Stöckl test is not as high as reported in the literature.

The finite element evaluations show that the new test method can clearly be an alternative to the Hofmann & Stöckl and triplet tests.

6.2.2 Experimental work

A new test arrangement was constructed using simple equipment which can be found in any civil engineering laboratory. The new test method was used to test 50 couplets. The tests conducted were divided into eight series with varying levels of pre-compression. The load-displacement behaviour of 40 specimens based on measurements using Linear Strain Converters (LSCs) proves that the new test method generates reproducible results. The peak values for load-displacement behaviour measured during the experimental work were affected by the amount of mortar that flowed into the holes of the bricks when the specimens were constructed and the resulting mechanical action between these mortar cylinders and the bricks.

The remaining ten specimens were used in combination with the GeoPIV measurement system to gain insight into the state of normal and shear stress that are induced in the mortar bed joint using the new test method. The specimen behaviour during the testing was documented by means of digital images and the images were analysed using a MATLAB module to determine the relative displacement between user-defined points. To the best of the author's knowledge, this is the first time that the strain or stress in the joint has been evaluated in any micro-level joint shear test. The results obtained prove that the new test method produces uniform shear strain in the mortar joint. Assuming a constant shear modulus, the shear stress will be as uniform as the strain. However, for the shear stress calculation the application of Eq. (7), $\tau_{i,joint} = G * \gamma_{\alpha\beta_i}$, is questionable, since the assumption that masonry is an isotropic and homogenous material cannot be guaranteed at the micro-level. In addition, Eq. (7),

$\tau_{i,joint} = G * \gamma_{\alpha\beta_i}$, is derived for materials subjected to pure shear which was not the case for the test method used in this research because the eccentrically applied load also produces a bending moment.

The distribution of the normal strains did not show uniformity, most likely due to the bending moment from the eccentrically applied horizontal load, and that the graphical resolution was not sufficient to capture the extremely small normal deformations. The irregularity of the results of normal and shear strain in the middle of the joint may also be a result of the small order of magnitude of the values and from dilation that occurs during the testing procedure.

6.3 Recommendations for future work

The results obtained from the experimental work and the GeoPIV measurements indicate that the specimen is subjected to a small rotation during the test. This rotation is a result of the eccentrically applied horizontal load, and of the compressibility of the rubber sheets used to accommodate the unevenness of the surface of the bricks.

The rotation of the specimens is the main disadvantage of the new test method. To overcome this limitation, the test setup should be modified as presented in Figure 6.1. The modification consists of adding a support plate connected by four threaded rods to the upper flange of the lower beam. This support plate will prevent the overturning of the specimen to a large degree. The increase of pre-applied vertical load during the testing phase can then be measured by the load cells placed between the support plate and hex-nuts. In addition, a load plate with circular cross section is added to provide a surface for

the manually operated jack. Further improvement can be achieved either by removing the rubber sheets and using an alternative material that is able to accommodate the unevenness of the surface of the brick with high compressive resistance, e.g. plaster of Paris. Further, it was concluded that the peak values measured during the experimental work were affected by the amount of mortar that flowed into the holes of the bricks while the specimens were constructed. Therefore, more studies about the effect of the mortar cylinder on the load-displacement behaviour are necessary. In this regard, the cores should be covered or plugged partially or completely to prevent mortar entering. A study should be undertaken with the cores of the specimens unfilled and filled to four different heights, namely: quarter, half, three-quarter, and full. This procedure will provide knowledge about the effect of the mortar cylinders.

Besides the above suggested modifications and recommendations, the following points are recommended:

1. The use of a digital camera with a graphical resolution of at least 15 megapixels is recommended. This combined with the above suggested modification should significantly reduce the scatter of the results for normal strain.

2. More research is needed to determine the stress distribution in the mortar joint precisely.

3. FE analysis with a non-uniform compressive stress is recommended to compare to the actual test results. The analysis is feasible with the

modified test arrangement and the magnitude of the vertical load that will be provided by the cell loads, see Figure 6.1.

4. In order to compare the state of strain/stress for the triplet and Hofmann & Stöckl test methods, experiments using the GeoPIV measurement system would be necessary, and are recommended.

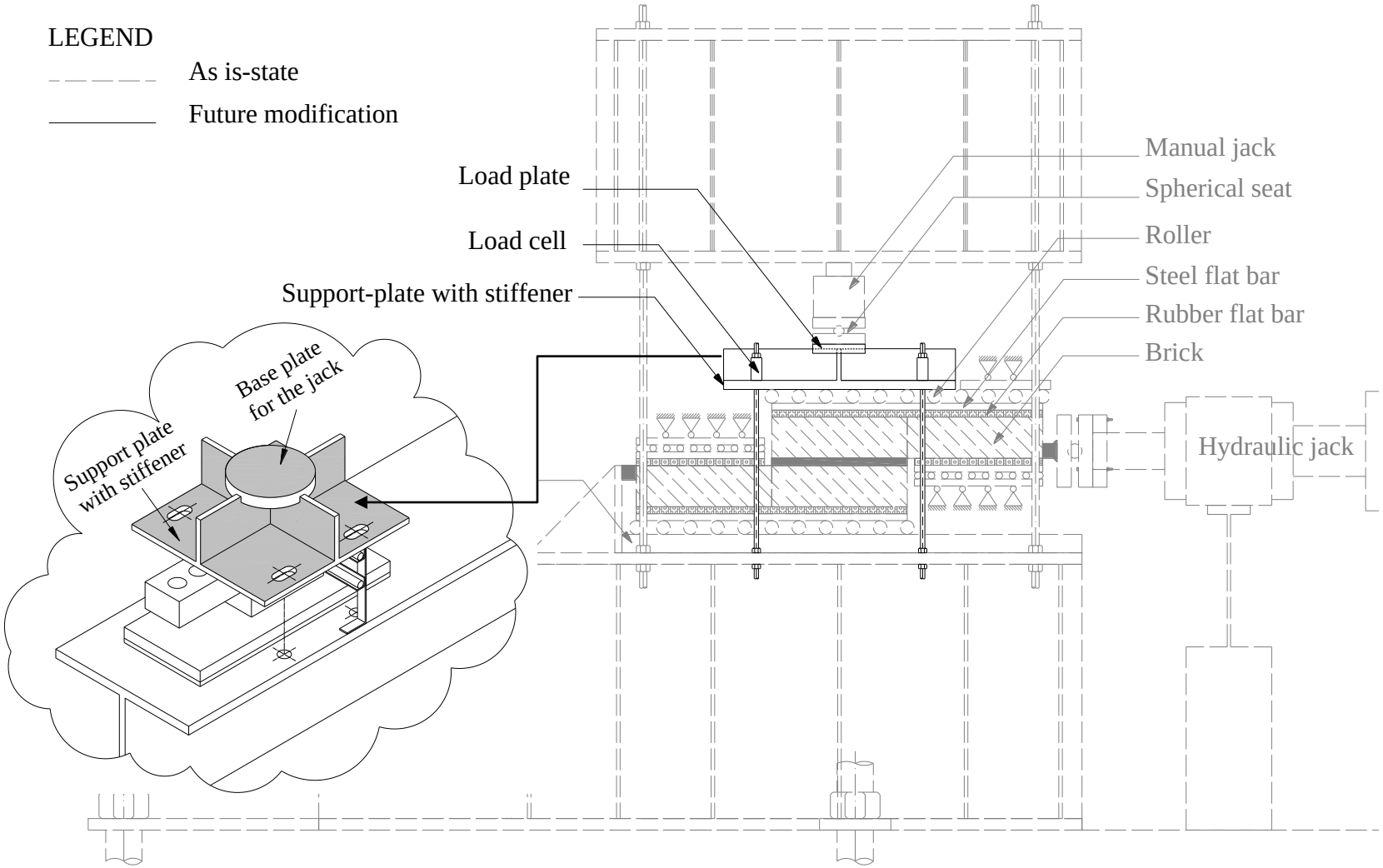

Figure 6.1: Suggested modifications to as is-state of the test setup

REFFERENCES

Adrian, R. J., 1991. Particle imaging techniques for experimental fluid mechanics. *Annu. Rev. of Fluid Mech.,* Volume 23, pp. 261-304.

Bisby, L. A. & Take, W. A., 2009. *Strain localisations in FRP confined concrete: new insights.* s.l., s.n., pp. 1-9.

Bisby, L., Take, W. & Caspary, A., 2007. *Quantifying strain variation in FRP confined concrete using digital image analysis.* Hong Kong, s.n., pp. 599-604.

Bouzeghoub, M., Jukes, P. & Riddington, J., 1995. Influence of loading arrangement on the initial mode of failure of brick triplet shear specimens. In: *Comput. Mehtod in Structural Masonry - 3. Eds.* s.l.:s.n., pp. 117-126.

CSA A179-04, C. S., 2004. *Mortar and grout for unit masonry,* Ontario: Canadian Standards Association.

CSA A82-06, C. S., 2006. *Fired Masonry Brick Made from Clay or Shale,* Ontario: Canadian Standard Association.

DIN EN 1052-3, I. 9., 2007. *Methods of test for masonry – Part 3: Determination of initial shear strength; German version EN 1052-3:2002 + A1:2007,* Brussels: EUROPEAN COMMITTEE FOR STANDARDIZATION.

Ghazali, M. & Riddington, J., 1986. *Shear strength of brickwork.* Bankok, s.n., pp. 593-604.

Ghazali, M. & Riddington, J., 1988. Simple test method for masonry shear strength. *Proc. Institution of Civil Engineers, Part 2,* Volume 85, pp. 567-574.

Hamid, A. A. & Drysdale, R. G., 1982. The shear behaviour of brickwork bed joints. *Proc. of the British Ceramic Soc.*, 09, Volume 30, pp. 101-109.

Hamid, A., Drysdale, R. & Heidebrecht, A. C., 1979. Shear strength of concrete masonry joints. *J. of the Structural Division,* Volume 105, pp. 1227-1240.

Hansen, K. F., Nykanen, E. & Gottfredsen, F. R., 1998. Shear behaviour of bed joints at different levels of precompression. *Masonry Int.,* 12(2), pp. 70-78.

Hansen, K. F. & Pedersen, C. M., 2008. Torsion testing of bed joints. *Int. Masonry Society,* 12(1), pp. 43-48.

Hansen, K. & Pedersen, E., 2009. Shear and torsion testing of brick-mortar joints. *Masonry Int.,* Volume 22, pp. 31-38.

Hofmann, P. & Stöckl, S., 1986. Tests on shear-bond behaviour in the bed-joints of masonry. *Masonry Int.,* 12, Volume 9, pp. 1-15.

Jiang, D.-H. & Xiao, X.-S., 1994. *A new masonry shear test method determining masonry shear strength.* Calgary, s.n., pp. 1013-1019.

Jukes, P. & Riddington, J., 1997. A review of masonry joint shear strength test methods. *Masonry Int.,* Volume 11, pp. 37-43.

Khalaf, F., 1995. *Simple bending test for the determination of masonry bond shear strength.* s.l., s.n.

Khalaf, F. M. & Naysmith, M. W., 1997. Shear strength of masonry bed joints. *The Masonry Society,* 15(2), pp. 13-22.

Lissel, S. L., 2001. *Behaviour and Design of CFRP Post-Tensioned Masonry Diaphragm Walls,* Calgary: University of Calgary.

Masia, M. J., Han, Y. & Correa, M. R. S., 2006. Torsion testing for the characterisation of the shear behaviour of mortar joints in masonry. *J. of the British Masonry Soc., Masnory Int.,* 19(2), pp. 77-88.

Masia, M. J., Petersen, R. B., Han, Y. & Correa, M. R. S., 2010. Torsion shear test for mortar joints in masonry: experimental evaluation. *J. of the Int. Masonry Soc.,* 09, 23(3), pp. 91-102.

Pook, L., Stylianou, M. & Dawe, J., 1986. *Experimental investigation of the influence of compression on the shear strength of masonry joints.* s.l., s.n., pp. 1053-1062.

Popal, R. & Lissel, S. L., 2010. *Numerical evaluation of existing mortar joint shear tests and a new test method.* Dresden, s.n., pp. 795-802.

Riddington, J., Fong, K. & Jukes, P., 1997. Numerical study of failure initiation in different joint shear test. *Masonry Int.,* Volume 11, pp. 44-50.

Riddington, J. & Jukes, P., 1994. *A masonry joint shear strength test method.* s.l., s.n., pp. 267-274.

Riddington, J. R., Gambo, A. H. & Edgell, G. J., 1991. *An assessment of the influence of unit aspect ratio on bond shear srtength values given by the proposed CEN triplet test.* Berlin, s.n., pp. 1321-1328.

Riddington, J. R. & Ghazali, M. Z., 1987. *Shear strength of masonry joints at high normal stress levels.* Kuala Lumpur, s.n., pp. 1-11.

Riddington, J. R. & Ghazali, M. Z., 1990. Hypothesis for shear failure in masonry joints. *Proc. Institution of Civil Engineers, Part 2,* 03, Volume 89, pp. 89-102.

Samarasinghe, W. & Lawrence, S., 1994. *Behaviour of masonry under combined torsion and compression.* Calgary, s.n., pp. 1057-1066.

Stöckl, S. & Hofmann, J., 1990. A Comparative finite element evaluation of mortar joint shear tests. *Masonry Int.,* Volume 3, pp. 101-104.

Sutcliffe, D. J., Yu, H. S. & Page, A. W., 2001. Lower bound limit analysis of unreinforced masonry shear walls. *Comput. and Structures,* pp. 1295 - 1312.

van der Pluijm, R., 1992. *Material properties of masonry and its components under tension and shear.* Saskatoon, s.n., pp. 675-686.

van der Pluijm, R., 1993. *Shear behaviour of bed joints.* Philadelphia, s.n., pp. 125-136.

van Vliet, i. M., 2004. *Shear tests on masonry panels; Literature survey and proposal for experiments,* s.l.: s.n.

Vermeltfoort, A. T., 2010. *Variation in shear properties of masonry.* Dresden, Int. Masonry Society.

White, D. & Take, W., 2002. *GeoPIV: Paritcale Image Velocimety (PIV) software for use in geotechnical testing,* s.l.: Cambridge University Engineering Departement.

White, D., Take, W. & Bolton, M., 2001a. *Measuring soil deformation in geotechnical models using digital images and PIV analysis.* Tucson, Arizona, Balkema, Rotterdam, pp. 997-1002.

White, D., Take, W., Bolton, M. & Munachen, S., 2001b. *A deformation measurement sustem for geotechnical testing based on digitla imaging, close-range photogrammetry, and PIV image analysis.* Instanbul, Turkey, Balkema, Rotterdam, pp. 539-542.

APPENDIX A: RAW DATA

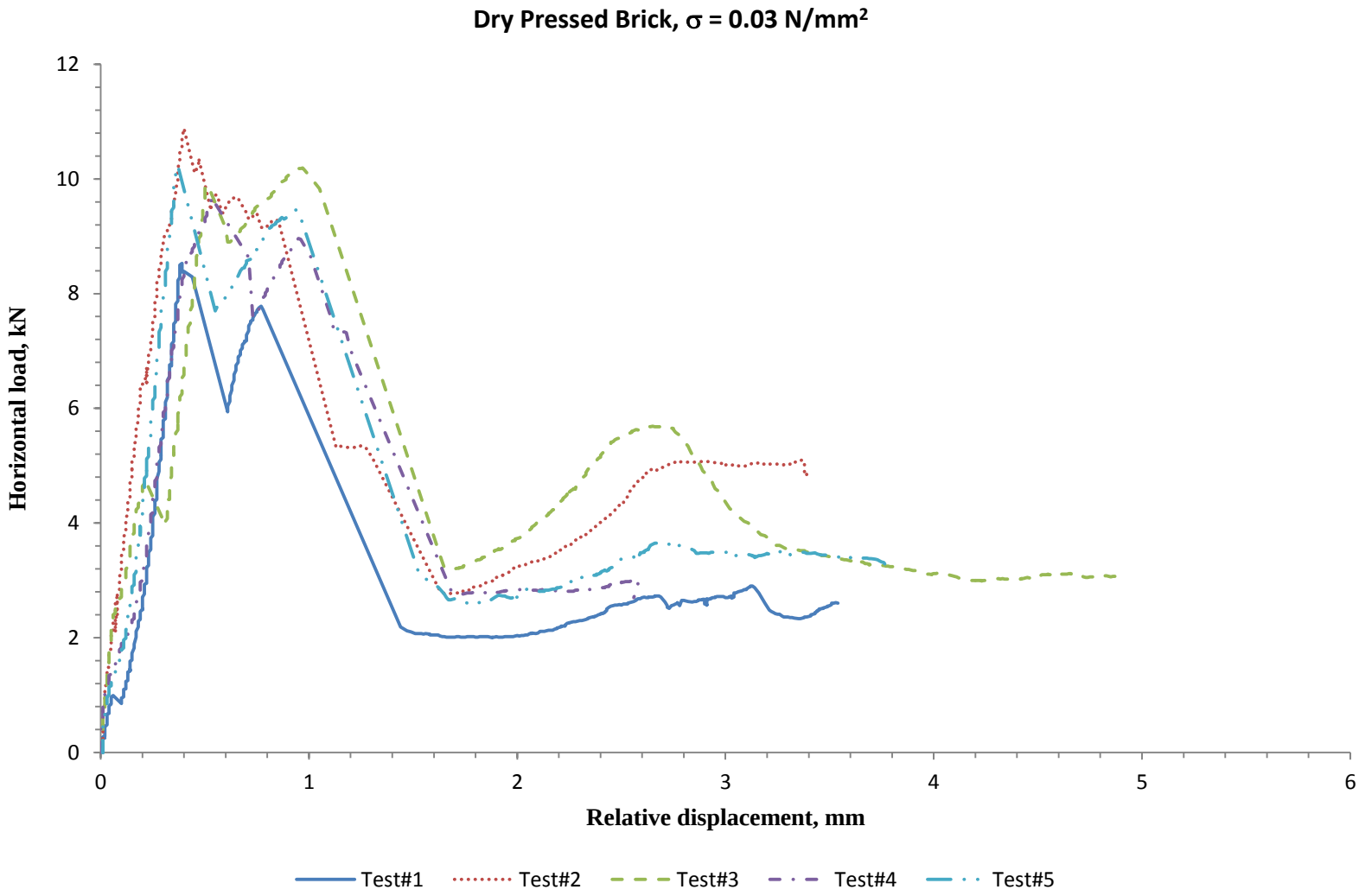
Dry Pressed Brick, σ = 0.03 N/mm²
Horizontal load, kN
Relative displacement, mm
0
2
4
6
8
10
12
0
1
2
3
4
5
6
Test#1
Test#2
Test#3
Test#4
Test#5

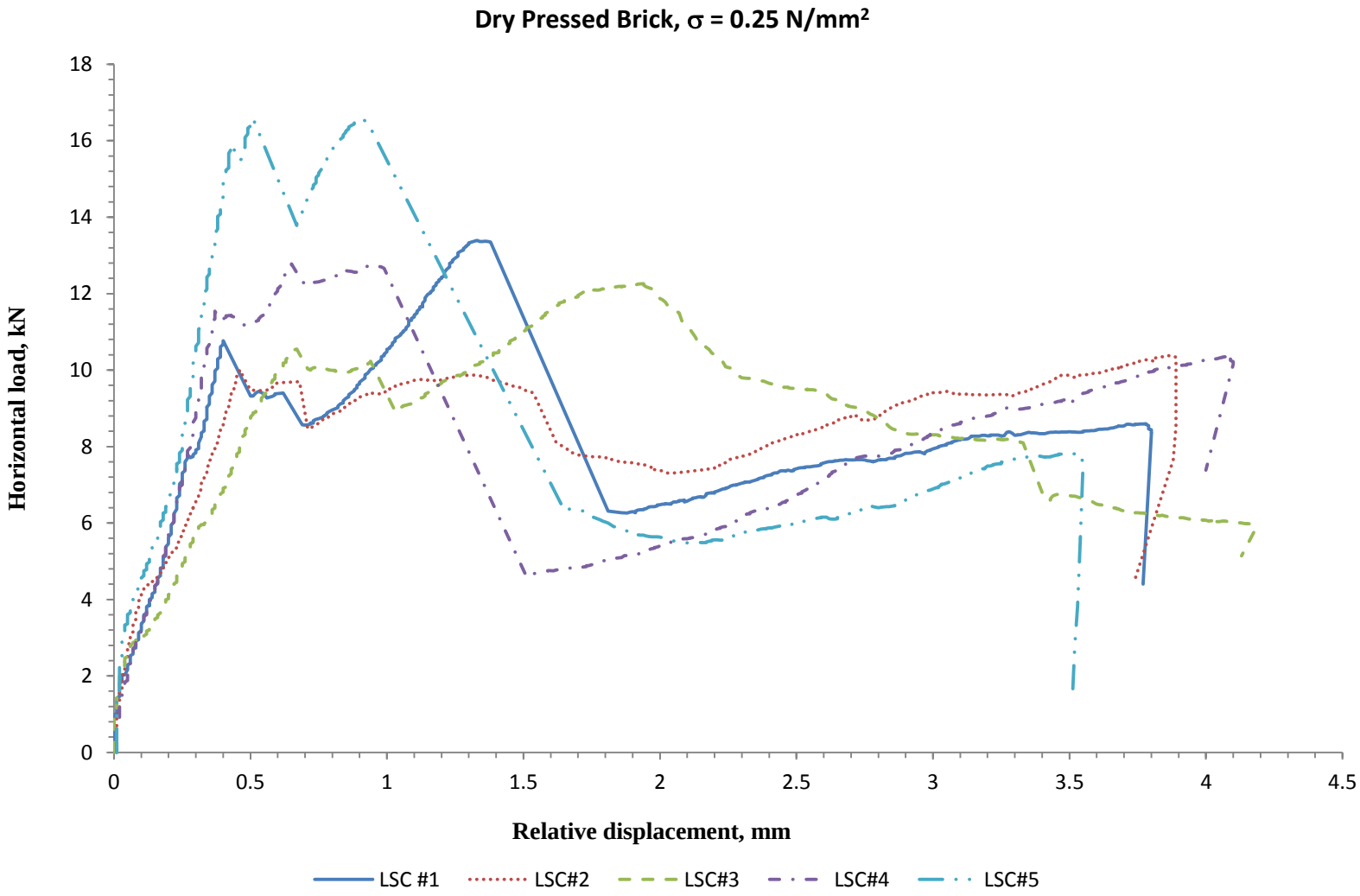
Dry Pressed Brick, σ = 0.25 N/mm²
Horizontal load, kN
Relative displacement, mm
0
2
4
6
8
10
12
14
16
18
0
0.5
1
1.5
2
2.5
3
3.5
4
4.5
LSC #1
LSC#2
LSC#3
LSC#4
LSC#5

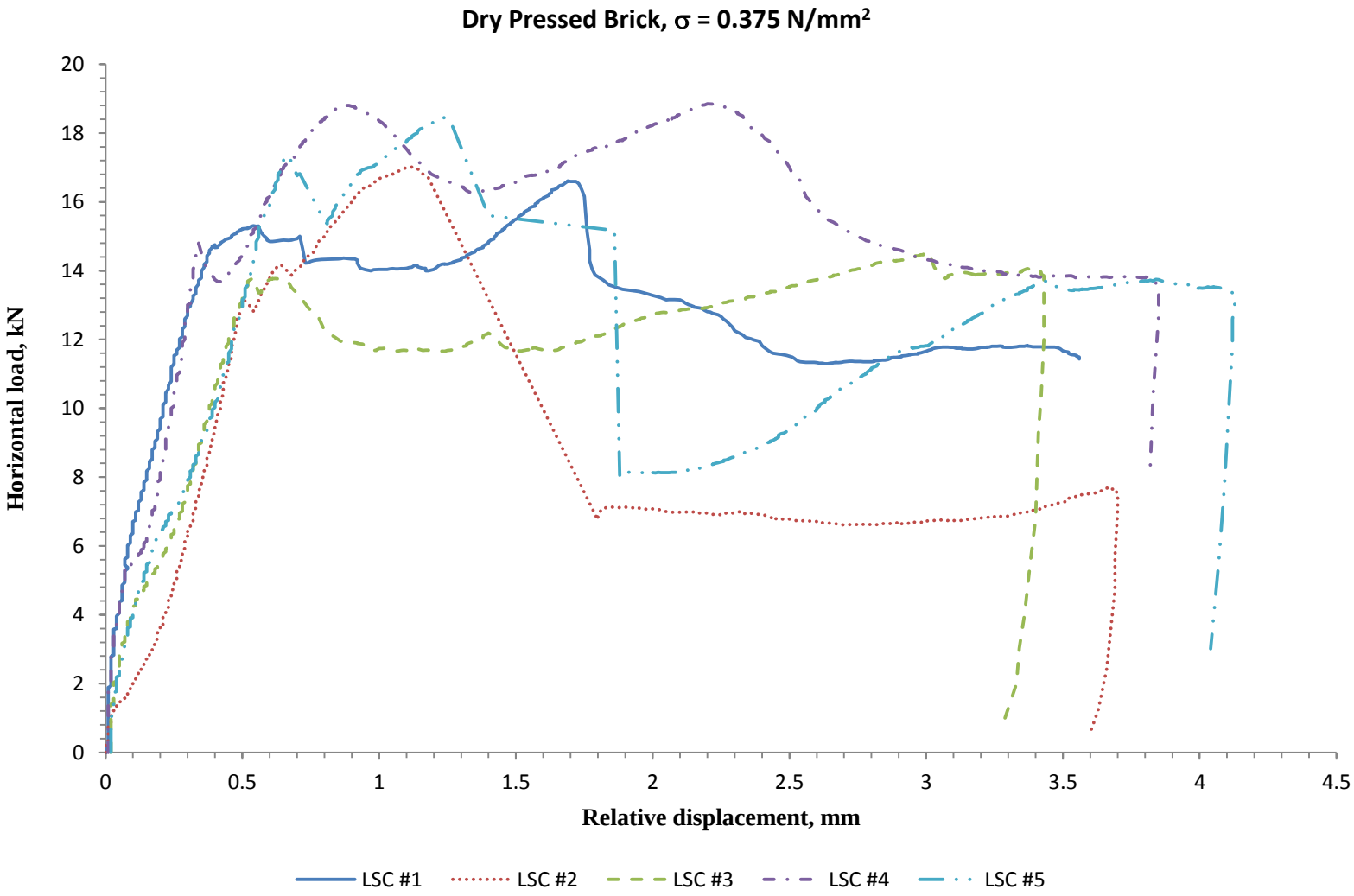
Dry Pressed Brick, σ = 0.375 N/mm²
Horizontal load, kN
Relative displacement, mm
0
2
4
6
8
10
12
14
16
18
20
0
0.5
1
1.5
2
2.5
3
3.5
4
4.5
LSC #1
LSC #2
LSC #3
LSC #4
LSC #5

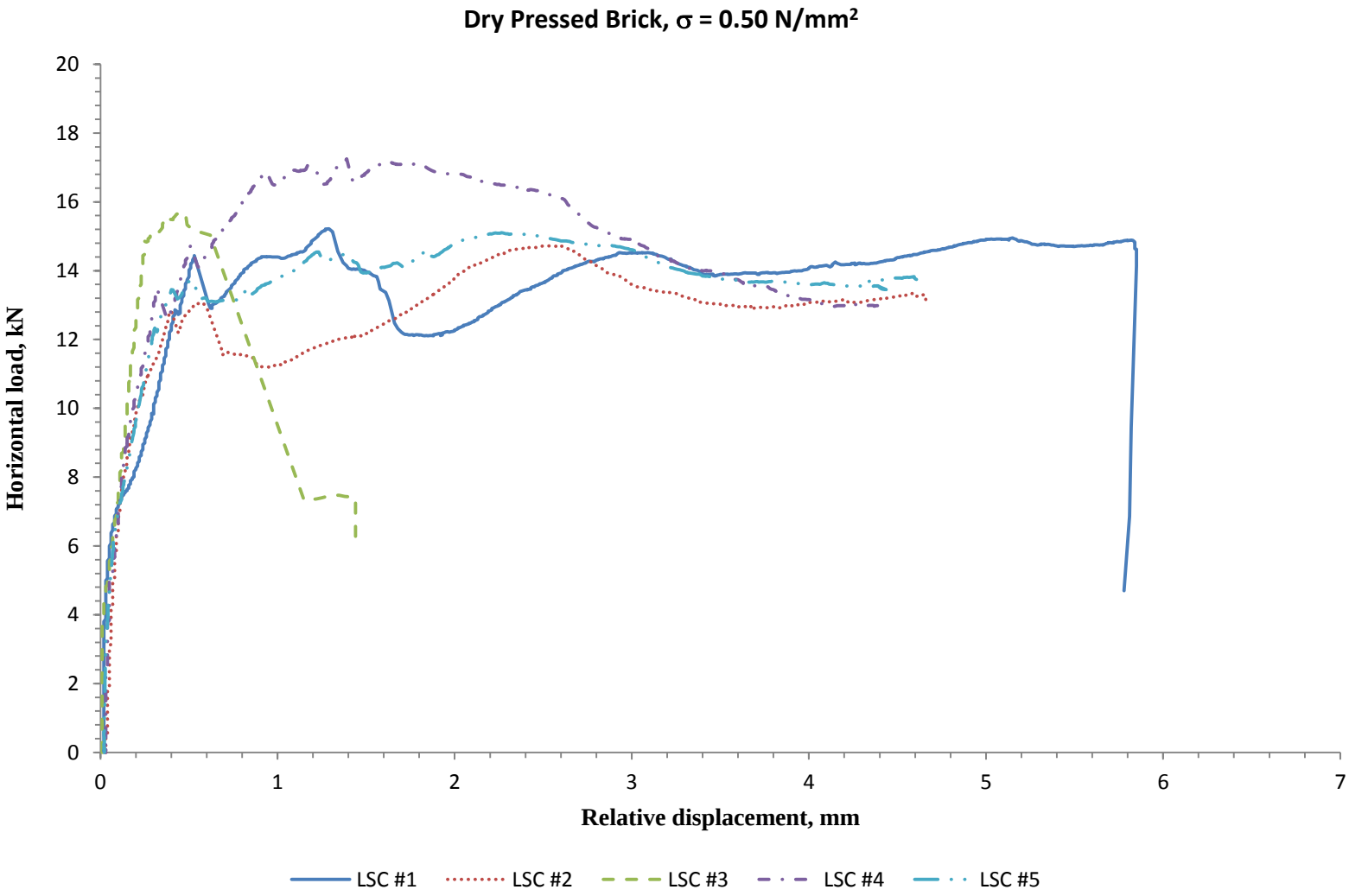
Dry Pressed Brick, σ = 0.50 N/mm²
Horizontal load, kN
20
18
16
14
12
10
8
6
4
2
0
0
1
2
3
4
5
6
7
Relative displacement, mm
LSC #1
LSC #2
LSC #3
LSC #4
LSC #5

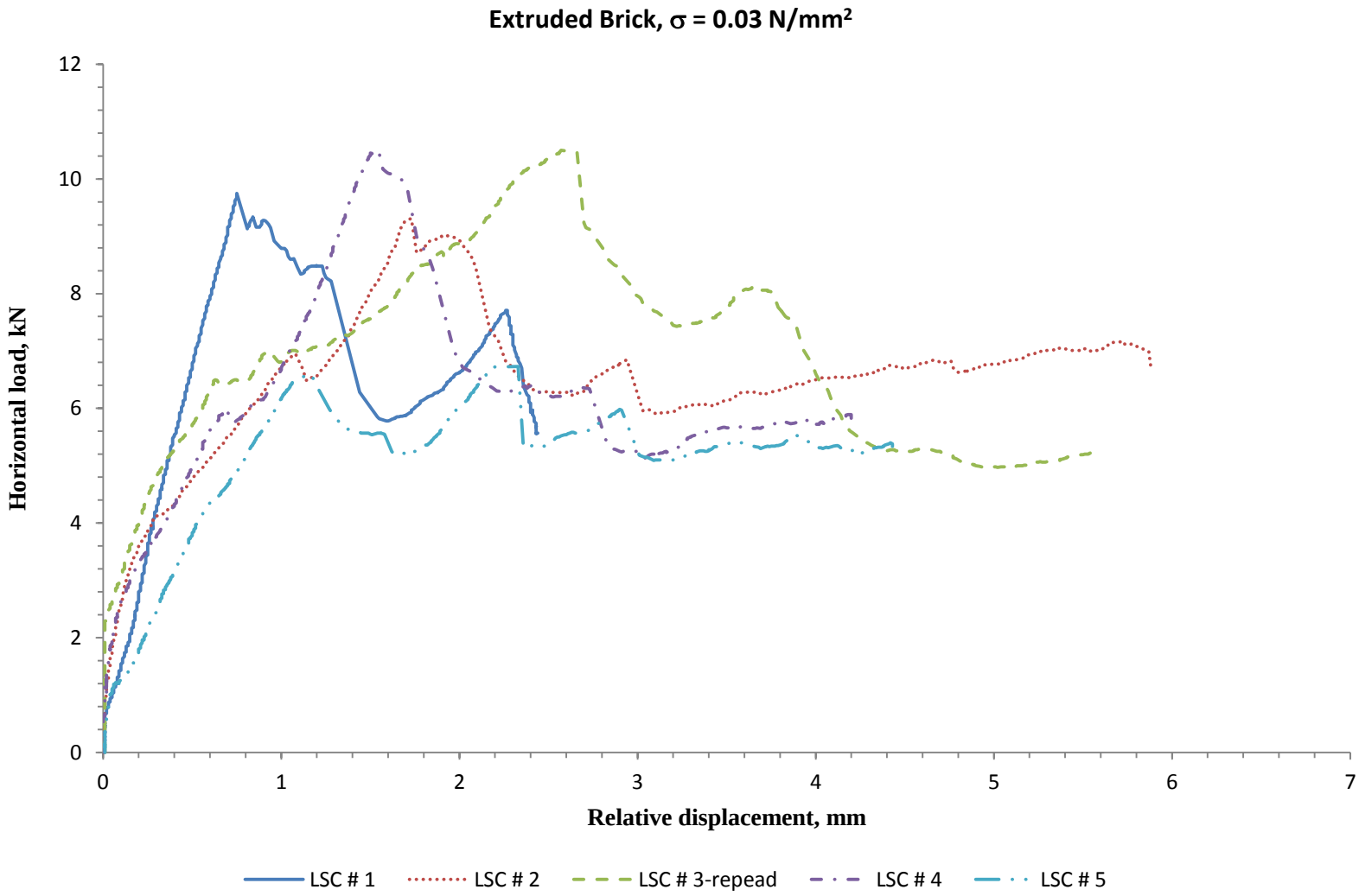
Extruded Brick, σ = 0.03 N/mm²
Horizontal load, kN
Relative displacement, mm
0
2
4
6
8
10
12
0
1
2
3
4
5
6
7
LSC # 1
LSC # 2
LSC # 3-repead
LSC # 4
LSC # 5

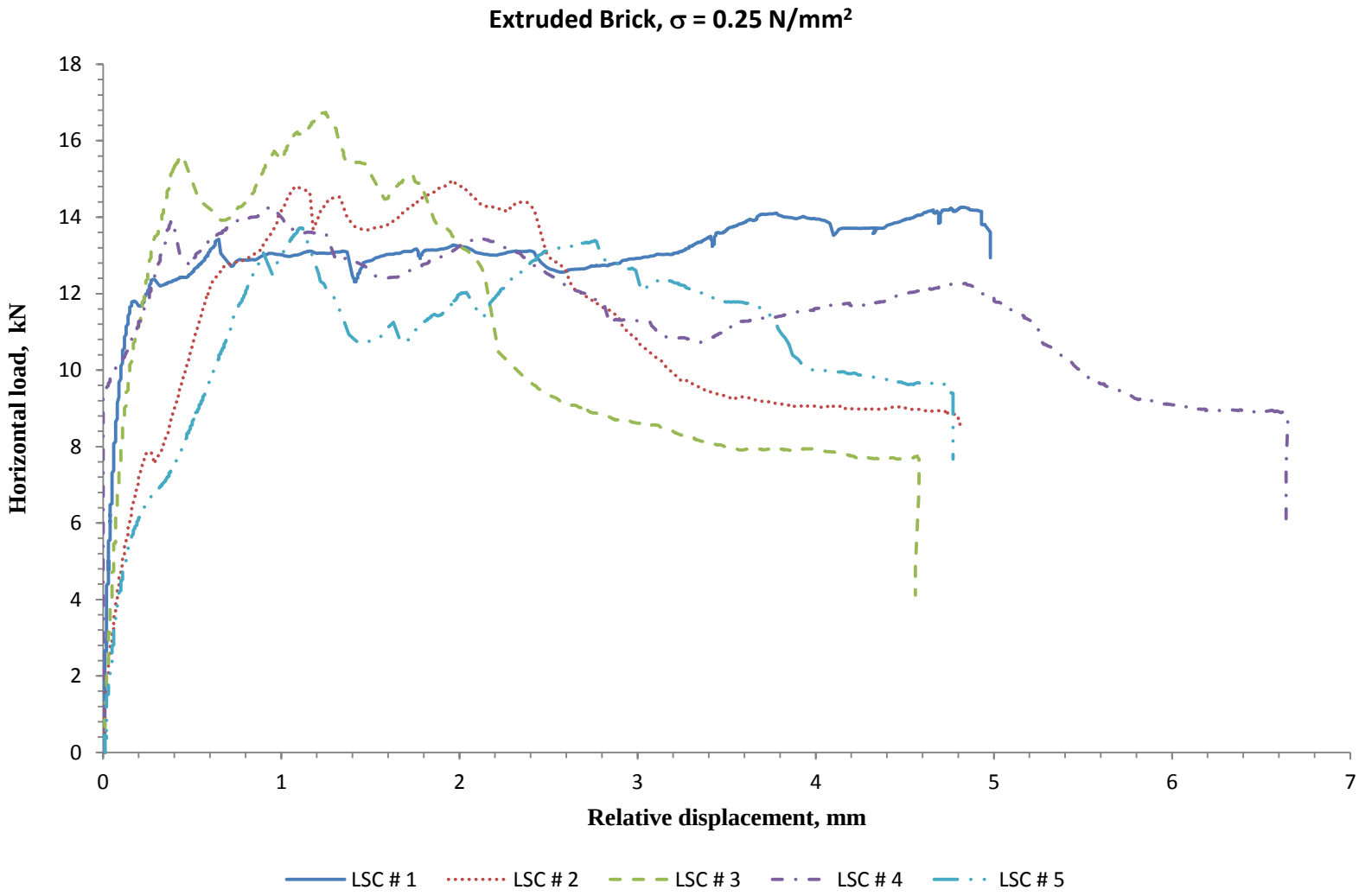
Extruded Brick, σ = 0.25 N/mm²
Horizontal load, kN
Relative displacement, mm
0
2
4
6
8
10
12
14
16
18
0
1
2
3
4
5
6
7
LSC # 1
LSC # 2
LSC # 3
LSC # 4
LSC # 5

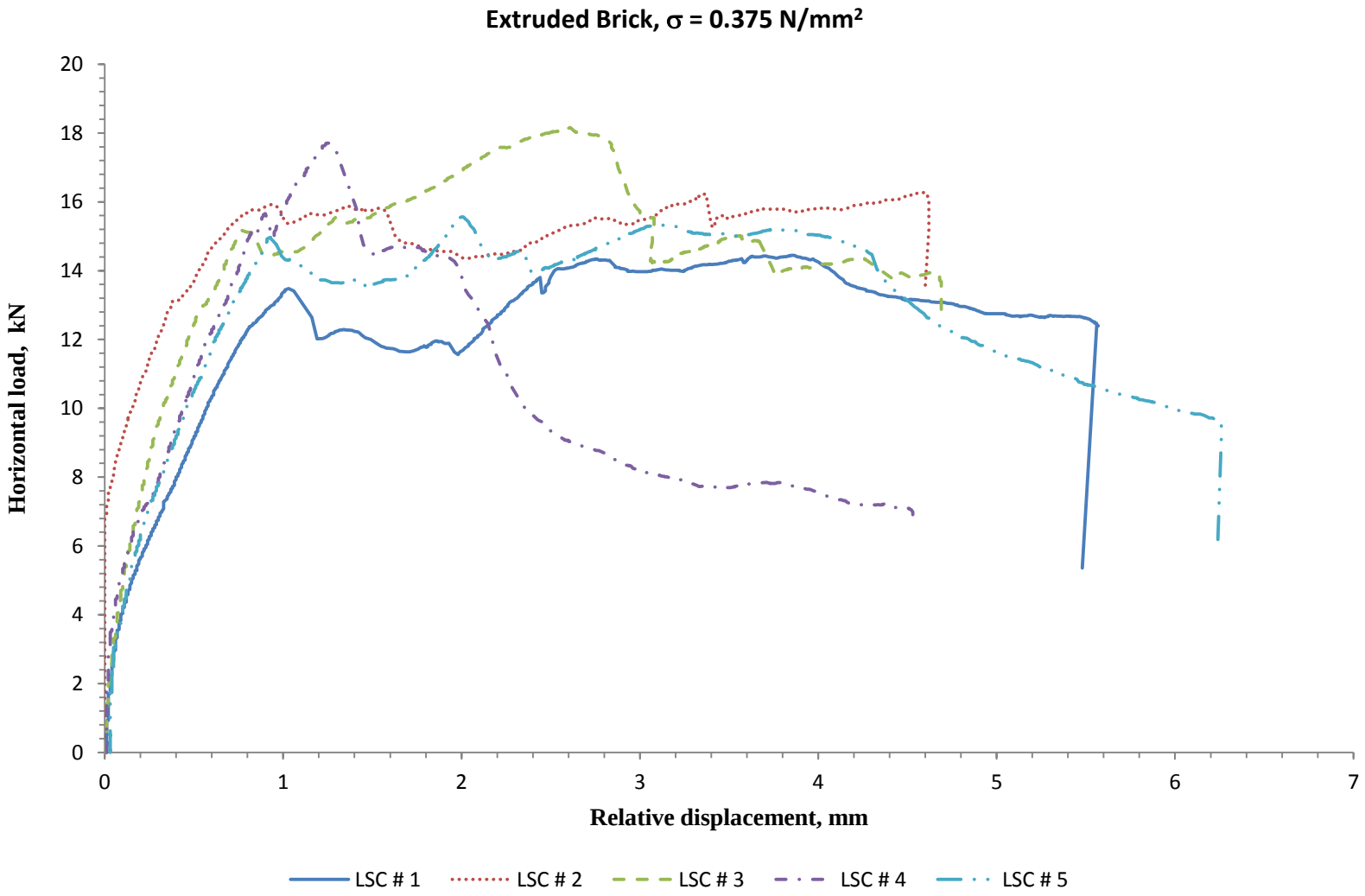
Extruded Brick, σ = 0.375 N/mm²
Horizontal load, kN
Relative displacement, mm
0
2
4
6
8
10
12
14
16
18
20
0
1
2
3
4
5
6
7
LSC # 1
LSC # 2
LSC # 3
LSC # 4
LSC # 5

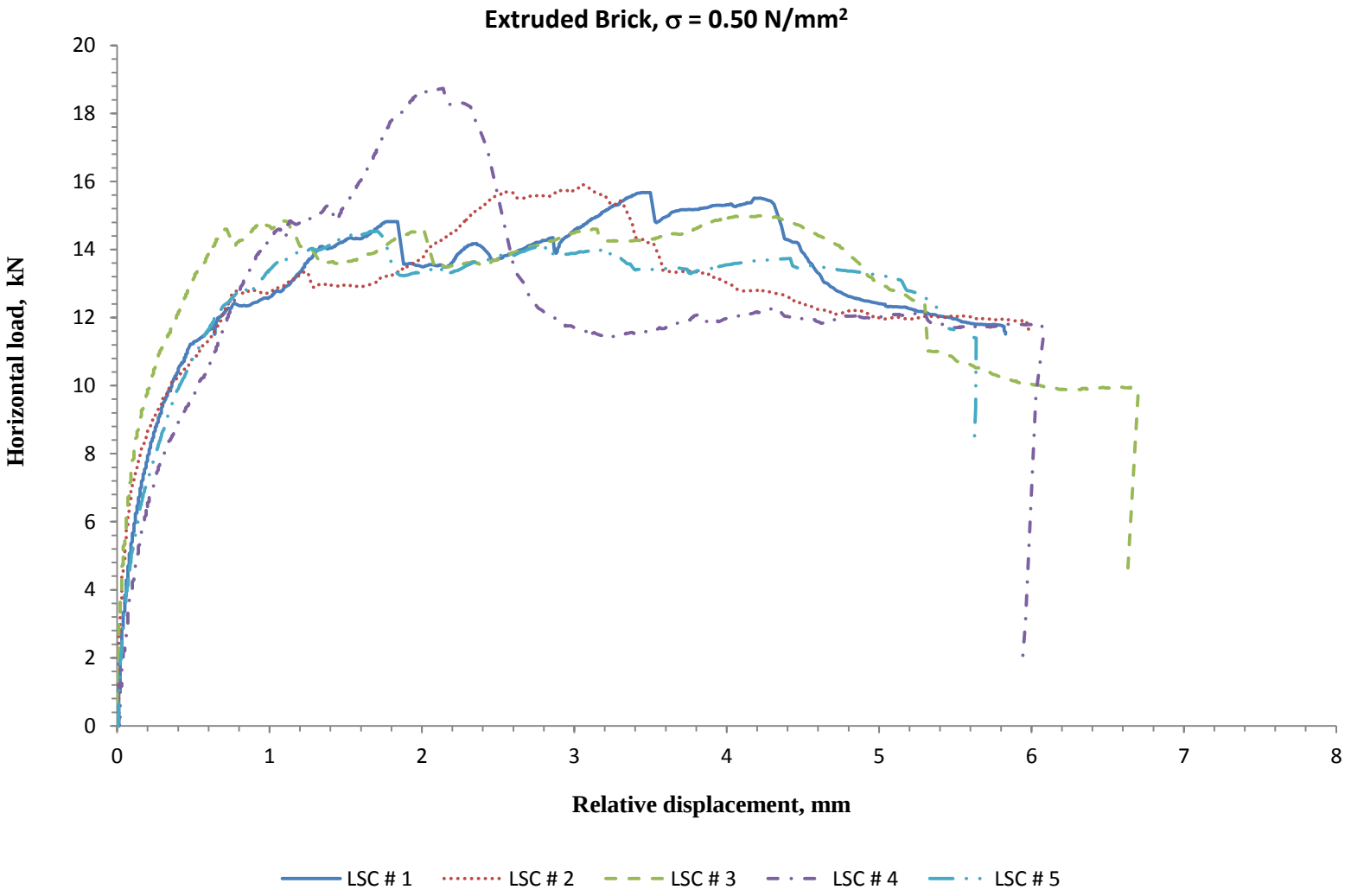
Extruded Brick, σ = 0.50 N/mm²
Horizontal load, kN
Relative displacement, mm
0
2
4
6
8
10
12
14
16
18
20
0
1
2
3
4
5
6
7
8
LSC # 1
LSC # 2
LSC # 3
LSC # 4
LSC # 5

APPENDIX B: HOFMANN & STÖCKL TEST

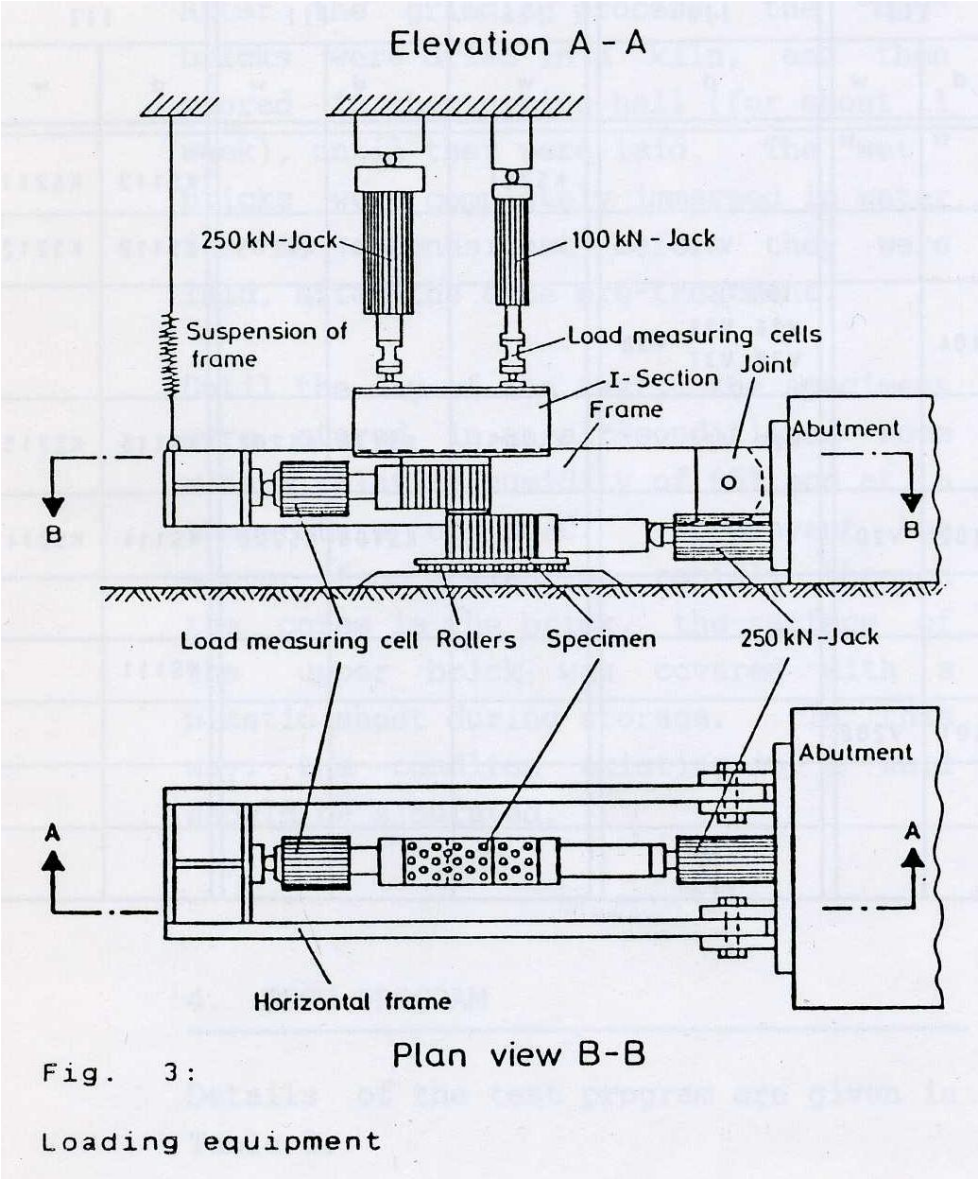

Fig. 3:

Loading equipment

(Hofmann & Stöckl, 1986)